Alpha-synuclein modulates the repair of genomic DNA double-strand breaks in a DNA-PK_{cs}-regulated manner

By

Elizabeth P. Rose

A DISSERTATION

Presented to the Neuroscience Graduate Program at the Vollum Institute and the Oregon Health & Science University School of Medicine in partial fulfillment of the requirements for the degree of Doctor of Philosophy

May 31st, 2024

School of Medicine
Oregon Health & Science University

CERTIFICATE OF APPROVAL

This is to certify the PhD dissertation of

Elizabeth P. Rose

has been approved

Mentor/Advisor: Vivek Unni, MD, PhD

Committee Chair: Michael Cohen, PhD

Member: Amanda McCullough, PhD

Member: Ian Martin, PhD

Member: Gregory Scott, MD, PhD

Table of Contents

List of Abbreviations

αSyn	Alpha-synuclein
AA	A53T Syn-GFP mouse line
AD	Alzheimer's Disease
ATM	Ataxia-Telangiectasia Mutated
ATR	Ataxia-Telangiectasia and Rad3-related protein
CK2	Casein Kinase II
CRISPR	Clustered Regularly Interspaced Short Palindromic Repeats
DNA-PK_{cs}	DNA-dependent Protein Kinase, catalytic subunit
DNMT3B	DNA Methyltransferase 3 Beta
DMSO	Dimethyl Sulfoxide
DSB	Double-strand Break
FRET	Fluorescence Resonance Energy Transfer
GBA	Glucocerebrosidase (lysosomal enzyme gene code)
GRK	G-protein-coupled-receptor kinase
HAP1	Human Haploid Cell Line
HR	Homologous Recombination
IHC	Immunohistochemistry
Indel	insertion/deletion
KO	Knockout
LBD	Lewy Body Dementia
LRRK2	Leucine-Rich Repeat Kinase 2
NAC	Non-Amyloid-beta Component

NGS	Next Generation Sequencing
NHEJ	Non-homologous End-joining
MOI	Multiplicity of Infection
MRE11	Meiotic Recombination 11 homolog 1
PARP	Poly ADP Ribose Polymerase
PD	Parkinson's Disease
PDD	Parkinson's Disease Dementia
PFF	Preformed Fibril
PLK	Polo-Like Kinase
PPIB	Peptidylprolyl Isomerase B
pSyn	S129 Phosphorylated Alpha-synuclein
SNCA	Gene encoding for Alpha-synuclein
SSA	Single Strand Annealing
T7EI	T7 Endonuclease I
WT	Wild-Type

Acknowledgements

Firstly, I would like to thank my PhD mentor, Dr. Vivek Unni MD,PhD. Thank you for guiding me throughout my scientific journey and always being eager to see the data. I joined the lab in a tumultuous time during the 2020 COVID pandemic, and I will never forget you taking the initiative to teach me bench skills when the rest of the lab was working from home. You elegantly pivoted my rotation to a virtual writing rotation, and you selflessly gave me access to your parking spot during the pandemic so I wouldn't have to use public transit when we were allowed back in the lab. You have always supported my career aspirations and always financially backed my conference attendances and career development endeavors. You provide such a unique teaching environment as you still see movement disorder patients at OHSU, and I appreciate you being so open with me shadowing you in clinic. You have taught me to think critically, and I feel lucky to have been able to learn from you.

I also kindly thank my Dissertation Advisory Committee for providing me with scientific guidance, grant writing assistance, and help navigating me through these past five years. Dr. Michael Cohen, thank you for acting as chair of my committee and always sharing neuronal culture dissection equipment. Whenever I came to you with a scientific roadblock, you would jump into action and offer a lab collaboration to help progress my science. Dr. Amanda McCullough, thank you for serving as the DNA repair expert on my committee and for the moral motivation in grant writing and experiments. Dr. Ian Martin, thank you for training me how to culture neurons and sharing incubators and hood space. Your expertise on PD and helpful feedback has been essential to my graduate education. I would also like to thank Dr. Gregory Scott for serving as my external reader for my dissertation defense.

If it were not for the support of past and present labmates, classmates, NGP, and all organizations at OHSU, my degree completion would not have been possible. Thank you to Moriah Arnold, Jovin Singh Banga, Valerie Osterberg, Sydney Weber-Boutros, Anna Bowman, Dr. Carlos Soto Faguas, Elias Wisdom, and Jessica Keating. Thank you for making the Unni Lab a wonderful place to work and for your constant assistant with experiments. Thank you to all NGP students, the Vollum Institute, Jungers Center, Dr. Kelly Monk, Dr. Kevin Wright, and Jessica Parks for making the NGP the most wholesome, supported, well-funded graduate program I have ever seen. The recruitment events, seminars, and events have kept me going through these past 5 years, and I rarely have to think about lunch with all the food provided at these spectacular events which has extremely improved my mental health and well-being. Thank you to Staci Wade-Hernandez for supporting me throughout all of the challenges of life and graduate school. Thank you to the School of Medicine Alumni Association

Council, the Graduate Researchers United, and the Graduate Student Organization for your dedication to graduate students and letting me serve as student representatives over the years. OHSU and the NGP has been an outstanding institution and graduate program, and I am honored to join their esteemed alumni.

Thank you to all the support outside of OHSU I have had along the way. Thank you to friends in Portland and Vancouver for your unwavering support and always being delighted to hear about my experiments. Thank you to Olivia Decelles, Cole Brashaw, Dan Orlin, Katy Lehmann, Gabby Thuillier, Katy Halverson, Joyce Vu, Holly Scrugham, Zane and Keith Franke, Austin and Natasha Morissette, and Tyler Scacco. Thank you to my wonderful friendships from Pomona College with Sabine Scott, Sara Sherburne, Jenny Thompson, Maddie Zug, Eliana Kaplan, Melissa Hooke, Kayla Lanker, Sarah Binau, and Leah Rosenzweig for long distance phone calls of enthusiasm and inspiration. Thank you to Cas and Tess Majewski at Congruency Collective for providing me with a creative outlet through tap fusion dance and for graciously welcoming me back into performing on stage after a long hiatus. Through the performing arts, book club, D&D, TV watch parties, lake vacations, or 2000's night at Crystal Ballroom, you all have created a home for me in the PNW and I am forever grateful.

Lastly, thank you to my inner circle of family and friends for daily encouragement and reassurance. Thank you to Moriah Arnold, labmate and best friend, for navigating the woes of scientific discovery with me and for always including me in your plans whether it be sauna spa days, camping at Crater Lake, or wine tasting in Southern Oregon. Thank you to my parents and sister, Catherine, Hugh, and Grace Rose and my entire extended family for cheering me on from the sidelines and visiting me in Portland. Lastly, thank you to my partner, Chris, and our cats, Meeka and Moose, for grounding me and creating a positive and peaceful environment to come home to. You always remind me that what I do is important and meaningful. I could not have persevered through this last year without your patience, compassion, kindness, and selflessness.

Dissertation funding: NGP, NIA T32 AG055378, The David Johnson Family Foundation, The Lacroute Fellowship, NINDS R01 90269398

Abstract

In Parkinson's Disease, the protein alpha-synuclein (αSyn) misfolds and aggregates to form Lewy Bodies. Although its role in the presynaptic terminal is to bind synaptic vesicles, the role of αSyn in the nucleus is still unknown. In Chapter 1, background information on Parkinson's Disease, αSyn, a potential nuclear role in DNA repair, and its most common post-translational modification of a serine 129 phosphorylation site are discussed.

Chapter 2 dives into these topics experimentally and highlights my work to investigate the role of αSyn in the repair of genomic DNA double-strand breaks. I hypothesized that αSyn is involved in non-homologous end-joining because it is thought to be the only double-strand break mechanism relevant in post-mitotic cells. In Chapter 2, I provide evidence for αSyn modulating DNA double-strand break repair using a CRISPR/Cas9 lentiviral approach and show evidence that this repair is modulated by DNA-PK_{cs}. Chapter 2 closes with experiments showing that altering clearance of αSyn via pharmacological kinase inhibition can lead to increased levels of histone modifications associated with DSB repair and increased survival rate of cells with αSyn inclusions.

Chapter 3 describes additional studies that I performed related to this project that either yielded negative data or were difficult to interpret due to technical reasons. In Chapter 4 is a discussion of the project as a whole and proposes future experimental approaches to add to the current body of work.

Chapter 1: Introduction

Parkinson's Disease (PD) is a movement disorder that affects more than 10 million people worldwide. It is the second most common neurodegenerative disease after Alzheimer's Disease and 1.2 million people in the United States alone are expected to be diagnosed by 2030. PD was first described by James Parkinson in 1817 as the "shaking palsy" (Parkinson, 1817) and then further characterized and differentiated from other diseases such as multiple sclerosis by Jean-Martin Charcot in the mid 1800s (Goetz, 2011). Since then, symptom onset, diagnosis, environmental factors, and genetic mutations have been clearly defined. Although therapeutics ameliorating symptoms have been developed and studies have begun to elucidate the pathological progression of this disease, there are currently no widely effective disease-altering treatments.

1.1 Parkinson's Disease

Symptoms and Diagnosis

Parkinson's Disease consists of two types of symptoms: motor symptoms and non-motor symptoms. Motor Parkinsonism symptoms such as bradykinesia, rigidity, tremors, and postural instability are due to a loss of a subset of dopamine neurons in the substantia nigra. Non-motor symptoms, such as dementia, psychosis, blood pressure regulation problems, and sleep disorders, are due to neurodegeneration of various non-dopamine neurons in other nervous system regions. Non-dopamine-related

motor symptoms such as freezing of gait and difficulty swallowing are also associated with Parkinsonism. For most patients, motor symptoms arise in the later stages of life, with an average diagnosis age of 60. While every patient is unique with their disease progression, the parkinsonian symptoms almost universally worsen over time, if untreated. The most effective therapeutic treatment option for patients is levodopa, the catecholamine precursor to dopamine that helps replenish its levels when dopaminergic neurons are reduced in the substantia nigra. Although many potentially promising new therapies are currently in clinical trials, there are no disease-modifying therapies to date.

Over the progression of the disease, patients' diagnoses can change with the development of dementia. Cases in which patients experience dementia at least one year after their motor symptoms develop are categorized as having developed Parkinson's Disease Dementia (PDD). Whereas if cognitive impairment precedes or occurs within one year of motor symptom onset, patients are diagnosed with Dementia with Lewy Bodies (DLB) (Gomperts, 2016). PDD and DLB both fall under the umbrella term of Lewy Body Dementias (LBD) (Milán-Tomás et al., 2021). Lewy Bodies are cytoplasmic inclusions found in surviving neurons that contain misfolded and aggregated α-synuclein (αSyn), which will be discussed at length later in this chapter.

Prevalence and Comorbidities

PD affects 1% of the population above 60 years old, 4% of the population above 80 years old (Dexter & Jenner, 2013), and 1-2 per 1000 people at any time. PD has recently undergone the fastest growth in prevalence out of all neurological disorders and is one of the leading causes of disability in the world (GBD 2015 Neurological Disorders Collaborator Group, 2017). Globally, the age-standardized incidence,

prevalence, and years lived with disability has increased from 1990 to 2019 by over 150% in a study of 204 countries (Ou et al., 2021). Men are at a higher risk of developing PD and have a documented higher prevalence globally compared to women, however women have a higher mortality rate and faster progression than men (Cerri et al., 2019; Heller et al., 2014; Solla et al., 2012). Studies have shown that motor and non-motor symptoms, risk factors, and pathogenic mechanisms may differ in men and women. Specifically, vulnerability of the dopaminergic system to neurodegeneration, neuroinflammatory responses, and oxidative stress mechanisms may be behind these sex differences in pathophysiology (Cerri et al., 2019).

Several risk factors are connected to PD, including age, gender, pesticide exposure, stress, and traumatic brain injury. PD also interacts with several other diseases. Comorbidities include anemia, depression, diabetes, gastrointestinal dysfunction, restless leg syndrome, and melanoma (Santiago et al., 2017). PD patients are at a higher risk of developing melanoma and vice versa. This may be because both diseases are associated with increased levels in αSyn. Increased levels of αSyn within the skin elevates the risk of melanoma, and increased aggregation of αSyn in the brain can form cytoplasmic inclusions called Lewy Bodies in PD patients. Comorbidities such as this may be important to understanding the etiology of PD and how other risk factors impact the development of this disease.

Prevalence of PD also differs based on geographic location, and rural living has been linked to PD incidence. Early studies suggested a connection between farming, rural living, and drinking well water with PD risk (Gorell et al., 1998; Priyadarshi et al., 2001). For many years PD was thought to be purely caused by environmental factors.

Influential twin studies (Duvoisin et al., 1981; Ward et al., 1983) and research on pesticide exposure increasing PD risk (Baldi et al., 2003; Kamel et al., 2007; Liew et al., 2014) all strengthened this environmental-only hypothesis. Specifically rotenone, paraquat, diquat, and maneb are the most heavily linked chemical pesticides associated with PD (Costello et al., 2009; Pezzoli & Cereda, 2013; Pouchieu et al., 2018; Tanner et al., 2011). However, the field of PD underwent an unprecedented dogma shift for neurodegenerative diseases when the first gene linked to PD was discovered.

Genetic Risk

In 1997, αSyn was genetically linked to PD (Polymeropoulos et al., 1997) in an autosomal dominant fashion. αSyn, including its structure and function will be discussed at length in Chapter 1.2. Since this first fundamental genetic evidence linking αSyn, other monogenic mutations in Parkin, PTEN-induced putative kinase 1 (PINK1), and Daisuke-Junko-1 gene (DJ-1) have been associated with rare autosomal recessive forms of early-onset PD (Kitada et al., 1998; Valente et al., 2001; Bonifati et al., 2003). Parkin is an E3 ubiquitin ligase; PINK1 is a protein kinase with a mitochondrial targeting domain, and both are involved in mitochondrial regulation and mitophagy (Seirafi et al., 2015). In PD, Parkin is the most frequently mutated autosomal recessive gene and makes up nearly 50% of early-onset familial cases, followed by PINK1 accounting for up to 8% of early-onset genetic cases (Kalia & Lang, 2015). DJ-1 makes up 1-2% of early-onset familial PD, and has been shown to be involved in regulating apoptosis, autophagy, inflammatory responses, chaperone processes, and recently cellular metabolism (Mencke et al., 2021).

More prevalent than Parkin, PINK1, and DJ-1, genetic point mutations in leucine-rich repeat kinase 2 (LRRK2) were subsequently discovered as the most common monogenic form of PD leading to autosomal dominant PD (Zimprich et al., 2004). LRRK2 is a large protein that contains a GTPase and a kinase domain and functions in several different cellular signaling pathways, including autophagy, vesicle trafficking, cytoskeletal dynamics, protein translation, immune response, and lysosomal and mitochondrial function (Tolosa et al., 2020). The G2019S mutation is the most prevalent LRRK2 mutation and accounts for 5-6% of autosomal dominant cases and 1% of idiopathic PD cases (Xiong et al., 2017). LRRK2 kinase activity is commonly increased in LRRK2 mutation familial PD, and may also be increased in idiopathic PD due to oxidative stress or endolysosomal stress (Rocha et al., 2022). Furthermore, although rare, some LRRK2 carriers do not exhibit Lewy Body pathology, yet still most carriers present neuronal degeneration in the striatum (Rocha et al., 2022). It is still unclear how increased LRRK2 kinase activity in idiopathic PD may lead to these differing mechanisms of disease progression.

The most prevalent genetic risk factor for PD comes from mutations in the gene GBA, which encodes for a lysosomal enzyme glucocerebrosidase. About 5-15% of the PD population have mutations in GBA, and GBA-associated PD is clinically identical to idiopathic PD with nigrostriatal dopaminergic neuron loss and Lewy pathology (Smith & Schapira, 2022). Interestingly, a polymorphism found within the SNCA gene encoding αSyn was associated with an increased risk of developing PD in GBA carriers (Blauwendraat et al., 2020), and associated with an accelerated motor decline in GBA-PD patients (Stoker et al., 2020). Out of at least 15 genes in which monogenic

mutations are connected to PD, GBA mutations are the most widespread genetic risk for PD and are important to investigate further in the diverse population of PD patients.

Other than mutations causing protein coding changes, there are SNCA gene multiplications that also lead to PD. Duplications and triplications in SNCA were first studied in the early 2000s by following extremely rare families that developed severe early onset PD (Singleton et al., 2003). Several kindreds were found where duplications in SNCA can lead to early-onset PD with an approximate average age of onset of 50 and triplications can lead to early-onset PD at around age 35 (Chartier-Harlin et al., 2004). This was later confirmed in a study from over 50 families, and generally triplication patients have rapidly progressive symptoms whereas duplication patients have symptoms similar to late-onset parkinsonism (Book et al., 2018). Although extremely rare, these genetic multiplication cases directly shed light on how just increasing expression of normal protein sequence αSyn can heavily influence PD progression.

Out of all the genetic mutations discussed here, in total these familial cases only make up 10% of all PD cases. The remaining 90% of cases are idiopathic forms of PD. Although rare, these genetic mutations can provide critical insight into the mechanisms of neurodegeneration and can lead to the creation of cell lines and animal models to better study the disease relevant intricacies of PD.

Animal Models

Although there is no perfect animal model for representing the human experience of PD, several models are useful for researching specific aspects of disease progression. As expected, transgenic models exist for almost all PD-associated genes

discussed in the previous section. Mouse, rat, non-human primates, *Drosophila*, and *C. elegans* models with genetic mutations targeting Parkin, PINK1, LRRK2, GBA, or αSyn have been studied for decades (Dovonou et al., 2023). These have provided valuable insights for understanding familial PD biology and progression. Scientists have also turned to genetically engineering mice which lack genes encoding for transcription factors such as Lmx1a/b, Otx2, Foxa1/2, and Pitx3 which are required for midbrain dopaminergic neuronal survival and lead to their degeneration when deleted (Dovonou et al., 2023). Transgenic models targeting well-known PD-associated genes and transcription factors have been incredible useful to recapitulate some familial and idiopathic phenotypes of PD in animals.

Drug-induced animal models have also had a long and important history of reproducing certain motor deficits of Parkinsonism. The first ever PD model was developed almost 7 decades ago with reserpine injected animals to induce motor impairments via inhibition of the vesicular monoamine transporter type 2 (Carlsson et al., 1957; Fernandes et al., 2012). Haloperidol, a dopaminergic D2 receptor antagonist, has also been used to induce catalepsy and modeling rigidity and dyskinesia (Ionov & Severtsev, 2012, 2022; Waku et al., 2021). These historical drug-induced parkinsonism models are important for investigating motor symptoms, but fall short in reproducing the neuropathology of PD.

In a similar vein, neurotoxic animal models have greatly improved over the years to replicate nigral loss and movement deficits. A well established and popular rodent model can be achieved by intracranial injections of 6-hydroxydopamine (6-OHDA) to lesion the nigrostriatal dopaminergic system (Blandini et al., 2008). This long-standing

model has been essential for researchers to study rapid and specific neurodegeneration, but it fails to replicate αSyn aggregation or Lewy pathology. Additionally, in the 1980's another animal model was discovered when humans mistakenly self-administered 1-methyl-4-phenyl-1,2,3,6-tetrahydropyridine (MPTP) a synthetic heroin, resulting in Parkinsonism in young adults (Langston et al., 1983). The MPTP model has shown to reproduce motor symptoms such as tremors, rigidity, postural instability, and freezing and neurodegeneration of dopaminergic neurons in the substantia nigra and putamen in humans and non-human primates (Ding et al., 2008; Przedborski et al., 2001). Lastly, intracranial injection of Lipopolysaccharide (LPS) into rodents has also proved to be a reliable model for studying loss of nigral dopaminergic neurons (Le et al., 2001). LPS is an endotoxin normally used for studying inflammation, but was also utilized as a PD model when a laboratory worker developed Parkinsonism and dopaminergic neuronal loss after accidental LPS exposure in an open wound (Dovonou et al., 2023). Unlike the 6-OHDA model, the MPTP mouse model also demonstrates upregulation of αSyn (Hu et al., 2020) and the LPS neuroinflammation model shows increased nitration of αSyn in rats although Lewy pathology is not generally observed (Choi et al., 2010). Though some were discovered by accident, these neurotoxic models now allow researchers control over dopamine neuron degeneration and replicate some of the molecular and neuropathological characteristics of PD.

As previously described, PD is heavily linked to environmental toxins and pesticide exposure through multiple epidemiological studies. Using this knowledge, animal models were developed using similar environmental toxins such as rotenone,

paraquat, and maneb. First established as a model over 20 years ago, rotenone inhibits proteasomal activity, prompts selective nigrostriatal dopaminergic neuron loss, causes motor impairments, and induces αSyn aggregation and inclusions (Betarbet et al., 2000; Fleming et al., 2004; Yuan et al., 2015). Paraquat can also be used to model partial neurodegeneration and increased αSyn aggregation (Manning-Bog et al., 2002). Paraquat alone may not fully cause motor deficits, but the combination of paraquat and maneb has been utilized to replicate motor impairments along with neuronal loss in mice and with mixed results in rats (Cicchetti et al., 2005; Saint-Pierre et al., 2006; Thiruchelvam et al., 2000). Toxin based models can be efficient at reproducing PD associated hallmarks like dopamine neuron loss, but in general do not cause Lewy pathology; there also can be experimental variability, as seen in epidemiological studies in humans exposed to these toxins.

Most recently the field has adopted the αSyn overexpression and Lewy pathology seeding models to more precisely investigate αSyn pathogenesis. The first transgenic mouse line expressing WT human αSyn was the M-line, resulting in increased αSyn aggregation and inclusions and loss of dopaminergic terminals (Masliah et al., 2000). Then, the transgenic mouse line 61 (M61) was developed, overexpressing human WT αSyn using a neuron specific promotor. This line successfully modelled motor impairments, αSyn inclusions, and mitochondrial dysfunction but shows only mild effects on dopaminergic neurons (Rockenstein et al., 2002; Subramaniam et al., 2014). Other genetic models have targeted familial PD-associated point mutations within αSyn such as E46K, A30P, and A53T. Rodent, *Drosophila*, and *C. elegans* versions of these models have shown varying levels of αSyn accumulation and motor symptoms (Ekmark-

Lewén et al., 2018; Emmer et al., 2011; Mizuno et al., 2010; Perni et al., 2021; Piltonen et al., 2013). The M83 line overexpressing human A53T αSyn demonstrates increased phosphorylated αSyn aggregation and motor symptoms after about 8 months, but lacks any dopaminergic neuron loss in homozygous mice (Giasson et al., 2002). Interestingly, the hemizygous M83 mice spontaneously develop motor impairments between 22 and 28 months of age (Giasson et al., 2002).

New αSyn animal models were developed when Kelvin Luk in Virginia Lee's lab discovered that recombinant αSyn that was aggregated into preformed fibrils (PFFs), sonicated and then injected into WT mouse dorsal striatum causes hyperphosphorylation of endogenous αSyn, Lewy body-like pathology, extensive spreading of this pathology, long term motor deficits and neurodegeneration of striatal dopaminergic neurons (Luk, Kehm, Carroll, et al., 2012). Because this method allows researchers to control the PFF injection location, intracranial, peripheral stomach, and hindlimb gastrocnemius muscle injections have all demonstrated pathology spread to the brain. The PFF model has become widely used and is a gold standard in the field for generating Lewy pathology. However, αSyn pathology spread can take several months after PFF injection to develop in WT mice; therefore researchers have also turned to PFF or whole brain homogenates from symptomatic M83 mice injected into A53T αSyn mutant mice to accelerate pathology induction (Luk, Kehm, Zhang, et al., 2012; Schaser et al., 2020). Groups have also developed viral-vector mediated models to overexpress WT and A53T αSyn in rodents and non-human primates to better model the different stages of PD (Decressac et al., 2012; Kirik et al., 2003). As the PFF model proves to be one of the most widely accepted models in the field for studying αSyn pathology

progression, I adopted a PFF cortical injection protocol, which will be discussed further in Chapter 2, in an A53T αSyn-GFP accelerated mouse model to study longitudinal αSyn progression *in vivo* using multiphoton microscopy.

1.2 Alpha-synuclein

Alpha-synuclein (αSyn) is a small 140 amino acid long protein highly conserved among vertebrates, originally discovered in the sting ray *Torpedo Californica* (Maroteaux et al., 1988). It was first named for its location in the (syn)apse and (nucle)us. In presynaptic terminals it functions to bind synaptic vesicles, but in the nucleus its role is more unclear. As seen in Figure 1.2.1, the N-terminal segment (residues 1-60) of the protein takes on an alpha-helical shape in the presence of synaptic vesicles and is responsible for binding to these vesicles. The hydrophobic Non-amyloid-beta Component (NAC) domain (61-95) is prone to aggregation and allows for αSyn to form β sheet structures. The C-terminal segment (96-140) inhibits aggregation, potentially by electrostatic repulsion via its multiple anionic residues (Bisi et al., 2021). αSyn is generally accepted as an intrinsically disordered protein when in solution that folds into an alpha-helical conformation when binding vesicles, however there is some controversy in the field over whether it can exist physiologically as a tetramer under unpurified and non-denaturing conditions (Bartels et al., 2011).

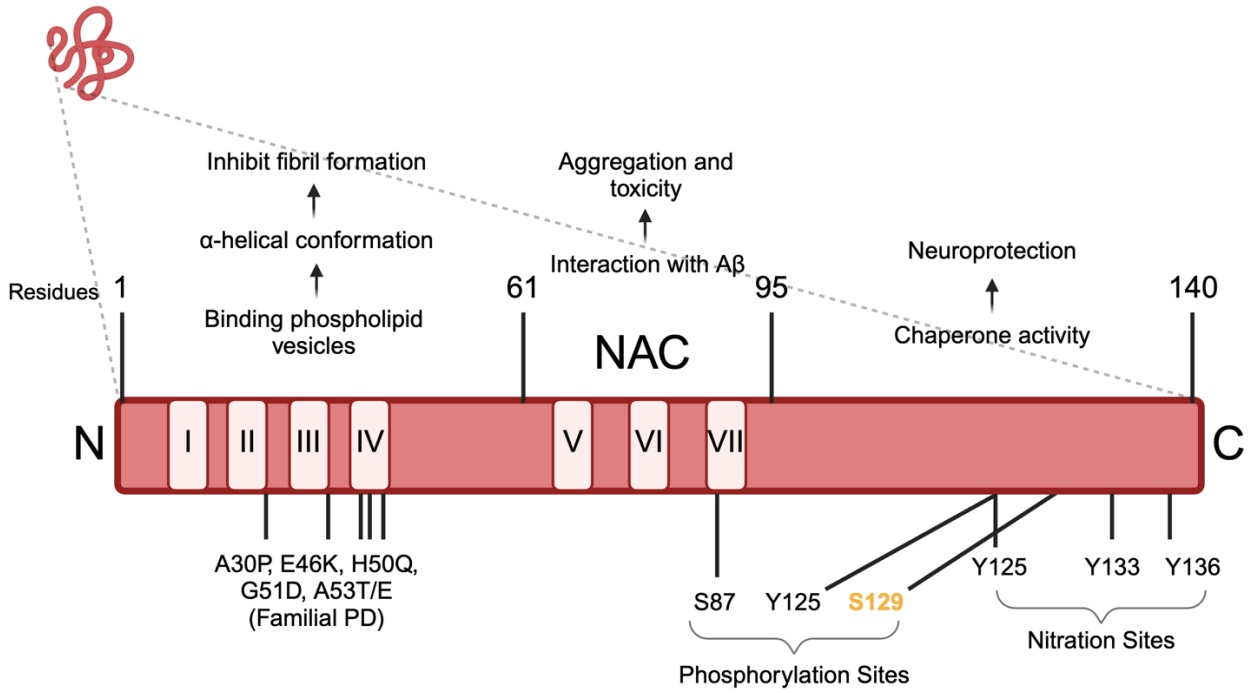

Figure 1.2.1. Cartoon of αSyn Primary Structure. Adapted from Cheng et. al 2010. Intrinsically disordered αSyn stretched linearly to display N-terminal, NAC, and C-terminal segments denoted by residue. Familial PD mutations found within the N-terminal segment and post-translational modifications (PTMs) within the NAC and the C-terminal segment with the most common and pathologically relevant PTM, S129, highlighted in yellow.

αSyn and Genetic PD

αSyn was the first gene linked to PD in the 1990's and now there are several mutant variants associated with familial PD. A30P, E46K, A53T, A53E, H50Q, and G51D are the main variants studied in the field, with emerging evidence calling for A30G and A53V to also be added to this list. Interestingly, all of these missense mutations are located within a specific region in the N-terminal segment of αSyn, which suggests some functional role for this region of αSyn in PD pathogenesis. As previously described, many animal models exist for A30P, E46K, and A53T mutations, yet no

animal models exist for A30G, A53E, A53V, H50Q, G51D at this point in time (Dovonou et al., 2023). The A30P, E46K, and A53T mutations were first discovered in German, Spanish, and Italian/Greek pedigrees, respectively (Krüger et al., 1998; Polymeropoulos et al., 1997; Zarranz et al., 2004). Additionally, duplication and triplication αSyn copy number variations lead to early onset of PD symptoms. Overall, the αSyn mutation familial PD cases are extremely rare and make up less than 0.01% of cases, but these studies have been crucial for understanding protein dynamics and their impact on disease biology.

These single point mutations within αSyn alter the way the protein interacts on a molecular level. Through NMR spectroscopy, researchers concluded that the A30P mutation disrupts the alpha-helical preference of the N-terminal segment and the A53T mutation enhances its propensity to form β sheet-like conformations (Bussell & Eliezer, 2001). Meanwhile via fluorescence resonance energy transfer (FRET), researchers determined A30P and A53T mutations did not alter N- and C- terminal interactions with membranes, but observed a closer vicinity between N- and C- terminal segments with the A30P mutant (McLean et al., 2000). As computational techniques improved, researchers were better able to model the specific dynamic changes of PD-associated mutants. After running replica exchange molecular dynamic simulations, it was suggested that β sheet propensity was increased in the N-terminal segment compared to the NAC domain or the C-terminal segment after A53T mutation (Coskuner & Wise-Scira, 2013), confirming Bussel & Eliezer's previous work. Conversely, the same research group showed that the A30P mutation produced the opposite results in which β sheet formation decreased in the N-terminal segment, but was enhanced in the NAC

domain and C-terminal segment (Coskuner & Wise-Scira, 2013). Although tightly located within the N-terminal segment, the A30P and A53T mutated αSyn forms can potentially widely differ in protein dynamics, although how they both lead to PD requires further investigation.

αSyn Aggregation and Pathology

Not only is αSyn genetically associated with PD, but it is pathologically interconnected with the disease as well. αSyn misfolds to form oligomers which then accumulate to form larger aggregates like fibrils which make up the Lewy Bodies (LBs) found in surviving neurons in the brain. The prion-like hypothesis is that αSyn aggregates act as a seed to induce monomer αSyn to convert into an aggregated form and that this process in one cell can "infect" other cells via neuron transfer or glial cell transfer (Brundin & Melki, 2017). The prion-like theory still leaves several questions, such as how and where does the first aberrant αSyn aggregation start in the body. LBs can be found extensively in the peripheral nervous systems in PD patients, especially in the gut, which suggests a connection to the gut-brain axis. Braak's hypothesis states the initial onset of Lewy pathology begins in the digestive system and olfactory system, and spreads peripherally to centrally from either of these two places (Rietdijk et al., 2017). However, not all patients follow the stereotypical Braak staging system.

αSyn aggregation does not only occur in PD patients. Glial cytoplasmic inclusions are also found in in Multiple System Atrophy (MSA) and αSyn inclusions can sometimes be found in brain autopsies from elderly non-symptomatic patients. This begs the question whether there is a threshold of Lewy pathology patients must meet before experiencing symptoms. Additionally, LBs are commonly found in patients

diagnosed with Alzheimer's Disease (AD) (Kotzbauer et al., 2001). Interestingly, the NAC domain of αSyn is the second most common protein identified in Amyloid Beta Plaque in AD, which is why one of its original names was the non-amyloid-beta component precursor (NACP). The NAC domain can either be membrane bound or exposed to the cytosol where it can recruit monomer αSyn and induce accumulation (Hijaz & Volpicelli-Daley, 2020; Lv et al., 2019). The A30P and G51Q mutations have been shown to increase cytosol exposure of the NAC domain which could suggest a pathophysiological mechanism for those genetic cases (Ysselstein et al., 2015). Other members of the synuclein gene family exist, such as β-synuclein, which lacks the NAC domain and has been implicated in neuroprotection. Due to its crucial role in aggregation, the NAC domain has been highly studied to understand the biology behind αSyn aggregate assembly.

Throughout the past decade researchers have questioned whether αSyn aggregation itself causes cell death and ultimately neurodegeneration. As αSyn pathology is prevalent in brain areas with neurodegeneration (Fearnley & Lees, 1991), some groups have maintained that LBs directly cause neuronal cell death (Greffard et al., 2010; Lu et al., 2005). Opposingly, others have argued that LBs are a byproduct of a cell surviving the neurodegenerative mechanism (Bodner et al., 2006; Gertz et al., 1994). However, when the Unni Lab longitudinally followed LB formation, maturation, and cell death via chronic *in vivo* multiphoton imaging in a Syn-GFP mouse model induced to form LB by PFF injection, this data strongly supported a model where LBs were tightly associated with that cell's death (Osterberg et al., 2015). Still, whether Lewy

pathology promotes or prevents neurodegeneration is still an active area of study within the field.

Functional Studies

As αSyn is highly implicated in PD genetics and pathogenesis, many research groups turned to functional studies to test whether an αSyn gain-of-function model or loss-of-function model could be used to explain PD pathogenesis. Several groups have shown evidence for a gain-of-function model by demonstrating that αSyn aggregates can have toxic properties and can lead to many problems in the cell. Among the list of potential problems caused by αSyn aggregates are mitochondrial malfunction (Parihar et al., 2009), synaptic dysfunction (Schulz-Schaeffer, 2010), ubiquitin proteosome system impairment (Kumar et al., 2018; McNaught et al., 2003), and problems with autophagy (Cuervo et al., 2004; Winslow et al., 2010; Xilouri et al., 2016). However, none of these ideas have led to a treatment targeting a mechanism that slows or halts the progression of motor symptoms in patients. This could suggest a gain-of-function model is not a perfect fit for the complex nature of PD progression.

Loss-of-function models for αSyn are less studied in the PD field. The main reason for this is that αSyn KO mice show no severe phenotype. Although this suggests that loss-of-function may be less important, other groups have detected that synaptic transmission is interrupted and neuronal function is altered in αSyn KO mice (Greten-Harrison et al., 2010; Steidl et al., 2003). Additionally, potential compensation by β-synuclein and γ- synuclein has been detected in the constitutive αSyn KO mouse. Curiously, triple αSyn, β-synuclein, and γ- synuclein KO mice have no severe phenotype, but die prematurely at approximately 8 months for an unexplained reason. It

is also vague whether the αSyn KO must be present before or after birth, and whether one or both copies of the gene are necessary (Anwar et al., 2011; Garcia-Reitboeck et al., 2013; Greten-Harrison et al., 2010). Although understudied, loss-of-function experiments may be crucial to understanding αSyn's role in PD.

A loss-of-function model for soluble αSyn garnered more attention when the Unni Lab captured the maturation of LB-like αSyn inclusions in WT Syn-GFP mouse cortex with longitudinal *in vivo* imaging. After cortical PFF injection, inclusions developed into an immature stage in which both soluble and aggregated αSyn is present in the soma of cells. This soluble αSyn disappears from the nucleus of the cell when the somatic inclusion fully matures and takes on a fibrillar tendril shape wrapping its processes around the nucleus of the cell. The Unni Lab reported that neurons with mature inclusions die at a significantly faster rate compared to cells without inclusions (Osterberg et al., 2015). This finding was confirmed with an analogous protocol with a different mouse line expressing A53T Syn-GFP and an accelerated pathology seeding phenotype (Schaser et al., 2019). These novel findings suggest the disappearance or loss of soluble αSyn in the maturation of the inclusion may contribute to the cell's demise. We will next discuss what the nuclear role of αSyn may be and whether when this role is lost that could lead to cell vulnerability and death.

Role of αSyn *in the Nucleus*

One potential role αSyn may perform in the nucleus is facilitation of DNA double-strand break (DSB) repair. Autopsies of brains from children who have suffered from Ataxia Telangiectasia (AT), a rare DSB repair deficiency, reveal LB-like inclusions that resemble LB found in PD (Agamanolis & Greenstein, 1979). Additionally, the Ataxia

Telangiectasia Mutated (ATM) KO mouse line displays increased αSyn aggregation and a progressive loss of dopaminergic neurons in the substantia nigra (Eilam et al., 2003). These two phenotypes with stark similarity to PD suggest there may be a link between αSyn and DSB repair. The Unni Lab conducted several pivotal experiments supporting this connection.

In 2019, the Unni Lab observed baseline colocalization of nuclear αSyn foci with γH2AX, a classical marker for DSBs, and the DNA damage response marker poly ADP-ribose (PAR). After widespread DNA DSB damage induced by bleomycin, αSyn KO human haploid (HAP1) cells developed increased γH2AX, as assayed by IHC and western blot, compared to WT cells. One caveat is that γH2AX is not a perfect correlate of DSB levels and can be associated with other DNA damage repair processes. γH2AX is a histone modification that occurs early in the signaling pathway to notify the cell of the DSB and help coordinate its repair. Since γH2AX is not an exact readout of DSB levels, the Unni Lab conducted neutral comet assays and found that αSyn KO cells treated with bleomycin had increased percent of DNA in comet tail and therefore more DSBs than WT cells treated with bleomycin. In support of this hypothesis, αSyn is rapidly recruited to the specific local site of laser-induced-DNA damage in mouse cortex *in vivo*. Lastly, IHC reveals that γH2AX levels increase in neurons bearing αSyn inclusions compared to cells without, suggesting heightened DSB levels are correlated with a Lewy pathology mouse model (Schaser et al., 2019).

More recent work from the Unni Lab demonstrates that αSyn is not just found in the nucleus in general, but is specifically enriched in a sub-compartment, the nucleolus, where it regulates DSB repair of ribosomal DNA in a melanoma model (Arnold et al.,

2024). This work outlines a mechanism by which αSyn facilitates the recruitment of the important DSB repair protein 53BP1 to DSB sites in the nucleolus, and the absence of αSyn leads to increased γH2AX levels and decreased 53BP1 recruitment, with potential functional consequences like micronuclei formation (Arnold et al., 2024). These nuclear and nucleolar findings further suggest a potential loss-of-function mechanism in which loss of αSyn within the nucleus/nucleolus could lead to genomic instability.

These findings implicating αSyn in DNA DSB repair are the first characterization of this possible nuclear function for αSyn. Although these mechanisms appear to be operative, it is unclear exactly the mechanism of how αSyn could be involved in DSB repair in the nucleus of neurons. Previous co-immunoprecipitation experiments did not show a direct binding interaction between αSyn and γH2AX, though it is possible that αSyn could be interacting with γH2AX indirectly or modulating another DSB repair factors downstream in the pathway. To fully introduce this topic, an in depth understanding of DSB repair is required.

1.3 DNA Double-strand Break Repair

Each cell in the human body is exposed to tens of thousands of DNA lesions and breaks every day. Cells have developed complex, redundant, and highly conserved mechanisms to repair this damage. Each mechanism is extremely specific to the type of DNA damage, which can include a base pair mismatch, base oxidation, deamination and alkylation, a single-strand break, intra-strand crosslink, inter-strand crosslink, and double-strand break (DSB). DSBs are the most severe and toxic form of DNA damage in the cell, and approximately 10-50 DSBs occur in each cell every cell cycle (Tripathy

et al., 2021). DSBs are especially of interest as neuronal DSBs are associated with neurodegeneration and AD (Dileep et al., 2023) and αSyn has been implicated in DSB repair (Schaser et al., 2019). There are several pathways that cells utilize to combat this constant assault of DSB lesions including homologous recombination (HR), classical non-homologous end-joining (c-NHEJ), alternative non-homologous end-joining (alt-NHEJ), single-strand annealing (SSA), which we will discuss in detail here.

Homologous Recombination

HR is one of the main cellular pathways to repair a DSB, and the only pathway that allows for direct copying of genetic information from the sister chromatid in order to ensure perfect or faithful repair. It does this by accessing genetic information lost at the break site from DNA strands within the sister chromatid generated during DNA replication. HR, therefore, is constrained to late S and G2 phases of the cell cycle in which template DNA is accessible from the duplicated sister chromatid. DSBs can be induced by environmental factors like ionizing radiation, but also from replication errors in S phase, which HR is effective at repairing. Because of this cell cycle limitation, HR is only functional in dividing cells, and not relevant in post-mitotic cells including neurons.

The pathway of HR begins, after recognition of the break site, with a large 5' to 3' resection on one strand of DNA normally of greater than 50 base pairs creating a single stranded overhang. The MRN complex consisting of MRE11, Rad50, and Nbs1 along with CtIP and BRCA1 initiate short resection. Additional long-range resection is performed by EXO1 with assistance from the BLM helicase. The RPA filament coats these overhangs until the Rad51 protein is recruited by BRCA2. This filament then invades the template DNA on the sister chromatid, forming a D-loop. The D-loop is

resolved by either synthesis dependent strand annealing or double Holliday junction. These non-crossover or crossover events of the sister chromatid ensure the DNA is repaired faithfully. End processing is performed either by Pol δ or Pol ε and Ligase I to repair the DSB. Figure 1.3.1 visually depicts this process. HR can collaborate and compete with other pathways to repair DSB, but large DNA end resection is the defining feature that is exclusive to HR and NHEJ lacks (Jasin & Rothstein, 2013; X. Li & Heyer, 2008; Wright et al., 2018).

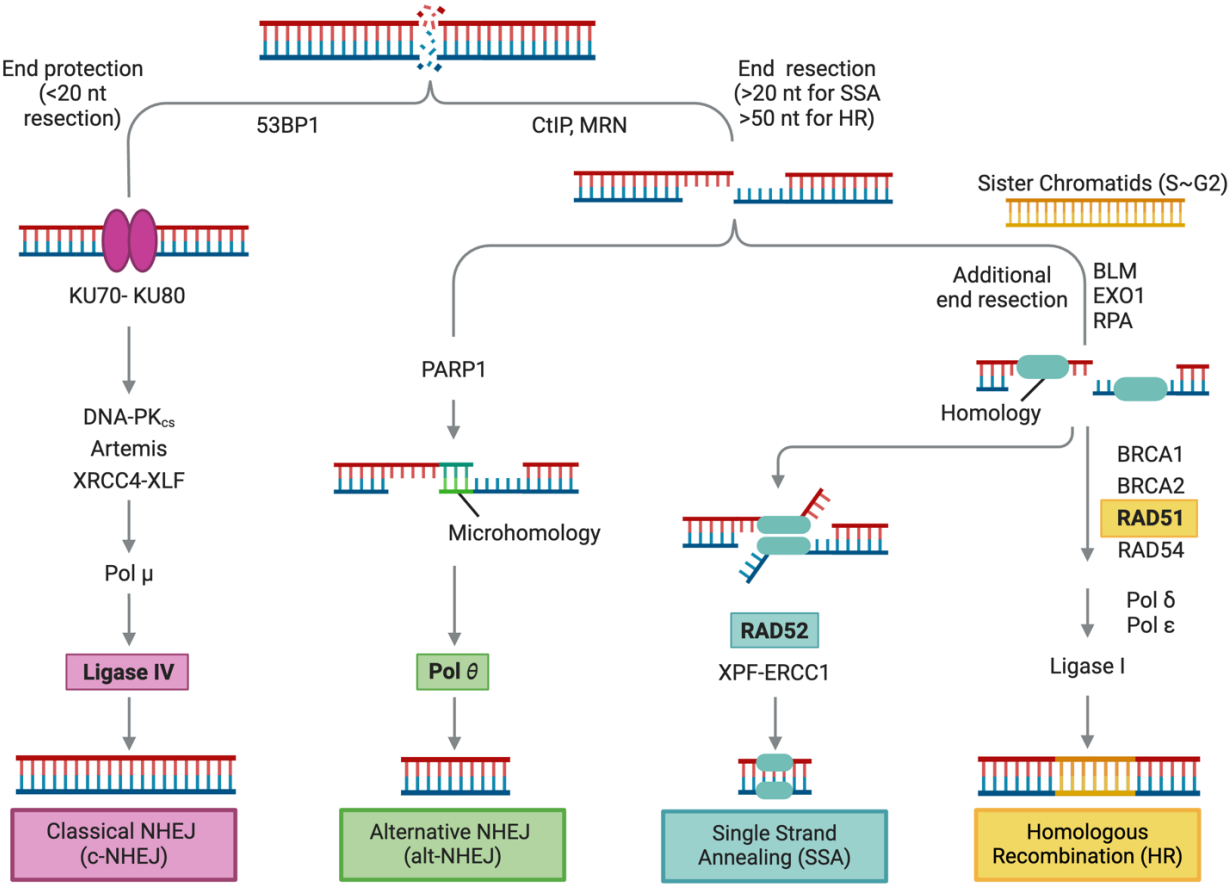

Figure 1.3.1. DSB Repair Pathways. Cartoon depicting c-NHEJ, alt-NHEJ, SSA, and HR, adapted from Chang et. al 2017. C-NHEJ associated with few and small indels due to smaller end resection (less than 20 nt) is shown with a repaired end product without deletions. Error-prone alt-NHEJ is dependent on Pol θ (highlighted in green) and results in deletions (shown by a shorter end product size). SSA produces repaired end

products with larger deletions due to an additional end resection step (shortest end product size). HR always faithfully repairs DNA by using sister chromatids but is limited to phases of the cell cycle.

Classical NHEJ

Traditionally in the DNA repair field, DSB repair is categorized into HR and NHEJ, however emerging evidence strongly suggests that there are multiple alternative pathways of NHEJ. Classical NHEJ (c-NHEJ) is the best studied of these pathways with hallmarks of limited end resection and Ku70/80 dependency, whereas alt-NHEJ is a recently discovered mechanism that relies on microhomology and Pol θ for end joining. C-NHEJ and alt-NHEJ can operate throughout the cell cycle and can repair breaks that occur at all times during the cell cycle regardless of the cause, but some studies have suggested that they predominantly function in G1 (Zhao et al., 2017). One notable difference between HR and NHEJ is the speed of repair, NHEJ has an average time of 30 minutes to repair, compared to HR that can take up to 7 hours to complete (Mao et al., 2008). NHEJ is thought to be the only DSB pathway relevant in post-mitotic cells, including neurons.

The mechanism of c-NHEJ initiates by Ku70/80 recognizing the DSB with rapid kinetics, within minutes of damage formation (Kim et al., 2005). Ku recruits DNA-PK_{cs} which then interacts with Artemis to form a complex where autophosphorylation can occur to activate the nuclease activity of Artemis (Neal & Meek, 2011). DNA-PK_{cs} is a member of the phosphatidylinositol 3-kinase-related kinase (PIKK) family and some groups argue that DNA-PK_{cs} plays a role in how the cell chooses between HR, c-NHEJ, or alt-NHEJ using its kinetics, enzymatic competition, and/or autophosphorylation

checkpoints (Neal & Meek, 2011). After end processing, Polymerase λ and Polymerase μ, members of the Pol X family, promote ligation by XLF, XRCC4, and Ligase IV to repair the DSB (Chang et al., 2017). Both polymerases can function in template-dependent and template-independent synthesis (Nick McElhinny et al., 2005), which can lead to base pair mutations. Traditionally, NHEJ is referred to as an "error-prone" pathway in comparison to HR. While it is true that NHEJ does not have the fail-safe of template DNA to produce consistently faithful repair, recent evidence suggests that c-NHEJ can be fairly accurate, especially when rejoining simple breaks where the DNA ends have not be extensively modified as part of the damage-inducing process, while alt-NHEJ because of its mechanism is much more error-prone (Bétermier et al., 2014).

Alternative NHEJ

alt-NHEJ is the newest member of DSB pathways to be categorized by the DNA repair field. Referred to by many names, including microhomology-mediated end joining (MMEJ) and Pol θ-mediated end joining, alt-NHEJ was first observed in cells lacking core c-NHEJ machinery components, when somewhat surprisingly, it was found that they were still able to perform end-joining (Kabotyanski et al., 1998). Studies show that alt-NHEJ incorporates much larger deletions into the repaired product than c-NHEJ and that alt-NHEJ is generally dependent on microhomology regions found near to the break site on each end to ligate the two ends together (Neal & Meek, 2011). Researchers believe that alt-NHEJ operates with slower kinetics than c-NHEJ due to the requirement of further resection to search for microhomology regions (Chang et al., 2017). Most of the work investigating alt-NHEJ has been performed under conditions where c-NHEJ is

removed, thus additional work is required to fully elucidate whether alt-NHEJ also has a purpose when c-NHEJ is intact.

Recent work suggests little resemblance between the two pathways in terms of mechanistic components. For example, new evidence shows alt-NHEJ uses poly ADP-ribose polymerase 1 (PARP1), CtIP, and the MRN complex at early steps (Sfeir & Symington, 2015), which is more similar to HR than c-NHEJ. Pol θ then synthesizes new DNA, which can incorporate larger deletions (greater than 10 nucleotides), than the Pol λ and Pol μ used in c-NHEJ (Wyatt et al., 2016). Pol θ does likely inhibit additional resection and larger deletions that could occur via SSA, after which Ligase I and Ligase III are able to join DNA ends together (Chang et al., 2017). Although significantly different than c-NHEJ, it remains unknown whether alt-NHEJ is simply a redundant backup mechanism for when c-NHEJ fails, or if it has its own physiological role/s in DSB repair under certain specific conditions.

In some ways, alt-NHEJ has more in common with SSA than c-NHEJ since both alt-NHEJ and SSA require end resection to uncover microhomology regions, but SSA necessitates more homology, requiring longer resection lengths (like HR), and therefore employs MRN and CtIP to create 3' single-strand DNA ends and the EXO1 nuclease and the BLM helicase to resect, similar to HR. RPA coats and protects exposed single-stranded DNA and RAD52 anneals complimentary single-stranded DNA. Next, the nucleotide excision repair complex XPF-ERCC1 cleaves the non-homologous single-strand DNA tails and ligation occurs. SSA is prone to the largest deletions due to the large resection needed and is not as highly conserved as other DSB repair pathways. Understanding HR, c-NHEJ, alt-NHEJ, and SSA and their individual properties will be

important for understanding our experimental approaches and results manipulating αSyn in Chapter 2.

1.4 Serine 129 Phosphorylation

The most common post-translational modification αSyn will undergo is a serine phosphorylation at residue 129 in the C-terminal segment. S129 phosphorylated αSyn (pSyn) has been a major subject of study in the field due to its correlation with disease progression. pSyn has also been of interest to the Unni Lab because it alters how αSyn interacts with DNA. The Unni Lab confirmed that αSyn can bind to the major groove of DNA, but pSyn has a lower propensity to bind linear DNA and is unable to bind circular DNA forms (Dent et al., 2022). This could suggest that the S129 phosphorylation site is important for how αSyn interacts with DNA and modulates DSB repair.

pSyn and Aggregation

Although other post-translational modification sites within αSyn, such as acetylation, ubiquitination, truncation, phosphorylation Y39, S87, Y125 and nitration Y39, Y125, Y133, and Y136 (Figure 1.2.1) have been described, none have been as closely studied as S129 phosphorylation. This is because pSyn is tightly correlated with pathology spread in PD, as over 90% of the αSyn found in LBs is phosphorylated compared to only 4% of αSyn in the healthy brain (Anderson et al., 2006). While total αSyn levels decrease in human CSF in PD patients, pSyn CSF levels are associated with disease severity (Stewart et al., 2015; Y. Wang et al., 2012). PD patient CSF analysis of pSyn has also been proposed to help distinguish between MSA and other

synucleinopathies (Foulds et al., 2012). In the periphery, pSyn levels in plasma can help detect PD (El-Agnaf et al., 2003; Foulds et al., 2012), and pSyn aggregation was detected in small and large nerves in skin (Donadio et al., 2014; Doppler et al., 2014), leading to the suggestion that pSyn could serve as a potential biomarker for PD.

Not only is upregulation of pSyn interconnected with human cases of PD, but increased accumulation of pSyn is also observed in several animal models described in Chapter 1.1. A genetic PD mouse model, a viral αSyn gene transfer rat model, a PFF model in mice, and two separate drosophila models all reported increased pSyn levels and aggregation (Chen & Feany, 2005; Neumann et al., 2002; Takahashi et al., 2003; Xu et al., 2021; Yamada et al., 2004). Yet the question remains if and how phosphorylation at S129 drives this pathology progression or if this modification occurs after LB formation. S129 phosphorylation has also been shown to alter αSyn properties and physiological function, which could also contribute to abnormal proteostasis and pathology progression. Phosphorylation at S129 can increase membrane binding (Nübling et al., 2014; Pronin et al., 2000) and can switch protein interaction affinity of non-phosphorylated αSyn from mitochondrial electron transport proteins to binding cytoskeletal and vesicle-trafficking presynaptic proteins once phosphorylated (M. A. McFarland et al., 2008). Most relevant to the nuclear αSyn field, S129 phosphorylation partly regulates translocation of αSyn from the cytoplasm to the nucleus (Gonçalves & Outeiro, 2013a). While these physiological changes represent promising starting points, more investigation is needed to clearly define what role S129 phosphorylation plays in disease.

In Vitro *and* In Vivo *Studies*

While the correlation between pSyn and aggregation has been shown many times in the patient population, investigation of this topic *in vitro* and in *in vivo* animal studies has been conflicting. It has long been contested whether pSyn promotes or protects against aggregation (Oueslati, 2016; Tenreiro et al., 2014). *In vitro* studies have shown S129 phosphorylation has no effect or reduces αSyn fibrilogenesis, utilizing pharmacological and S129D/E phosphomimic approaches (Paleologou et al., 2008; Waxman & Giasson, 2011). In contrast, other *in vitro* studies show that S129 phosphorylation can promote fibrillar aggregation (Fujiwara et al., 2002; Ma et al., 2016; Samuel et al., 2016). Because of this controversy, many groups turned to *in vivo* studies to try to shed light on this issue.

While *in vivo* studies can potentially offer more biologically relevant results, disagreements over the role of pSyn in promoting aggregation have still arisen from this work. One body of work, employing a phospho-deficiency approach where S129 is mutated to alanine, observed an increase in αSyn accumulation in flies (Chen & Feany, 2005). Another study in a rat genetic PD model displays increased αSyn aggregation and cell loss, supporting the initial result (Sato et al., 2011). However, the same S129A in other rat studies showed no effect on or reduced αSyn aggregation compared to the phospho-mimic S129D mutation *in vivo* (Azeredo da Silveira et al., 2009; Gorbatyuk et al., 2008; N. R. McFarland et al., 2009). It is therefore difficult to conclude if *in vivo* studies can better untangle this controversy, as animal models, IHC protocols, and approaches to measure phosphorylation are different across laboratories. Therefore, exploring these questions without using the phospho-deficiency and phospho-mimic

approach may yield useful information. Measuring pSyn levels with specific antibodies and manipulating the endogenous kinases that phosphorylate αSyn could help us to unravel this complex matter, although this strategy has proven difficult.

Over 50 αSyn and pSyn antibodies are currently commercially available (Vaikath et al., 2019), but many have problems with specificity that can lead to misleading conclusions. Research into the role of nuclear αSyn has been somewhat contentious over the years because of disagreement about whether αSyn exists in the nucleus or not, likely in part because of these antibody specificity issues (Z. Huang et al., 2011). Some αSyn and pSyn antibodies can display non-specific cross-reactivity with another nuclear epitope which has made the interpretation of some work difficult. This makes it critical to validate any nuclear αSyn and pSyn antibody signal in a KO αSyn condition (Arnold et al., 2024; Schaser et al., 2019), and in the past decade a consensus has emerged using multiple different approaches that synuclein is present in the nucleus (Lashuel et al., 2022; Surguchov, 2015). For these reasons, in our work we have only included nuclear antibody data that has been validated in this way.

Kinases

Another factor that is important to consider is that there are several kinases that phosphorylate αSyn at S129. G-protein-coupled receptor kinases (GRKs), Casein Kinase II (CK2), and the Polo-like Kinase (PLK) family can all phosphorylate αSyn to varying degrees. LRRK2 has also been implicated as a synuclein kinase, although this is more controversial. GRK2 preferentially phosphorylates αSyn (Kawahata et al., 2022), while GRK5 is involved in trafficking αSyn to the nucleus (Gonçalves & Outeiro, 2013b). CK2 is an essential suppressor of apoptotic cell death and received attention

when CK2β was discovered in the outer rings of LBs in PD patients (Ahmad et al., 2008; Ryu et al., 2008). Additionally CK2α regulates phosphorylation of αSyn at Y136 in brains from DLB patients (Sano et al., 2021). LRRK2 and αSyn co-localize in substantia nigra neurons and LBs in PD brains and knockdown of LRRK2 increases αSyn inclusions *in vitro* (Guerreiro et al., 2013). Though some evidence exists for all of these kinases, the most evidence exists for the PLK family as an important S129 kinase.

Several groups have suggested that the PLK family is the main kinase responsible for αSyn S129 phosphorylation (Bergeron et al., 2014; Inglis et al., 2009; Mbefo et al., 2010). There are 5 PLK family members and PLK2 and PLK 3 can phosphorylate αSyn to a higher degree than PLK1 and PLK4. PLK5 lacks a functional kinase domain. Furthermore, PLK2 and PLK3 can promote αSyn shuttling from the nucleus to the cytoplasm (Gonçalves & Outeiro, 2013b), and PLK2 can regulate the clearance of αSyn via autophagy. The Unni Lab tested if PLK2 is the kinase responsible for phosphorylating αSyn within Lewy pathology. Interestingly, we found neurons with αSyn inclusions from PLK2 KO mice survived at a higher rate than those from WT mice, there was no difference in S129 phosphorylation of Lewy pathology after genetic deletion of PLK2 (Weston et al., 2021). Therefore, the question remains as to which kinase is responsible for phosphorylating αSyn within a LB. Understanding the answer to this question could be key to revealing the connection between pSyn and pathological progression. The PLK family and this connection is examined in experiments detailed in the results and discussion sections of Chapter 2.

In conclusion, uncovering which kinase is the lewy pathology kinase in vivo is one of the major gaps in the literature of PD pathological progression. My dissertation

aims to test my hypothesis that the PLK family is the lewy pathology kinase in vivo. The second question of this dissertion is how specifically does αSyn influence DSB repair. Several pieces link αSyn to DSB repair, but how it contributes mechanistically is unknown. I hypothesized that αSyn is involved in NHEJ because it is thought to be the only DSB repair mechanism relevant in post-mitotic cells. Both of these overreaching questions are investigated experimentally in Chapter 2.

Chapter 2

Alpha-synuclein modulates the repair of genomic DNA double-strand breaks in a DNA-PK$_{cs}$ regulated manner

Elizabeth P. Rose[1, 2], Valerie R. Osterberg[1], Jovin S. Banga[1], Vera Gorbunova[3], Vivek K. Unni[1, 4]

[1] Jungers Center for Neurosciences Research, Oregon Health & Science University, Portland, OR 97239
[2] Neuroscience Graduate Program, Vollum Institute, Oregon Health & Science University, Portland, OR 97239
[3] Departments of Biology and Medicine, University of Rochester, Rochester, NY, 14620
[4] OHSU Parkinson Center, Department of Neurology, Oregon Health & Science University, Portland, OR 97239

Published on BioRxiv March 4th, 2024

In Review at *Neurobiology of Disease*

Abstract: 247 words

Introduction: 1161

Discussion: 1495

Figures: 6

Supplemental Figures: 4

Abstract

α-synuclein (αSyn) is a presynaptic and nuclear protein that aggregates in important neurodegenerative diseases such as Parkinson's Disease (PD), Parkinson's Disease Dementia (PDD) and Lewy Body Dementia (LBD). Our past work suggests that nuclear αSyn may regulate forms of DNA double-strand break (DSB) repair in HAP1 cells after DNA damage induction with the chemotherapeutic agent bleomycin (Schaser et al., 2019). Here, we report that genetic deletion of αSyn specifically impairs the non-homologous end-joining (NHEJ) pathway of DSB repair using an extrachromosomal plasmid-based repair assay in HAP1 cells. Notably, induction of a single DSB at a precise genomic location using a CRISPR/Cas9 lentiviral approach also showed the importance of αSyn in regulating NHEJ in HAP1 cells and primary mouse cortical neuron cultures. This modulation of DSB repair is regulated by the activity of the DNA damage response signaling kinase DNA-PK_{cs}, since the effect of αSyn loss-of-function is reversed by DNA-PK_{cs} inhibition. Using *in vivo* multiphoton imaging in mouse cortex after induction of αSyn pathology, we find an increase in longitudinal cell survival of inclusion-bearing neurons after Polo-like kinase (PLK) inhibition, which is associated with an increase in the amount of aggregated αSyn within inclusions. Together, these findings suggest that αSyn plays an important physiologic role in regulating DSB repair in both a transformed cell line and in primary cortical neurons. Loss of this nuclear function may contribute to the neuronal genomic instability detected in PD, PDD and DLB and points to DNA-PK_{cs} and PLK as potential therapeutic targets.

Introduction

Synucleinopathies, such as Parkinson's Disease (PD), Parkinson's Disease Dementia (PDD), and Lewy Body Dementia (LBD), are characterized by the presence of aggregated α-synuclein (αSyn) pathology, known as Lewy pathology, which is found in surviving neurons in brain regions vulnerable to cell death. Although these three synucleinopathies, in addition to several other neurodegenerative diseases, are characterized by this abnormal αSyn aggregation within cell bodies and neurites, known as Lewy bodies and neurites, respectively, it is still not clear how Lewy pathology relates to neuronal cell death. Evidence exists for both gain-of-function and loss-of-function mechanisms for how αSyn aggregation may play a role. Possible gain-of-function mechanisms include toxic αSyn aggregates taking on distinctly new properties and disrupting presynaptic (Greten-Harrison et al., 2010; Steidl et al., 2003) & mitochondrial function (Parihar et al., 2009), affecting protein degradation by the ubiquitin-proteasome system (Kumar et al., 2018; McNaught et al., 2003) or autophagy (Cuervo et al., 2004; Winslow et al., 2010; Xilouri et al., 2016).

αSyn is normally localized to the presynaptic terminal and nucleus of neurons, which is how it was originally named (Maroteaux et al., 1988). It is a 140 amino acid long protein that binds to the outer leaflet of synaptic vesicles and contributes to their trafficking (Burré et al., 2018). Extensive work has characterized its normal physiological function in modulating vesicle sorting and clustering at presynaptic terminals (L. Wang et al., 2014) during exo- and endocytosis (Greten-Harrison et al., 2010). Presynaptic loss-of-function hypotheses for the role of αSyn in synucleinopathies suggest dysregulation of these neurotransmitter vesicle processing steps in neurons with Lewy

inclusions. Conflicting evidence exists for whether αSyn knockdown is protective (Zharikov et al., 2015) or harmful (Benskey et al., 2018) in PD models. αSyn is also found in the nucleus of cells (Goers et al., 2003; Kontopoulos et al., 2006; Pinho et al., 2019), where its role is less clear. Selective localization of αSyn to the nucleus using a nuclear localization sequence has been associated with motor deficits independent of its aggregation in mice (Geertsma et al., 2022). Other evidence points to the importance of αSyn in regulating transcription, modifying histone biology, and directly binding DNA (Iwata et al., 2001; Lee Clough & Stefanis, 2007; Somayaji et al., 2021). It has also been recently suggested to influence mRNA stability in P-bodies (Hallacli et al., 2022). Our previous work highlights a normal physiologic role in regulating forms of DNA repair, including double-strand break (DSB) repair (Schaser et al., 2019), and was motivated, in part, by human pathological studies in patients with Ataxia-Telangiectasia (AT) showing that they can develop Lewy pathology (Agamanolis & Greenstein, 1979). AT is a result of defects in DSB repair caused by mutations in the Ataxia-Telangiectasia Mutated (ATM) gene, known to be a critical kinase involved in DNA damage response signaling after DSBs have been detected within a cell, where it then helps to coordinate repair. An important aspect of this signaling is the phosphorylation of the histone H2AX, creating a mark known as γH2AX that helps recruit downstream DSB repair components to the site of the break. Interestingly, work in a mouse ATM knock-out (KO) model also suggests that this DSB repair dysfunction can cause progressive dopamine neuron loss in the substantia nigra and αSyn aggregation similar to what is seen in people with PD (Eilam et al., 2003).

Our previous work demonstrated that the induction of DNA damage with the chemotherapeutic agent bleomycin in the leukemia-derived immortalized HAP1 cell line clearly increased DSB and γH2AX levels, and that this increase was even greater in the αSyn KO condition. Bleomycin is used extensively to chemically induce DSBs in multiple systems and this has been shown to be associated with increased γH2AX levels, however, a caveat of this approach is that bleomycin is also known to increase other forms of DNA damage besides DSBs (Caporossi et al., 2003; C.-H. Huang et al., 1981). Importantly, although γH2AX is widely used as a marker of DSB repair signaling, it can also be increased by other forms of DNA damage like clustered oxidative lesions or high levels of single-strand breaks (Mah et al., 2010). In order to directly test the role of αSyn in the repair of DSBs specifically, we set out here to use CRISPR/Cas9-based methods to selectively induce a single DSB at a prespecified site in the human genome in HAP1 cells to test the normal role of αSyn in the DSB repair process. In addition, we also set out to use this CRISPR/Cas9 strategy to induce a similar, prespecified DSB in the genome of primary cortical neurons from mice to test whether αSyn is important for modulating DSB repair in this cell type as well.

Our recent work studying the ability of αSyn to bind double-stranded DNA using an *in vitro* gel-shift assay suggested that it can directly bind in the major groove. Interestingly, phosphorylation of αSyn at serine-129 (S129) seemed to alter the properties of this binding and switched DNA binding to a different mode (Dent et al., 2022). S129 phosphorylation (pSyn) is the most common post-translational modification αSyn undergoes and is highly enriched in Lewy pathology (Anderson et al., 2006). It is unclear, however, whether pSyn promotes or protects against aggregation (Tenreiro et

al., 2014). While S129 phosphorylation has been shown to reduce αSyn fibrillogenesis *in vitro* (Paleologou et al., 2008), other *in vitro* studies suggest that it can also promote fibrillar aggregation depending on the exact conditions used (Fujiwara et al., 2002; Ma et al., 2016; Samuel et al., 2016). *In vivo*, studies utilizing a phospho-deficiency approach where S129 is mutated to alanine increased aggregation in drosophila (Chen & Feany, 2005), but this same S129A mutant had no effect (N. R. McFarland et al., 2009) or reduced (Gorbatyuk et al., 2008) aggregation compared to the phospho-mimic S129D mutation in rat brain. Another strategy to study the effects of S129 phosphorylation is to modulate the kinases and phosphatases that act at this residue. Several kinase families have been shown to produce pSyn *in vitro* (Ishii et al., 2007; Kawahata et al., 2022; Pronin et al., 2000; Qing et al., 2009; Wu et al., 2020), but several studies, including our own work, suggest that the Polo-Like Kinase (PLK) family members 1, 2, and 3 (Aubele et al., 2013; Basso et al., 2013; Bergeron et al., 2014; Inglis et al., 2009; Mbefo et al., 2010; Oueslati et al., 2013; Waxman & Giasson, 2011) may be the most important *in vivo* (Weston et al., 2021). Our previous work demonstrated that genetic knockout of PLK2 led to increased αSyn in nuclear DSB repair foci and to improved survival of cortical neurons bearing aggregated αSyn inclusions in mouse cortex *in vivo* (Weston et al., 2021). Given the attractiveness of kinases, specifically the PLK family and PI3KK family, important for DSB repair signaling (e.g. ATM, ATR, DNA-PK_{cs}), as drug targets, we also set out here to test their potential relevance to nuclear αSyn biology in modulating DSB repair, genomic stability and neurodegeneration.

Results

αSyn KO in HAP1 cells impairs non-homologous end-joining.

Our previous research in HAP1 cells suggested a role for αSyn in DSB repair using γH2AX levels as primary readout, however, there are two main mechanisms for repairing DSBs: non-homologous end-joining (NHEJ) and homologous recombination (HR). Perturbations in either can alter γH2AX levels. To directly test which pathway αSyn may be involved in, we used a previously established plasmid-based reporter system. This system involves two different plasmids, both of which can be linearized and transfected into cells. One is sensitive to NHEJ repair and will only produce fluorescent GFP expression when the plasmid is repaired by NHEJ and re-circularized in the process. An analogous plasmid assays HR and only produces functional GFP when HR repairs and re-circularizes this plasmid (Seluanov et al., 2010). After transfection of these linearized plasmids into HAP1 cells, we measured GFP expression and RFP expression (as a transfection control) using flow cytometry at 72 hours post-transfection (Fig. 1A). We only found a significant difference between WT and αSyn KO cells when using a plasmid reporting NHEJ repair (Fig. 1A). This suggests that the loss of αSyn impairs NHEJ repair efficiency. We did not find a significant difference between WT and αSyn KO cell lines with the HR reporter (Fig. 1A), although overall repair efficiency was lower with this plasmid, possibly making the assay less sensitive to HR repair differences.

One characteristic of NHEJ is that it is more error-prone compared to HR, since the repair that occurs is not templated using a faithful copy of the sequence from the

sister chromatid, as it is in HR. This often leads to the introduction of insertions and deletions (indels) at the repaired junction. In addition, NHEJ can be broken down to different subtypes, with classical NHEJ (c-NHEJ) being the most well studied and dependent on specific components like DNA-PK_{cs}, XRCC4/XLF and ligase 4 (Neal & Meek, 2011). c-NHEJ is thought to be the least error-prone of the NHEJ pathways, with a decreased likelihood of introducing indels during repair and smaller sized indels when they do occur. In addition to c-NHEJ, other alternative NHEJ (alt-NHEJ) pathways dependent on Pol θ, XRCC1, ligase 3, and single-strand annealing (SSA) pathways have been described. When alt-NHEJ is recruited to repair DSBs, higher levels and larger indel sizes are reported in the repaired products (Iliakis et al., 2004, 2015). With this in mind, we next wanted to investigate how the loss-of-function of αSyn affects the size and frequency of indels at the DSB repair junction. In order to do this, we transfected a ~500 bp linear double-stranded DNA into WT or αSyn KO HAP1 cells. DNA that had undergone DSB repair to produce a circular topology was purified from cells, then exposed to exonuclease treatment to remove remaining linear DNA from the sample, purified, linearized again (using a cut site opposite the repair junction) and analyzed by next-generation sequencing. This approach allowed us to detect the frequency of repair events that incorporated an indel during the repair process and to determine the exact size and position of these indels. Using this strategy, we found an increase in the frequency of sequenced junctions with deletions incorporated at the repair site in αSyn KO cells compared to WT cells (Fig. 1B). There was no apparent change in the size spectrum of deletions, however, and they were also relatively small (most <10 bp in length). This suggests that αSyn may be influencing specific sub-forms

of c-NHEJ, since alt-NHEJ and SSA are usually associated with larger deletions (>20 bp in length)(Chang et al., 2017). The repair of extrachromosomal DNA transfected into cells is likely, however, to involve different processes than occur in the context of genomic DSBs, where other important factors like DNA methylation, histone modifications, and higher order chromatin organization are important.

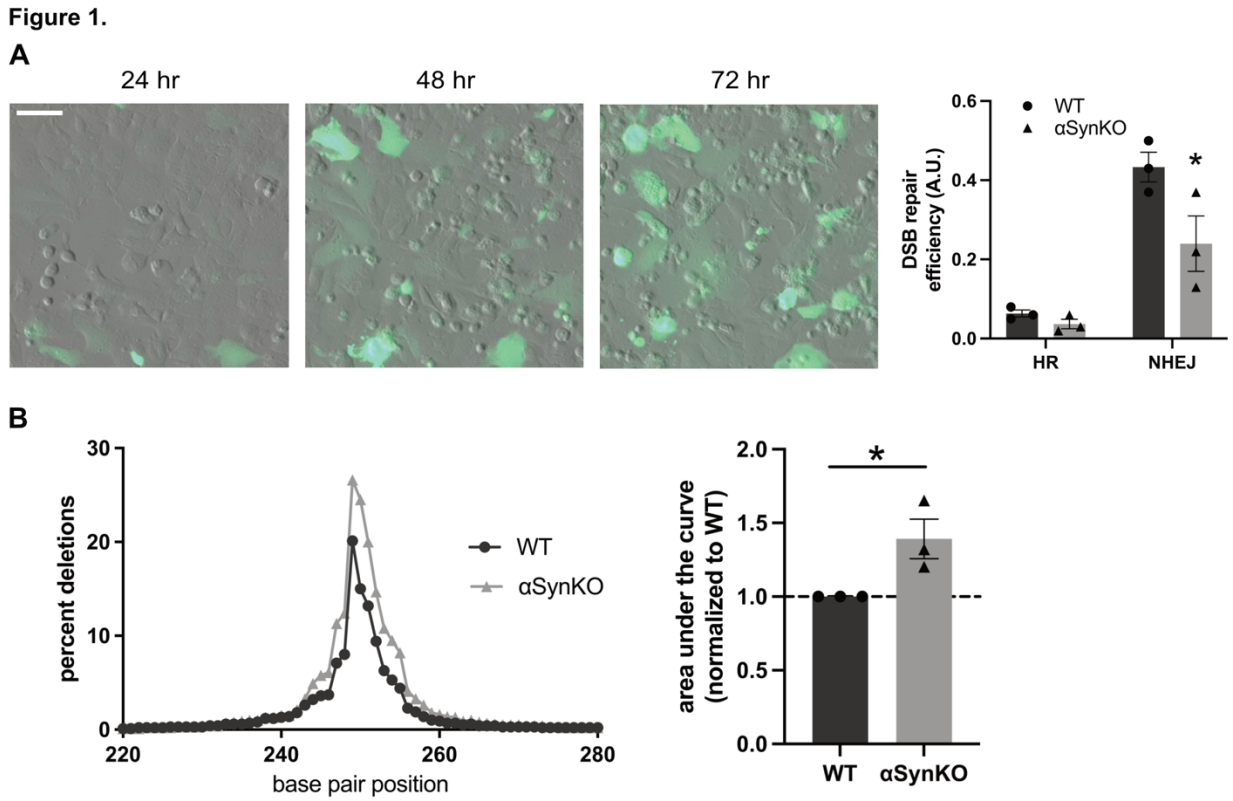

Figure 1. αSyn KO in HAP1 cells reduces NHEJ efficiency using a plasmid reporter system.

A) NHEJ reporting green fluorescing HAP1 cells after repair event at 24, 48, and 72 hours post transfection (Scale bar = 50 μm). RIGHT: Quantification from 72-hour timepoint. HR reporter in WT cells (0.063 ±0.009) vs HR reporter in KO cells (0.037 ±0.012) (p=0.2697), NHEJ reporter in WT cells (0.433 ±0.038) vs KO cells (0.240 ±0.070) (p=0.0276). N=~500,000 cells counted per replicate, 3 biological replicates. Two-tailed student's t-test. B) Next Generation Sequencing of repair junction from WT and KO HAP1 cells transfected with NHEJ reporter. Percent of deletions are increased in KO cells compared to WT cells. RIGHT: Quantification. Area under the curve of KO cells (1.392 ±0.134) significantly increased compared to WT cells (1.0 ±0.0) (p=0.0435) Two-tailed student's t-test. Data and analysis performed by Valerie Osterberg.

αSyn KO modulates repair fidelity after CRISPR/Cas9-induced DSB formation in HAP1 cells.

To assess whether αSyn is involved in NHEJ within this genomic DSB context, we turned to a CRISPR/Cas9 approach using lentiviral expression. Cells were transduced with lentivirus to introduce a single DSB in the *DNMT3B* locus. As a control for transduction efficiency, a similarly designed lentivirus expressing EGFP was used. WT and αSyn KO HAP1 cells were transduced by this lentivirus similarly when assayed using immunocytochemistry (Fig. 2A). In order to confirm this using a second approach, we also used flow cytometry to quantify transduction efficiency and no significant differences between WT and αSyn KO HAP1 cells were observed (Fig. 2B, see Methods).

To assess the effect of αSyn on the repair of single DSBs induced at the *DNMT3B* locus, we performed PCR to amplify a 288 bp product across the repair junction and analyzed these for indels using next-generation sequencing. Interestingly, similar to our data using transfected DNA (Fig. 1B), when we analyzed DSB repair junctions induced in genomic DNA we also found a significant increase in the frequency of repair junctions containing deletions in αSyn KO cells compared to WT cells (Fig. 2C), with little change in the spectrum of deletions induced and relatively small lengths (most <10 bp). This again suggests that the loss of αSyn compromises DSB repair fidelity and may be skewing DSB repair between sub-forms of c-NHEJ that are more likely to induce small deletions at the junction. This finding was confirmed by a secondary method for measuring repair fidelity using a T7 Endonuclease 1 (T7EI) assay. In this case, we amplified a longer PCR product flanking the repair junction (544

bp) and digested the products with T7EI, which recognizes and cleaves duplex DNA that contain imperfect base pairing. These cleaved fragments of DNA are measured to determine the ratio of edited to unedited PCR products in the sample. This provides a way to screen for indels that were introduced during the repair of the CRISPR-mediated DSB and these results were similar to our sequencing data. We found a significant increase in gene editing (T7EI cleavable product) using this approach in αSyn KO cells compared to WT cells (Fig. 2D). Together, these two assays for indel frequency show that αSyn loss-of-function leads to an increase in small indel frequency during the repair of DSBs induced at an individual site in the human genome.

Figure 2.

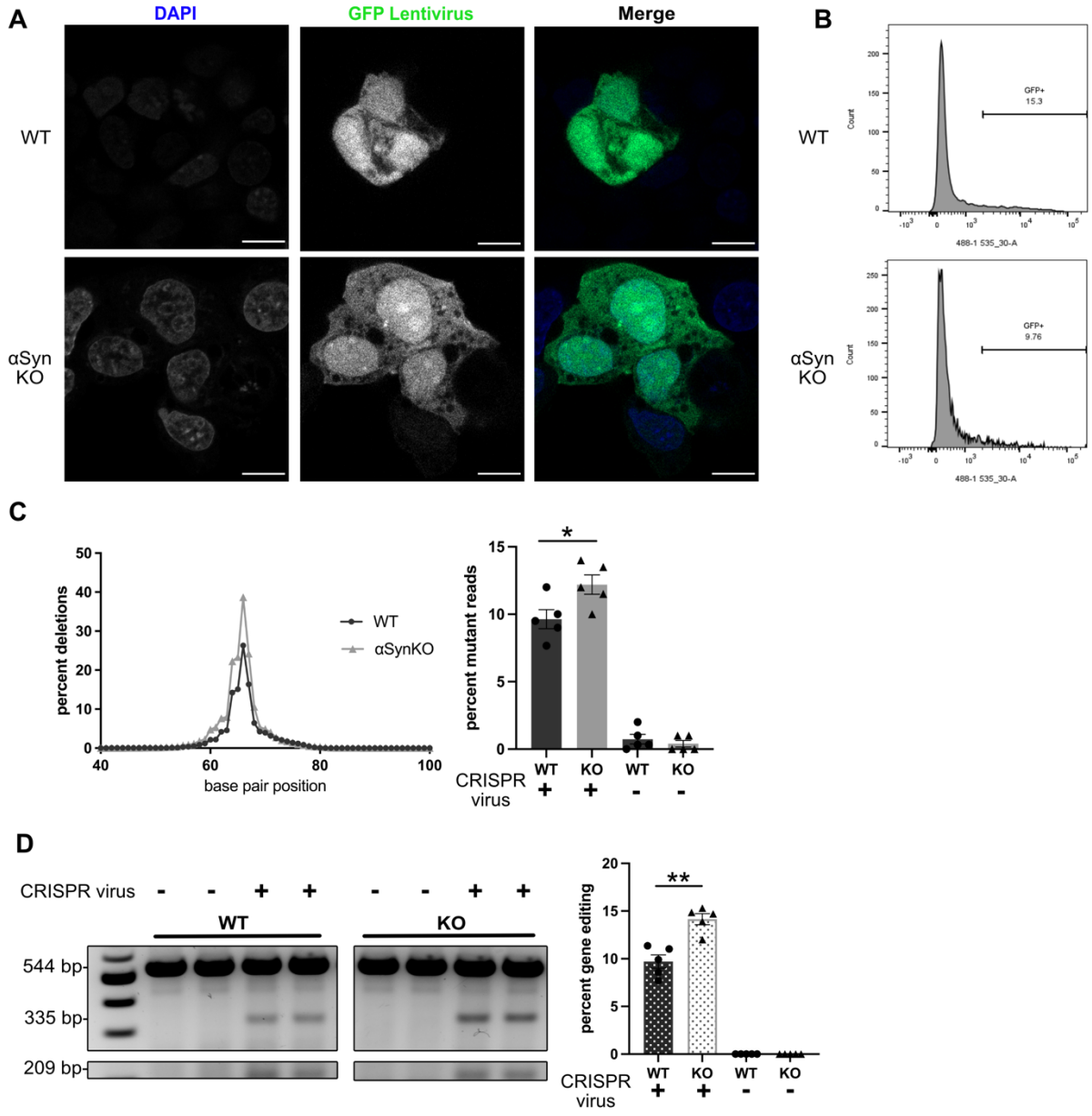

Figure 2. αSyn KO in HAP1 cells reduces genomic DSB NHEJ efficiency using a CRISPR/Cas9 system.

A) GFP tagged DSB inducing CRISPR/Cas9 lentiviral treated WT and αSyn KO HAP1 cells. Scale bar 10μm. B) Representative histograms of GFP tagged lentiviral transduction efficiency in WT and αSyn KO HAP1 cells using flow cytometry. No significant difference observed (see methods). C) NGS of 288bp repair junction with percent of reads containing deletions WT (black) and αSyn KO (gray) HAP1 cells transduced with CRISPR/Cas9 DSB inducing lentivirus. Mutant reads plotted against base pair position with cut site at base pair 67. RIGHT: Quantification. Increased mutant reads in αSyn KO cells (12.20 ±0.718) compared to WT cells (9.633 ±0.708) (p=0.0344). WT Nontargeting Virus (0.733 ±0.356), αSyn KO Nontargeting Virus (0.400

±0.245). N=5 biological replicates (2-3 technical replicates per biological replicate). Two-tailed student's t-test. D) T7 Endonuclease I enzymatic assay gel image of full-length unedited amplicon 544bp, edited fragmented products 335 bp and 209 bp. RIGHT: Quantification. % Gene Editing = 100 x (1 – (1- fraction cleaved)$^{1/2}$). Significant increase in gene editing in αSyn KO HAP1 cells (14.15 ±0.583) compared to WT cells (9.707 ±0.702) (p=0.0012). WT Nontargeting virus (0.0 ±0.0), αSyn KO Nontargeting Virus (0.0 ±0.0). N=5 biological replicates (2-3 technical replicates per biological replicate). Two-tailed student's t-test.

αSyn KO affects repair fidelity after CRISPR/Cas9-induced DSB formation in mouse primary cortical neurons.

We next wanted to investigate whether αSyn also affects DSB repair fidelity in neurons, where NHEJ is thought to be the primary mechanism for DSB repair. We cultured WT and αSyn KO E18 cortical mouse neurons *in vitro* and used an analogous *Dnmt3b* targeting CRISPR/Cas9 approach using lentiviral expression. We first measured transduction efficiency using lentivirus expressing EGFP in WT and αSyn KO neurons using immunocytochemistry and detected no significant differences (Fig. 3A, see Methods). We then measured the indel frequency after the repair of a single DSB introduced into the genome of WT and αSyn KO mouse neurons using a PCR amplification and sequencing assay similar to the one we used in HAP1 cells. We again found a significant increase in the fraction of repair junctions containing deletions in αSyn KO neurons compared to WT neurons (Fig. 3B), very similar to what we found in HAP1 cells (Fig. 2C). Interestingly, the deletions in neurons were smaller around the cut site (most <5 bp in length) than what we detected in HAP1 cells (Fig. 2C). We next tested whether loss of αSyn leads to increased indel frequency using the T7EI assay in

cortical neurons and again detected an increase in gene editing in αSyn KO neurons compared to WT (Fig. 3C).

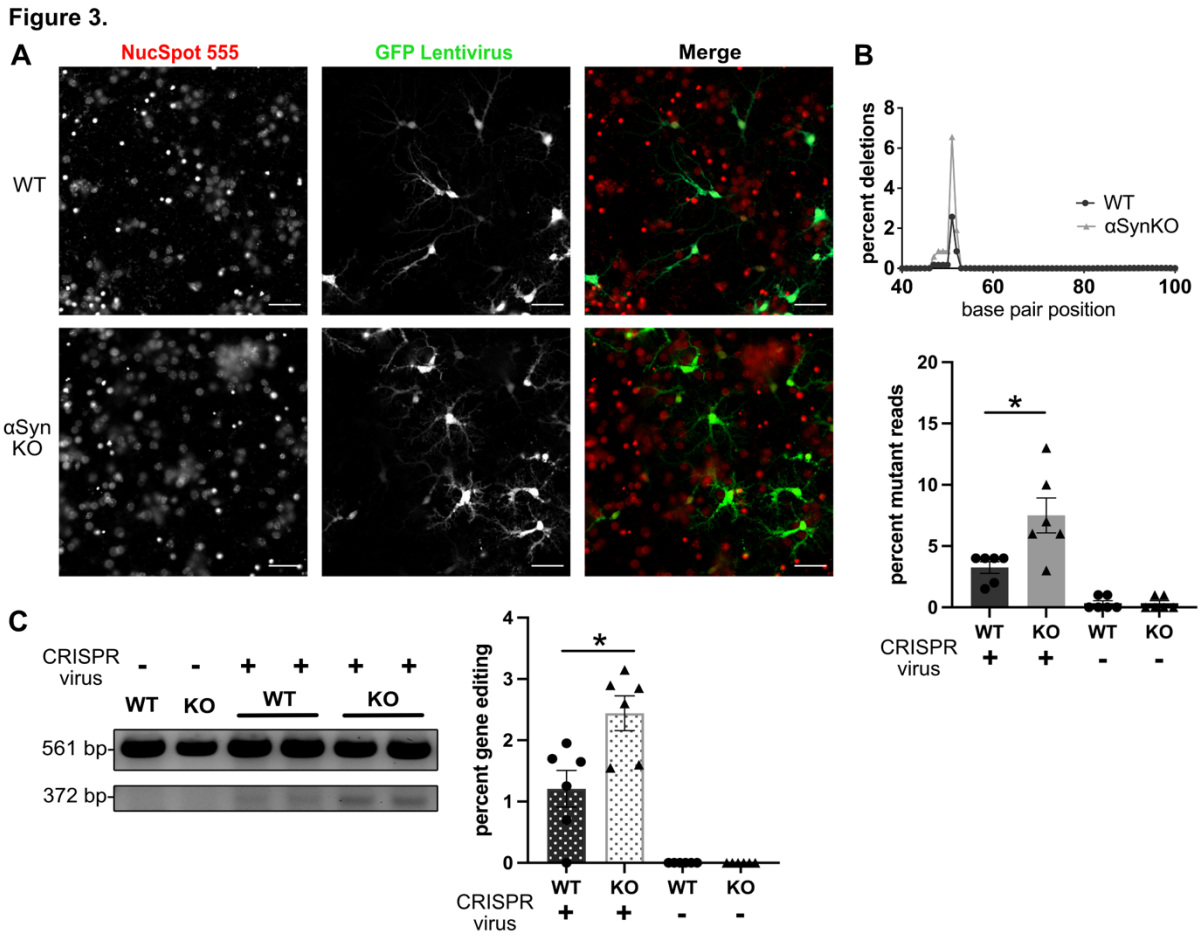

Figure 3. αSyn KO in mouse cortical neurons reduces genomic DSB NHEJ efficiency using a CRISPR/Cas9 system.

A) GFP tagged DSB inducing CRISPR/Cas9 lentiviral treated WT and αSyn KO mouse E18 cortical neurons. Scale bar 20μm. B) NGS of 272bp repair junction with percent of reads containing deletions from WT (black) and αSyn KO (gray) mouse neurons transduced with CRISPR/Cas9 DSB inducing lentivirus. Mutant reads plotted against base pair position with cut site at base pair 52. RIGHT: Quantification. Increased mutant reads in αSyn KO neurons (7.500 ±1.568) compared to WT cells (3.250 ±0.524) (p=0.0183). WT Nontargeting Virus (0.333 ±0.231), αSyn KO Nontargeting Virus (0.333 ±0.231). N=6 biological replicates (1-2 technical replicates per biological replicate). Two-tailed student's t-test. C) T7 Endonuclease I enzymatic assay gel image of full-length unedited amplicon 561bp, edited fragmented product 372bp. RIGHT: Quantification. % Gene Editing = 100 x (1 – (1- fraction cleaved)$^{1/2}$). Significant increase in gene editing in αSyn KO neurons (2.442 ±0.283) compared to WT cells (1.208 ±0.300) (p=0.0136). WT

Nontargeting virus (0.0 ±0.0), αSyn KO Nontargeting Virus (0.0 ±0.0). N=6 biological replicates (1-2 technical replicates per biological replicate). Two-tailed student's t-test.

αSyn modulates repair fidelity via DNA-PK$_{cs}$-regulated mechanism.

To test how αSyn interacts with polymerases, nucleases and kinases known to be important in various DSB repair pathways, we next set out to test how a panel of small molecule inhibitors interacted with DSB repair in αSyn WT and KO HAP1 cells using our CRISPR-mediated DSB induction approach. To test the roles of Polymerase θ and Mre11, we used pharmacological inhibitors of Polymerase θ (ART558) and Mre11 (mirin). We did not observe any consistent differences in the indel frequency after DSB repair in WT and αSyn KO HAP1 cells treated with either a Pol θ inhibitor (Pol θi) or Mre11i, compared to a vehicle control using both our sequencing and T7EI assays (Fig 4A-B).

We also investigated the role of three phosphatidylinositol 3-OH-kinase-related kinases (PI3KKs) that are known to phosphorylate H2AX to produce γH2AX, ATM, ATM-and Rad3-related (ATR), and DNA-dependent protein kinase catalytic subunit (DNA-PK$_{cs}$). We inhibited these three kinases with KU60019, VE822, and AZD7648, respectively. To determine the maximum concentration without toxic effects, we performed dose response curves for all 5 inhibitors in these cell lines and chose the maximum dose that did not cause toxicity (*data not shown*). Interestingly, we found a consistent effect in both our sequencing and T7EI assays that inhibiting DNA-PK$_{cs}$ reversed the indel frequency effect normally seen in αSyn KO cells. In our previous experiments αSyn KO cells always had a higher frequency of indels created during the

repair process. However, under the condition of DNA-PK_{cs} inhibition, this effect was reversed and αSyn KO cells had a lower deletion frequency than WT (Fig. 4B-C). As a control, we tested whether these inhibitors influenced cell proliferation and no significant changes were observed (Supplementary Fig. 1). These results suggest that αSyn's normal function may be to modulate forms of c-NHEJ where DNA-PK_{cs} is important, such as those which require the DNA-PK_{cs}-stimulated endonuclease activity of Artemis (Chang et al., 2017), since our data is consistent with αSyn loss-of-function skewing repair towards a pathway that increases small indel frequency.

In order to assess whether αSyn re-expression is sufficient to reverse the abnormalities we detected in DSB repair in αSyn KO cells, we used transient transfection to express WT αSyn and a variety of mutants in WT and αSyn KO cells. We transfected WT αSyn, and 6 other mutant forms (A53T, E46K, A30P, delNAC 61-95 (deletion in residues 61-95), S129A, S129D) into WT and αSyn KO HAP1 cells and measured the indel frequency at the repair junction after using our CRISPR/Cas9 DSB induction system targeting the *DNMT3B* gene as previously described. We confirmed rescue of αSyn expression for WT and all mutant forms via western blot (Supplementary Fig. 2), but unfortunately, the transient transfection approach to re-express αSyn altered our system so that there was no difference between WT and αSyn KO cells in indel frequency as assayed by sequencing or the T7EI assay, as we had previously detected. This made it difficult to interpret the effect of our attempted re-expression in this context where we found no significant difference between transfected WT and αSyn KO cells in indel frequency (Supplementary Fig. 2) or in their proliferation (Supplementary Fig. 3).

Figure 4.

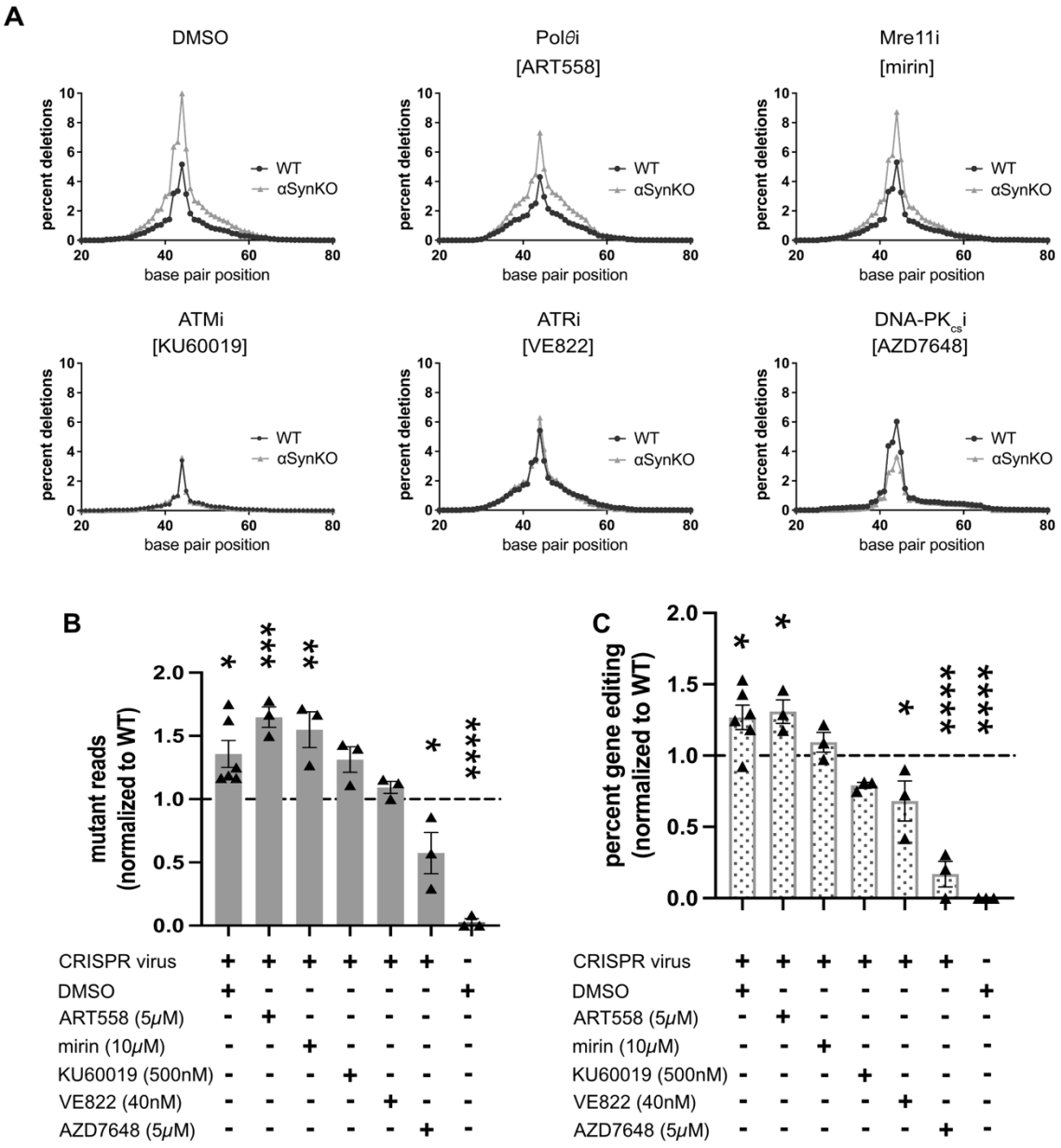

Figure 4. αSyn's modulation of DSB repair in human cells is reversed by DNA-PK$_{cs}$ inhibition.

A) NGS of repair junction with percent of reads containing deletions from WT and αSyn KO HAP1 cells transduced with CRISPR/Cas9 DSB inducing lentivirus. Mutant reads plotted against base pair position with cut site at base pair 45. Cells treated with 0.01% DMSO, Polθi (ART558 5μM), Mre11i (mirin 10μM), ATMi (KU60019 500nM), ATRi (VE822 40nM), DNA-PK$_{cs}$i (AZD7648 5μM). B) Quantification of NGS of αSyn KO samples with condition normalized to WT DMSO. ANOVA summary p<0.0001. Post-hoc multiple comparisons: Significant increase of mutant reads in repair junction of DMSO treated αSyn KO cells (1.358 ±0.166) compared to DMSO treated WT cells (p=0.0124),

in Polθi treated αSyn KO cells (1.648 ±0.081) (p=0.0002), and in Mre11i treated αSyn KO cells (1.549 ±0.142) (p=0.0014). ATMi treated αSyn KO cells (1.313 ±0.101) (p=0.1162). ATRi treated αSyn KO cells (1.093 ±0.047) (p=0.9816). Significant decrease in mutant reads of DNA-PK_{cs}i treated αSyn KO cells (0.5734 ±0.163) (p=0.0154). αSyn KO Nontargeting Virus (0.028 ±0.028) (p<0.0001). N= 3 biological replicates, 1-2 technical replicate per biological replicate. One-way ANOVA. C) T7 Endonuclease I enzymatic assay quantification of percent gene editing of WT and αSyn KO cells treated with inhibitors from A) and C). % Gene Editing = 100 x (1 – (1- fraction cleaved)$^{1/2}$). ANOVA summary p<0.0001. Post-hoc multiple comparisons: Significant increase of gene editing in DMSO treated αSyn cells (1.268 ±0.123) compared to DMSO treated WT cells (p=0.0212), and in Polθi treated αSyn KO cells (1.309 ±0.082) (p=0.0331). Mre11i treated αSyn KO cells (1.093 ±0.070) (p=0.9371). ATMi treated αSyn KO cells (0.7914 ±0.029) (p=0.2584). Significant decrease in mutant reads of ATRi treated αSyn KO cells (0.6812 ±0.106) (p=0.0262), and in DNA-PK_{cs}i treated αSyn KO cells (0.1694 ±0.090) (p<0.0001). αSyn KO Nontargeting Virus (0.0 ±0.0) (p<0.0001). N= 3 biological replicates, 1-2 technical replicate per biological replicate. One-way ANOVA.

Inhibition of PLK protects against neurodegeneration in Lewy pathology mouse model in vivo.

We next wanted to test how manipulating phosphorylation of αSyn may affect cell death in a Lewy pathology mouse model, given our recent work suggesting that pSyn binds DNA very differently than non-phosphorylated αSyn (Dent et al., 2022). We measured cell survival of Lewy inclusion-containing neurons longitudinally over 4 weeks utilizing an *in vivo* multiphoton imaging approach in our previously characterized A53T Syn-GFP mouse line (Schaser et al., 2020). Previous work shows that the GFP tag used does not affect synuclein aggregation in this experimental paradigm (Osterberg et al., 2015; Spinelli et al., 2014). Mouse cortical regions were imaged for a 2-week baseline period, and then for an additional 2 weeks during exposure to the PLK inhibitor BI2536 or saline control. This PLK inhibition started at day 60 after αSyn preformed fibril (PFF) injection to induce Lewy pathology, a time point we have previously shown leads

to robust cortical Lewy pathology that can be imaged *in vivo* with this approach (Schaser et al., 2020). No significant differences in the rate of Lewy inclusion-bearing neuron cell death were detected between the two groups of mice during the baseline imaging period. However, after the treatment period had begun, we measured an increase in survival rate of cells bearing Lewy inclusions in mice treated with twice-weekly BI2536 injections compared to those receiving saline control injections (Fig. 5A-5B). These results suggest that acute pharmacologic inhibition of PLK protects against neurodegeneration of neurons bearing Lewy inclusions and extends the result we obtained previously in PLK2 KO mice (Weston et al., 2021) by reproducing this neuroprotective effect with a more clinically relevant treatment paradigm.

We next tested how this inhibition of PLK may affect αSyn's role in DSB repair. We set out to do this by treating HAP1 cells with BI2536 to test its effect on αSyn modulated DSB repair in our CRISPR/Cas9-mediated DSB induction paradigm, but unfortunately, BI2536 treatment was toxic to HAP1 cells at the relevant concentrations. Because of this, we tested another PLK inhibitor GW843682X which had a better toxicity profile on HAP1 cells in our hands. We found an increased frequency of indels at the DSB repair junction of WT and αSyn KO cells when treated with GW843682X compared to vehicle treated cells (Supplementary Fig. 4A). In mouse cortical neurons, no significant differences were observed (Supplementary Fig. 4B). These differences between our *in vivo* imaging results and our DSB repair assay in cultured cells may be due to the specificity differences in the inhibitors we were required to use. BI2536 inhibits PLK1, 2 and 3 with a similar IC50, while GW843682X is more selective from PLK1 and 3, and previous work suggests that PLK2 may be the most important family

member for phosphorylating αSyn (Bergeron et al., 2014; Inglis et al., 2009; Lou et al., 2010; Weston et al., 2021).

Figure 5.

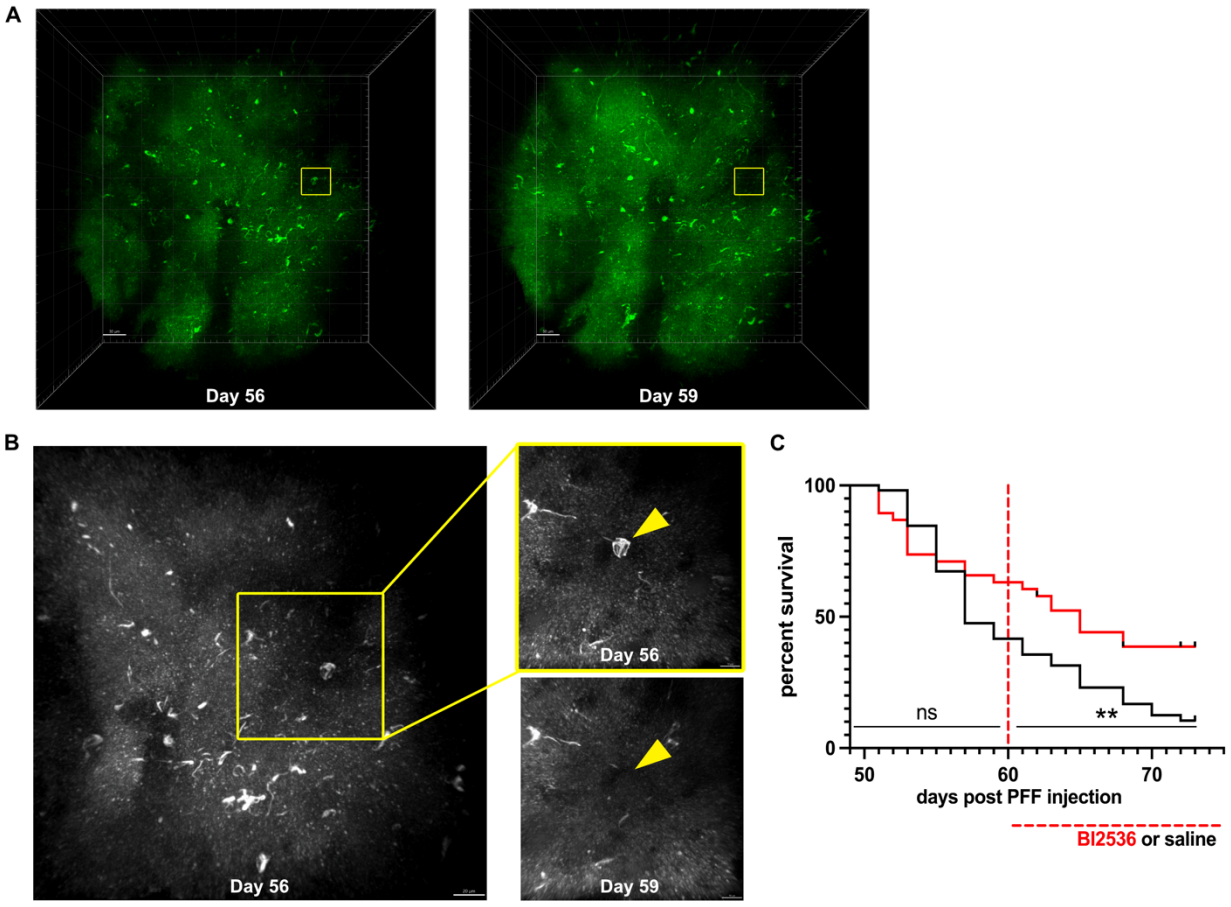

Figure 5: PLK inhibition protects against neurodegeneration in neurons bearing somatic Lewy inclusions *in vivo*.

A) 3D Reconstruction of mouse brain cortical pathology *in vivo* on Day 55 and Day 59 post PFF injection with inclusion represented in B) highlighted (yellow square). Scale bar 30 μm. 255 μm z-stack. B) Representative images of mouse brain cortex *in vivo* demonstrating loss of cell body bearing αSyn somatic inclusion (yellow arrowhead) from day 55 to day 59 post PFF injection. Scale bar 20 μm (LEFT), scale bar 10 μm (RIGHT). Images were taken as separate acquisitions of inclusions (top 21μm z-stack, bottom 36μm z-stack). C) Survival curve of somatic inclusions across 25 days of longitudinal imaging of cortical regions *in vivo* in mice treated with saline or PLK 1/2/3/4 Inhibitor BI2536 (15 mg/kg) IP injections for 2 weeks starting day 60 post PFF injection. Overall, Mantel-cox test p=0.0161. Pre BI2536/saline treatment p=0.1454. Post BI2536/saline

treatment p<0.0055. Saline treated group N= 4 animals. BI2536 treated group N=4 animals. 108 inclusions counted.

Inhibition of PLK increases levels of aggregated αSyn within somatic inclusions.

To investigate the effects of PLK inhibition on aggregated αSyn within Lewy pathology, we used fixed tissue immunohistochemstry (IHC) to study neuronal somatic inclusions from mouse cortex after BI2536 or saline treatment after our *in vivo* imaging experiment (Fig. 5) had ended. Interestingly, BI2536 treatment reduced the ratio of pSyn/αSyn as we predicted, but for reasons different than we originally expected. BI2536 treatment had no significant effect on absolute pSyn levels measured, but it did increase the level of αSyn protein within Lewy inclusions. This was the cause of the decrease in the pSyn/αSyn ratio we detected. This suggests that at PLK1, 2 and 3 are not specific Lewy pathology kinases, but can have effects on the levels of αSyn protein within the inclusion (Fig 6A-6B). Previous work has suggested that PLK inhibition leads to a decrease in degradation of αSyn within aggregates (Oueslati et al., 2013). Our data is consistent with this result. We next tested whether PLK inhibition leads to changes in γH2AX levels, via IHC. We found that BI2536 treatment caused an increase in γH2AX levels, both in cells with and without somatic Lewy inclusions (Fig. 6C). How PLK inhibition leads to an increase in γH2AX is not clear; it could be due to a specific effect on mediators of DSB repair like C-terminal binding protein (CtBP) interacting protein (CtIP), which are known to be phosphorylated by PLK (Barton et al., 2014; H. Wang et al., 2018) or potentially through its effect causing increased aggregated αSyn levels within cells.

Figure 6.

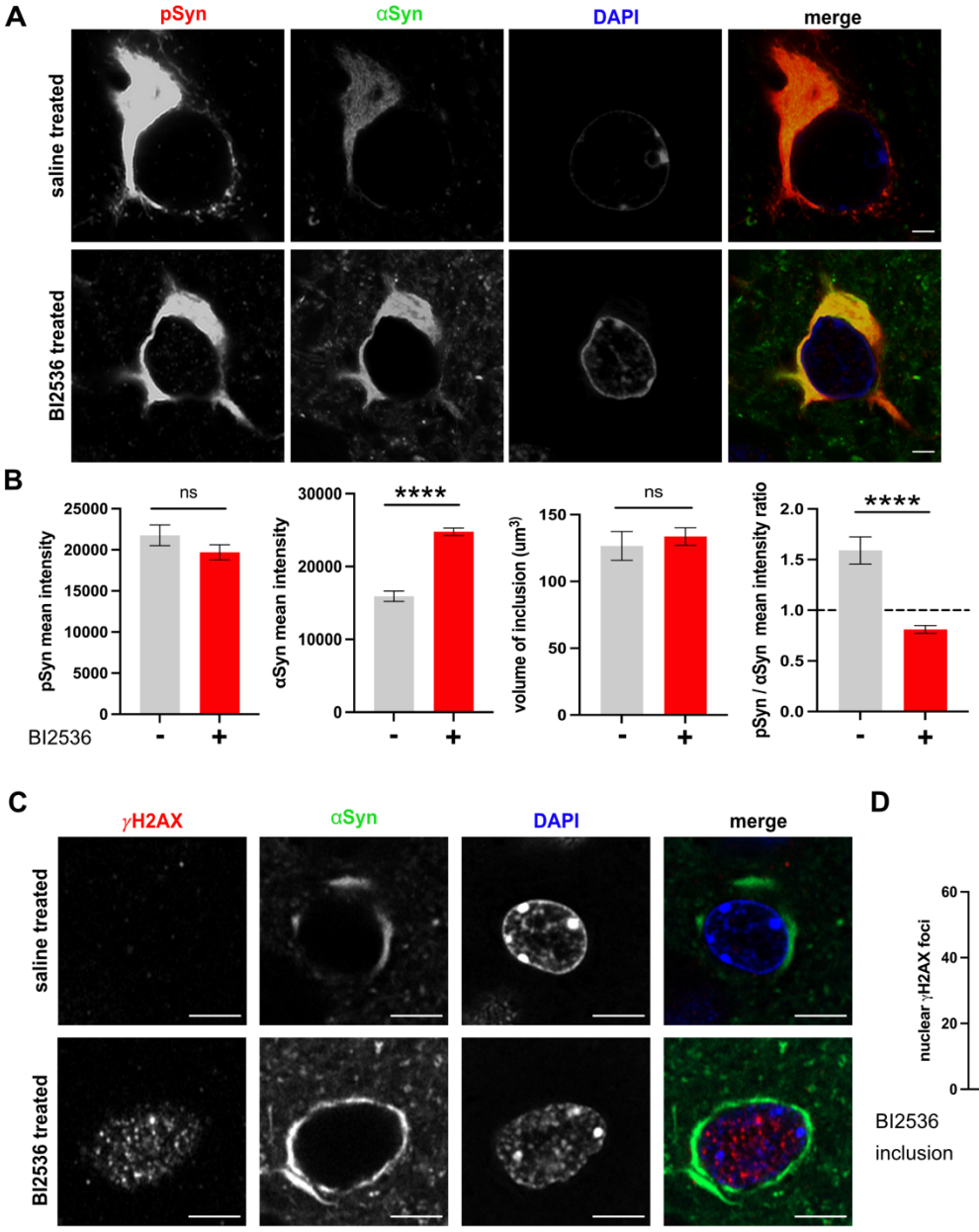

Figure 6. PLK inhibition increases levels of aggregated αSyn within somatic Lewy inclusions.

A) BI2536 treatment (15 mg/kg IP injections twice per week for two weeks) is associated with no change in pSyn levels but increased total αSyn levels within PFF-induced aggregated somatic inclusion. Scale bar 2 μm. B) Quantification of synuclein levels within the aggregate. No significant difference between pSyn mean intensity from saline treated mice (21766 ±1255.436) and BI2536 treated mice (19698 ±918.248) (p=0.1805). Significant increase of αSyn mean intensity from BI2536 treated mice

(24755 ±511.682) compared to saline treated mice (15920 ±707.861) ($p<0.0001$). No significant difference of volume of the inclusion between saline treated mice (126.6 ±10.803) and BI2536 treated mice (133.6 ±6.606) ($p=0.5559$). Significant decrease of pSyn/αSyn mean intensity ratio of BI2536 treated mice (0.8106 ±0.038) compared to saline treated mice (1.590 ±0.135) ($p<0.0001$). N= 5-6 mice in each group, n=143 inclusions. Two-tailed student's t-test. C) BI2536 treatment is associated with increased DSB levels in PFF-induced cortical Lewy pathology mouse model. Scale bar 5μm. RIGHT: Quantification. Significant increase of nuclear γH2AX foci in cells without inclusions from BI2536 treated mice (49.55 ±6.334) compared to cells without inclusions from saline treated mice (21.54 ±2.605) ($p=0.0007$), but no significant difference when compared to cells bearing inclusions from BI2536 treated mice (37.53 ±7.357) ($p=0.2178$). Significant increase of nuclear γH2AX foci in BI2536 treated cells bearing inclusions compared to saline treated cells bearing inclusions (9.812 ±1.886) ($p=0.0031$). Significant decrease of nuclear γH2AX foci in saline treated cells bearing inclusions compared to cells without inclusions ($p=0.0004$). N= 5-6 mice in each group, n=349 inclusions. Two-tailed student's t-test. Formal analysis of Figure 6D performed by Jovin Banga

Discussion

Here, we demonstrate that αSyn loss-of-function leads to impairment in the NHEJ pathway of DSB repair using a plasmid-based reporter assay in human cells (Fig. 1). Importantly, using a CRISPR/Cas9-based system to introduce a DSB at a single genomic location within a chromosomal context also showed an impairment in DSB repair in human cells (Fig. 2) and mouse cortical neurons (Fig. 3) in culture in the αSyn KO condition. The effect of αSyn KO is to increase the frequency of small indels found in the repaired DNA, suggesting that αSyn might function to promote forms of DSB repair that have a lower frequency of small indels, for example, alternative pathways of c-NHEJ. Interestingly, DNA-PK_{cs} inhibition reversed this effect and led to lower indel levels in the αSyn KO condition (Fig. 4). Inhibition of PLK in our *in vivo* multiphoton imaging paradigm suggested that acutely inhibiting this kinase can improve the survival

of these neurons (Fig. 5) and that this was associated with a reduction in pSyn/αSyn ratio within Lewy inclusions because of an increase in aggregated αSyn levels (Fig. 6).

Although a normal role for αSyn in DSB repair is a relatively new concept that we recently introduced to the field, several other groups have linked perturbations in αSyn with DNA damage. For example, both increased expression of αSyn or the PD-associated A30P mutation is correlated with down-regulation of genes involved in DNA repair, while only WT αSyn expression, and not the A30P form, induces DNA damage in dopaminergic neurons (Paiva et al., 2017). Other recent work shows that oxidized, misfolded αSyn can directly lead to DNA damage via an endonuclease activity, and that iron-dependent DNA breaks are associated with the triplication of the SNCA gene in a PD patient-derived IPSC line *in vitro* (Vasquez et al., 2017). Notably, αSyn pathology induced by PFF injection causes a DNA damage response *in vivo* signaled by increased γH2AX and 53BP1 foci (Milanese et al., 2018). Our work suggests that in addition to this effect of dysregulated and/or aggregated αSyn contributing to DNA damage, a normal physiologic function of αSyn could be to repair DSBs. Our previous work provided evidence for this by showing recruitment of αSyn to the sites of DNA damage in HAP1 cells and mouse cortex *in vivo*, and that αSyn loss-of-function led to higher DSB and γH2AX levels, including after treatment with the chemical inducer of DSBs, bleomycin (Schaser et al., 2019). The current study significantly extends these results and again suggests a normal function for αSyn in repair of DSBs, but now when they are induced in a selective way within a single site in genomic DNA, both in human cells and mouse cortical neurons. In addition, we have found that αSyn plays an important role to facilitate sub-forms of c-NHEJ which result in a lower frequency of indels during the

DSB repair process when αSyn is present at normal expression levels. It is interesting to consider how our data fits in with the previous work from other groups suggesting that αSyn aggregation leads to increased levels of DNA damage. We propose, given our data presented here, that αSyn facilitates c-NHEJ through a mechanism that is regulated by DNA-PK_{cs} activity, and that disrupting this process by overexpressing, mutating or aggregating αSyn leads to aberrant DSB repair. This could be due to a combination of factors, including shifting NHEJ towards a pathway that causes an increase in small indel frequency during DSB repair. In neurons, which are heavily dependent on NHEJ DSB repair, this could lead to a progressive increase in mutation burden with time in LB-containing cells. We speculate that when a certain level of these small indels accumulate, it may trigger dysregulation of critical gene expression and neuroinflammatory pathways that lead to programmed cell death. It will be important in future studies to test whether there is evidence for this in human patient-derived tissue or model systems exhibiting Lewy pathology using single-cell approaches, since our model directly predicts an increased frequency of small indels within the genome of LB-containing neurons.

One of our more unexpected results was the evidence for interactions between αSyn and DNA-PK_{cs} in our DSB repair assays. There are multiple pathways to repair a DSB, including c-NHEJ, alt-NHEJ, SSA and HR. How the cell decides which pathway to use is a critical question and previous work suggests that DNA-PK_{cs} is an important component in this decision. Because of its cellular abundance, DNA-PK_{cs} is thought to be an early repair factor that binds DSBs (Neal & Meek, 2011) and shunts cells towards f c-NHEJ that can introduce small indels (Chang et al., 2017) and away from alt-NHEJ

and HR (Mao et al., 2008). Consistent with this, our experiment blocking an alt-NHEJ polymerase, Pol θ, showed no effect (Fig. 4). In addition to the role DNA-PK$_{cs}$ has in inhibiting HR, which can be regulated by autophosphorylation (Neal et al., 2011), DNA-PK$_{cs}$ may also regulate a cell's decision between c-NHEJ and alt-NHEJ (Perrault et al., 2004; Udayakumar et al., 2003), although other data suggests that DNA- PK$_{cs}$ phosphorylation of ATM (Zhou et al., 2017) or Ku (Fattah et al., 2010) facilitates this choice. C-NHEJ can proceed via a pathway independent of DNA-PK$_{cs}$, involving Ku binding to XRCC4 and ligase 4 that does not introduce indels, or via other paths requiring DNA-PK$_{cs}$ activity that activates the endonuclease Artemis and introduces small deletions at the repair site (Chang et al., 2017). Our data suggests that αSyn promotes sub-forms of c-NHEJ which do not introduce small indels when DNA-PK$_{cs}$ is not inhibited. Our result that DNA-PK$_{cs}$ inhibition reverses this effect and αSyn switches to increasing the frequency of small indels suggests that these two molecules do potentially interact in potentially complicated ways. This interaction may be direct or indirect, and could also potentially involve modulation of liquid-liquid phase separation processes that are relevant to DNA repair and neurodegeneration (Webber et al., 2020), and in which αSyn has been recently implicated (Ray et al., 2020). One possibility is that αSyn could be acting like a partial agonist for DNA-PK$_{cs}$ activity. In the presence of DNA-PK$_{cs}$'s endogenous activator, Ku protein at DSB sites, αSyn acts to reduce the level of DNA-PK$_{cs}$ kinase activity, thereby reducing Artemis endonuclease activity and reducing the level of small indels created at the repair junction. However, in the presence of strong DNA-PK$_{cs}$ chemical inhibition, αSyn partial agonism could actually promote its kinase activity and promote Artemis-mediated endonuclease activity giving

rise to small indel formation. Multiple models are possible, however, including ones where αSyn could directly promote or inhibit other DSB repair pathways that could influence the frequency of small indels formed during repair. It will be interesting in future experiments to test which of these models could be operative.

Our *in vivo* multiphoton imaging data suggests that inhibiting PLK acutely can improve survival of Lewy inclusion-bearing neurons in cortex. This extends our previous work in PLK2 KO mice showing a similar result (Weston et al., 2021) by suggesting that pharmacologic inhibition may have similar effects and be potentially therapeutic. We originally expected that PLK inhibition with BI2536, which inhibits PLK1, 2 & 3, would have effects on pSyn levels within Lewy pathology, suggesting that PLK1 or 3 was a Lewy pathology kinase, since our previous work in PLK2 KO mice suggested that PLK2 was not a Lewy pathology kinase (Weston et al., 2021). However, our fixed tissue IHC analysis did not suggest that pSyn levels were lower after BI2536 treatment, suggesting that PLK is not a Lewy pathology kinase *in vivo*. We did detect changes in total aggregated αSyn levels within inclusions, with PLK inhibition leading to an increase. Our data is consistent with previous work from Lashuel and colleagues that finds that PLK2 regulates and enhances autophagic clearance of αSyn in a kinase-dependent manner (Oueslati et al., 2013). More investigation is required to decipher how PLK inhibition leads to increased neuronal survival and whether genomic stability plays a role, but it is interesting to speculate that increases in αSyn levels within the inclusion are mirrored by increases in potentially low levels of soluble nuclear αSyn as well that could be promoting more efficient DSB repair.

In summary, our data using powerful single genomic DSB induction approaches clearly demonstrates the importance of αSyn in NHEJ, favoring less error prone c-NHEJ pathways. This is the case both in a human cell line and in mouse primary cortical neurons, directly implicating αSyn-mediated DSB repair in this important cell type. Our data suggesting an interaction between αSyn and DNA-PK$_{cs}$ in this process is the first time, to our knowledge, this has been suggested and sets the stage for future work to test whether αSyn could act as a partial agonist of DNA-PK$_{cs}$ at DSBs. We also show how acute PLK inhibition can lead to neuroprotection in a Lewy pathology model and suggest that determining the mechanism for this effect could help lead to new treatments for clinically important forms of neurodegenerative disease.

Methods and Materials

Cell culture

HAP1 WT (item #C631 bath 29663) and HAP1 Human SNCA 103 bp deletion knockout (item #HZGHC003210c003 batch 2) cell lines were purchased from Horizon Discovery. Cells were maintained at 37°C 5% CO_2 and grown in IMDM media (Gibco #11995-065)+10% Fetal Bovine Serum +5% penicillin-streptomycin (Gibco #1514022). Cells were passed when ~75% confluent and discarded above passage number 10.

Plasmid NHEJ and HR reporters

HAP1 WT and SNCA KO cells were seeded for ~75% confluency and transfected with NHEJ and HR plasmid reporters(Seluanov et al., 2010) using X-tremeGENE HP DNA Transfection Reagent (1:3 DNA:reagent) in OptiMEM (Gibco #31985062). Images were taken on a Zeiss Axio Observer.D1 outfitted with an Excelitas X-Cite 120 LED GFP light at 24, 48, 72 hours. After 48 hours, cells were spun down and either submitted for flow cytometry or the DNA was processed with Qiagen's QIAprep kit. DNA was digested with T5 exonuclease for 1 hour at 37°C and cleaned up using Cytivia's mag-bind beads. DNA was digested with fspI for 45 minutes at 37°C and cleaned up again with mag-bind beads. DNA was normalized and sent to Azenta Life Sciences for AmpliconEZ illumina sequencing.

Flow Cytometry

All experiments were completed with the help of OHSU's Flow Cytometry core. GFP expression was measured in living cells, not fixed cells on the same day of experiment. HAP1 cells were trypsinized with 0.5% trypsin (Gibco #25300062) to transfer cells to a 0.6 mL tube. Cells were incubated in trypsin for 10 minutes on ice. Cells were spun down and resuspended in PBS. Cells were spun down and resuspended in FACS Buffer (PBS +1% FBS). Cells were strained and submitted to OHSU's Flow Cytometry for GFP expression analysis. Cells were first gated on a forward side scatter to exclude debris. Cells were next gated on forward side scatter height x forward side scatter area for doublet discrimination. GFP efficiency was measured by taking GFP positive singlets

over the total amount of single cells. For CRISPR/Cas9 lentiviral DSB assays, there was no significant difference in GFP efficiency between HAP1 WT cells treated with GFP lentivirus (21.54 ±4.92) and HAP1 KO cells (14.88 ±4.29) p=0.3653. Mutation values were not adjusted.

Incucyte proliferation

96 well image lock plates (Essen) were coated with 80µg/mL matrigel for 24 hours. 35K cells were plated per well in IMDM (10% FBS, 5% penicillin-streptomycin) with 6 replicates of WT and SNCA KO cells each and transferred to the Sartorius Incucyte S3 microplate holder maintained at 37°C at 5% CO_2. 4x brightfield scans were taken 3 hours after plating and continuously every 3 hours for the duration of the experiment. For proliferation assays post transfection, cells were seeded at 15 K per well to account for the different time course of the experiment.

CRISPR/Cas9 lentiviral double strand break repair assay

Human HAP1 WT and SNCA KO cells were maintained in IMDM (Gibco# 11995-065 +10% FBS, +5% penicillin-streptomycin) under passage number 10. Cells were seeded 16,000 cells per well in a 96 well plate coated in Poly-D-Lysine (Cultrex 343910001). 24 hours after seeding, cells were incubated with a Horizon Discovery Human DNMT3B mCMV-EGFP lentivirus (cat. #VSGH12131) (MOI 1) in 50 µL of IMDM. 150 µL of maintenance media was added to cells 5 hours after start of lentiviral treatment. Cells

were harvested 72 hours after lentiviral treatment with 0.05% trypsin. Cells were lysed in 20% 5x Phusion HF Buffer, 5% 20 mg/mL Proteinase K, and 5% 10 mg/mL RNaseA and stored at -80 °C. The repair junction was amplified using a standard PCR reaction with Phusion HotStart. Human cell line repair junction 288 bp product reference sequence:

TTTCTGAGCACAGAGGGTACAGGCCGGCTCTTCTTCGAATTTTACCACCTGCTGAA
TTACTCACGCCCCAAGGAGGGTGATGACCGGCCGTTCTTCTGGATGTTTGAGAAT
GTTGTAGCCATGAAGGTTGGCGACAAGAGGGACATCTCACGGTTCCTGGAGGTGA
GGGAATCTGGGGACCTGATTGTCACAGACAGCCAGGGCAGGGAAAGCGCTGCTG
GCAGTGATGATTGGTGGGTGTTGCCAACATTGGGAATGACTTTCCCGTTCTTGGTC
TGGCTAGATCCA with forward primer TTTCTGAGCACAGAGGGTACAG and reverse primer TGGATCTAGCCAGACCAAGAAC. Cut site at 45 bp CC^CC. Samples underwent a PCR cleanup protocol according to Qiagen's QIAquick PCR Purification Kit protocol and DNA levels were measured via Qubit dsDNA HS Assay Kit. Samples were normalized to 20 ng/uL and sent to Azenta Life Sciences for Next Generation Sequencing (AmpliconEZ).

Mouse E18 cortical neurons were transduced with an analogous mouse dnmt3b mCMV-EGFP lentivirus (cat. #VSGM12147) (MOI 0.35) in maintenance media DIV 6. Cells were harvested 72 hours after lentiviral treatment with 0.05% trypsin and submitted to the same protocol as listed above. Mouse neurons repair junction 272bp product reference sequence:

CTGTGCTGTTCCCATTACAGAGGGCACAGGAAGGCTCTTCTTCGAGTTTTACCACT
TGCTGAATTATACCCGCCCCAAGGAGGGCGACAACCGTCCATTCTTCTGGATGTTC

GAGAATGTTGTGGCCATGAAAGTGAATGACAAGAAAGACATCTCAAGATTCCTGGC
AGTGAGTGGATTGTCAGGGAAACCTGGCAGGGAAGGCGCCACTAACACGGAGGG
CTGAGAAAATTATTTCCTGCTCAGAGGAGGGTGTGGCTTAATCTGAGAAC with
forward primer CTGTGCTGTTCCCATTACAGAG and reverse primer
GTTCTCAGATTAAGCCACACCC. Cut site at 52 bp CC^CC.

T7 endonuclease I assay

The repair junction of the DNMT3b gene from human HAP1 cell lysates from the DSBR Assay was amplified with the same PCR protocol to create a 544 bp full length product. Samples were then heated for 10 min at 95°C and slowly cooled at 1°C per minute to room temperature. Samples were digested with T7 Endonuclease I for 25 minutes at 37 °C and run out on a 2% agarose gel at 100V for 2 hours. Human DNMT3b gene 544 bp product reference sequence:
TGAGAAGGAGCCACTTGCTTCTGGCCAAGTTACTGGCAGCATCAGGGGCCTGTTG
GTGCTGCCTACGCTCCATAGTAAATCCTCAGCCCACAAGGGAAATACCCTAGTAAA
TAGTGCCCTGCTGCTGCCTGTGTCCCTGCTGTCATTCAGGTGGACATAGACTGGTA
GGCATCACCCTGAACTGTCAGGAGGCCATTGGGAACCTGCTGGTCTCAGGGAATA
AGGTGGGTTGGGCTGGAGGTTTCAAATGAACCCTGCGCTGTCATCTTTTCTGAGCA
CAGAGGGTACAGGCCGGCTCTTCTTCGAATTTTACCACCTGCTGAATTACTCACGC
CCCAAGGAGGGTGATGACCGGCCGTTCTTCTGGATGTTTGAGAATGTTGTAGCCA
TGAAGGTTGGCGACAAGAGGGACATCTCACGGTTCCTGGAGGTGAGGGAATCTG
GGGACCTGATTGTCACAGACAGCCAGGGCAGGGAAAGCGCTGCTGGCAGTGATG

ATTGGTGGGTGTTGCCAACATTGGGAATGACTTTCCCGTTCTTGGTCTGGCTAGAT
CCA with forward primer TGAGAAGGAGCCACTTGCTT and reverse primer
ACTGAAAGGGCAAGAACCAG. Mouse dnmt3b gene 561 bp product reference
sequence:
ACTTGGTGATTGGTGGAAGCCCATGCAATGATCTCTCTAACGTCAATCCTGCCCGC
AAAGGTTTATATGGTAAGCAGGGTTTGGGAACCTCCAGCACCACTATGTGCCATGT
GTCTATGTTCAAATGGAAAATGGAGAAAAGAAGCTGTTGTCAGTTGTTCAGCCGTA
TTCATGACTCAGGCCCGGTCCTTCCCAGACACAACAAATCCAGTTGCTTTCTTTTAC
TGCAGTGTCCTGGGGACACTCTTGGTCTTTTGAGGCTCGTTTGGAATGAAGGCTTT
GACTAAACCTTGTCCTCCTGTGCTGTTCCCATTACAGAGGGCACAGGAAGGCTCTT
CTTCGAGTTTTACCACTTGCTGAATTATACCCGCCCCAAGGAGGGCGACAACCGTC
CATTCTTCTGGATGTTCGAGAATGTTGTGGCCATGAAAGTGAATGACAAGAAAGAC
ATCTCAAGATTCCTGGCAGTGAGTGGATTGTCAGGGAAACCTGGCAGGGAAGGCG
CCACTAACACGGAGGGCTGAGAAAATTATTTCCTGCTCAGAGGAGGGTGTGGCTT
AA with forward primer ACTTGGTGATTGGTGGAAGC and reverse primer
GTCTCCTCCCACACCGAATT.

Animals

All mice lines were housed in OHSU's Department of Comparative Medicine (DCM) facilities in a light-dark cycle vivarium. Animals were maintained under ad libitum food and water diet. All animal protocols were approved by OHSU IACUC, and all

experiments were performed with every effort to reduce animal lives and animal suffering.

Transgenic mouse lines

WT (C57BL/6NJ Strain#: 005304) and SNCA KO (C57BL/6N-*Sncatm1Mjff*/J Strain #: 016123) were obtained from The Jackson Laboratory. For embryonic cortical dissections, timed pregnancies were performed by breeding SNCA KO mice together or WT mice together for 72 hours and separating the female.

The A53T-Syn-GFP mouse line was genetically created (Schaser et al., 2019) and characterized (Schaser et al., 2020) according to our previous research.

Primary Cultured Neurons

Cortices were dissected from E18 mice and kept in Hibernate-E (Gibco #A1247601) at 4 °C until dissociation within 1 to 2 hours. Primary cortical neurons were cultured according to an adapted protocol from the Banker Lab (Kaech & Banker, 2006). Cortices were transferred to HBSS (Gibco #14025092) on ice. Neurons were dissociated with 2.5% trypsin (Gibco #15090046) for 15 minutes at 37 °C, gently inverting every 5 minutes. Neurons were dissociated in sterile filtered plating medium (Neurobasal Medium Gibco #21103049 +10% FBS, +1% GlutaMAX Supplement, +1% sodium pyruvate, +1% penicillin-streptomycin) and frozen down with MD Bioproduct's

NeuroFreeze kit. Neurons were kept in liquid nitrogen up to 4 months. Neurons were thawed according to the NeuroFreeze kit and plated for 4 hours in PDL coated 96 well plates. Media was exchanged for sterile filtered maintenance media (Neurobasal Medium +2% B-27 Supplement 50X Gibco #17504044, +0.5% GlutaMAX Supplement) and neurons remained in a humidified incubator at 37 °C with 5% CO_2 until DIV 5. One third of the media was exchanged for fresh maintenance media on DIV 5. Lentiviral Transduction for the DSB repair assay occurred on DIV 6.

Pharmacological Agents

All inhibitors were purchased, stored at -20 °C, diluted in DMSO, aliquoted, and immediately stored at -80 °C. Treatment concentrations were decided by a treatment curve, selecting the highest concentration possible without affecting cell health. Final concentrations were between 2x-2000x each inhibitor's IC50 for each desired target. 1000x Inhibitors were thawed and added to IMDM at 0.1%. Cells were treated with inhibitors concurrently with lentiviral treatment. Final Concentrations: 40nM ATRi (VE822), 500 nM ATMi (KU60019), 200 nM DNA-PK_{cs}i (NU7441), 5μM DNA-PK_{cs}i (AZD7648), 5 μM Pol θi (ART558), and 10 μM Mre11i (mirin).

Transfection

The mammalian expression vector pBApo-CMV-Pur (cat. #3421) was purchased from Takara. We used Genescript to insert the 144 amino acid sequence for WT synuclein

into the backbone and create 6 mutated strains: S129A, S129D, A53T, E46K, A30P, and delNAC(61-95). Plasmids were then transformed, miniprepped, and stored at -20C. 24 hours before transfection, HAP1 cells were seeded to be 60% confluent. The jetOPTIMUS reagent was added to the DNA+jetOPTIMUS buffer according to the Polyplus protocol using 0.15ug of DNA for each well in a 96 well format, 1:1.5 ratio DNA: jetOPTIMUS reagent. Transfection was performed in IMDM +5% FBS for 4 hours and then media was exchanged for IMDM +10% FBS, +5% penicillin-streptomycin. Reagents were scaled up for transfections in a 60mm dish for subsequent western blot confirmation.

Western Blot

The western blot protocol used in the paper was completed in accordance to previously published work (Schaser et al., 2019). Primary antibodies used were: anti-Syn 4B12, 1:500 dilution, mouse monoclonal, Biolegend, cat. 807804; GAPDH, 1:10,000 dilution, mouse monoclonal, Millipore, cat. MAB374.

Mouse brain in vivo imaging & analysis

2 to 3 month-old male and female mice were injected with mouse WT sequence PFFs using the same protocol as we have previously published (Schaser et al., 2019). Cranial window surgeries were performed 5 weeks post PFF injection according to our previous published protocols. Mouse cortex was imaged 3 weeks post cranial window surgery

using a Zeiss LSM 7MP multiphoton microscope. Zeiss Zen image acquisition software was used to collect z-stacks from layer 1 to layer 2/3 of the cortex with 3μm intervals at 63x zoom 1. Regions of interest (ROIs) were analyzed in FIJI and inclusions were verified visually for each day of imaging by hand. New inclusions were counted for each day of imaging and scored by hand. No detectible sex differences were observed. Survival curves were created with Prism10 (GraphPad). Cortical regions were imaged for 4 weeks at 3 times per week. After 2 weeks animals were given a 2-week treatment of saline or 15 mg/kg BI2536 IP injections twice per week. Animals were sacrificed after 4 weeks of imaging for IHC.

Immunofluorescence and Immunohistochemistry

HAP1 cells.

Cells were seeded on #1.5 coverslips or glass-bottomed 96 well plates coated in PLL. Cells were fixed, permeabilized, incubated in blocking buffer, stained with primary and secondary antibodies, and mounted according to previously published protocols (Schaser et al., 2019). Cells were imaged on a Zeiss 980 laser-scanning confocal microscope with Zen software. Z-stacks of optimal intervals were acquired at 63x zoom 1.

Primary Cortical Neurons.

Neurons were seeded into PDL coated Cellvis #1.5H glass-bottomed 96 well plates. After a 72-hour lentiviral treatment, neurons were fixed on DIV 9 with 4% PFA for 15 minutes and permeabilized with 0.25% Triton X-100 for 20 minutes at RT. Neurons

were incubated with Biotium NucSpot555/570 (cat. 41033) for 10 minutes at RT. Whole well images were acquired same day on a Zeiss Celldiscoverer 7 at 20x zoom 1. Images were stitched together using Zen software and an Imaris machine learning analysis protocol was used to exclude dead nuclei. A mean intensity 488 threshold was used to count GFP positive cells on Imaris and GFP efficiency was calculated. For CRISPR/Cas9 lentiviral DSB assays, there was no significant difference in GFP efficiency between WT E18 cortical neurons treated with GFP lentivirus (6.267 ±0.70) and KO E18 cortical neurons (16.05 ±6.18) p=0.1907. Mutation values were not adjusted.

Mouse Tissue.

Brains from 4-5 month old mice were dissected and fixed according to previously published protocols (Schaser et al., 2019). Brains were sectioned into 50μM coronal slices using a Vibratome LeicaVT1000S. Tissue was fixed, permeabilized, incubated in blocking buffer, stained with primary and secondary antibodies, and mounted as previously published (Schaser et al., 2019). Imaging was performed on a Zeiss 980 laser-scanning confocal microscope with a 63x oil objective zoom 7.0. Z-stacks of the αSyn inclusion and nucleus with optimal intervals. Analysis was performed in IMARIS using a 3D surface reconstruction of the inclusion and the DAPI channel to create a nuclear mask. We then used IMARIS to quantify the nuclear γH2AX foci count or αSyn and pSyn levels with an average intensity measurement.

Primary antibodies used were: anti-Syn1, 1:500 dilution, mouse monoclonal, BD Biosciences, cat. 610786; anti-Phospho-Histone H2a.X, 1:500 dilution, rabbit monoclonal, Cell Signaling, cat. 9718; anti-PhosphoS129-Syn EPY1536Y, 1:500

dilution, rabbit monoclonal, Abcam ab51253. Secondary antibodies used were: Alexa Fluor 555 goat anti-mouse, Abcam ab150114; Alexa Fluor 647 donkey anti-rabbit, Jackson ImmunoResearch Laboratories 711605152.

Acknowledgments

We would like to thank the lab of Kelvin Luk for providing αsyn PFFs, Lev Federov and the OHSU Transgenic Mouse Model Core for generation of A53T Syn-GFP mice, and the OHSU Advanced Light Microscopy core for their guidance and equipment on several experiments. We also thank Michael Cohen, Amanda McCullough, Ian Martin, and Peter McKinnon for helpful discussions. Lastly, we recognize Unni Lab members who helped with the revision process: Moriah Arnold, Dr. Sydney Boutros, Anna Bowman, Jessica Keating, Dr. Carlos Soto Faguas, and Elias Wisdom. This work was supported in part by the NIH (T32AG055378, R01NS102227), the David Johnson Family Foundation, and the Lacroute Fellows Program.

Author Contributions

Conceptualization, EPR & VKU. Methodology, EPR, VRO (Figure 1 only), VG, VKU (Figure 1 only). Formal analysis, EPR, VRO (Figure 1 only), JSB (Figure 6D only), VKU. Investigation, EPR, VRO (Figure 1 only), VKU. Writing - original draft, EPR. Writing - review & editing, EPR, VRO, VG, VKU, Visualization - EPR & VKU. Supervision, VKU. Project administration, VKU. Funding acquisition, EPR & VKU.

Data Availability

All materials, data, and protocols will be made available to readers without undue qualifications.

Disclosures

The authors have nothing to disclose.

Supplemental Materials

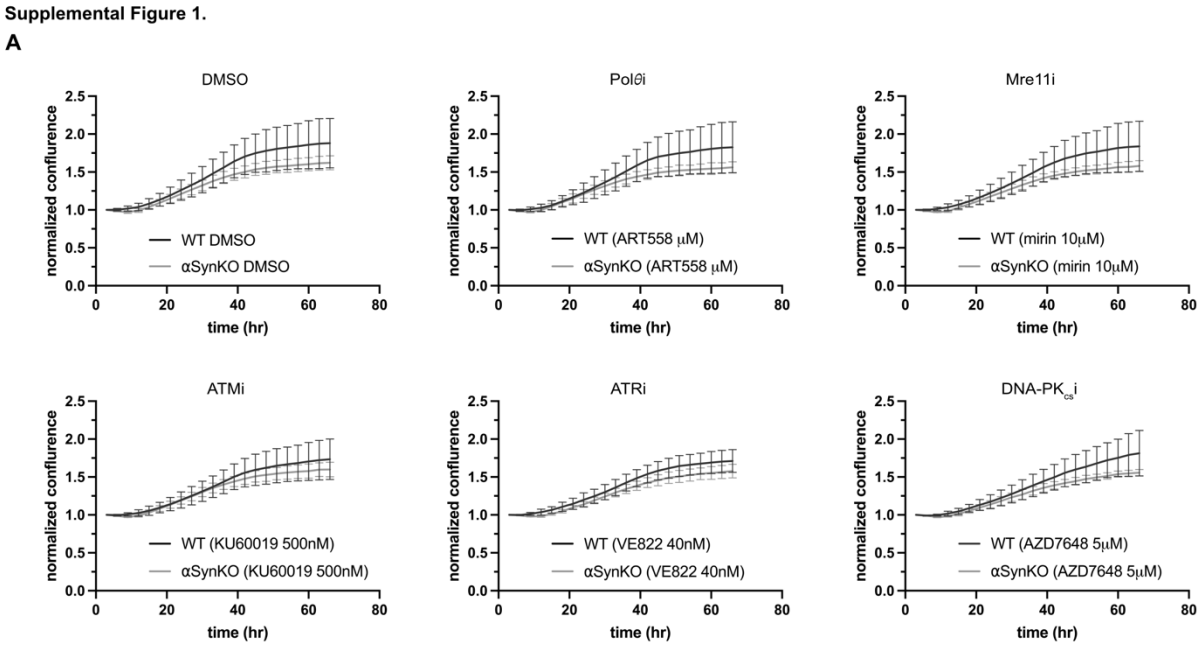

Supplemental Figure 1. WT and αSyn KO HAP1 cell proliferation is unchanged by inhibition of Pol *θ*/Mre11/ATM/ATR/DNA-PK$_{cs}$.

A) Normalized confluence of WT and αSyn KO cells treated with 0.01% DMSO, Pol *θ*i (ART558 5uM), Mre11i (mirin 10μM), ATMi (KU60019 500nM), ATRi (VE822 40nM), DNA-PK$_{cs}$i (AZD7648 5μM). No significant differences observed. WT DMSO= 95% CI 50% maximum (27.25-61.40). KO DMSO= 95% CI 50% maximum (27.11-32.87). WT Pol *θ*i= 95% CI 50% maximum (27.46-69.68). KO Pol *θ*i= 95% CI 50% maximum

(25.87-30.66). WT Mre11i= 95% CI 50% maximum (28.76-117.6). KO Mre11i= 95% CI 50% maximum (28.85-34.01). WT ATMi=95% CI 50% maximum (28.52-75.11). KO ATMi= 95% CI 50% maximum (27.98-33.98). WT ATRi= 95% CI 50% maximum (30.55-46.05). KO ATRi= 95% CI 50% maximum (31.14-37.96). WT DNA-PK$_{cs}$i = 95% CI 50% maximum (34.08-poor fit). KO DNA-PK$_{cs}$i = 95% CI 50% maximum (32.79-40.85). N=3 biological replicates, 6 technical replicates per biological replicate). Sigmoidal nonlinear regression.

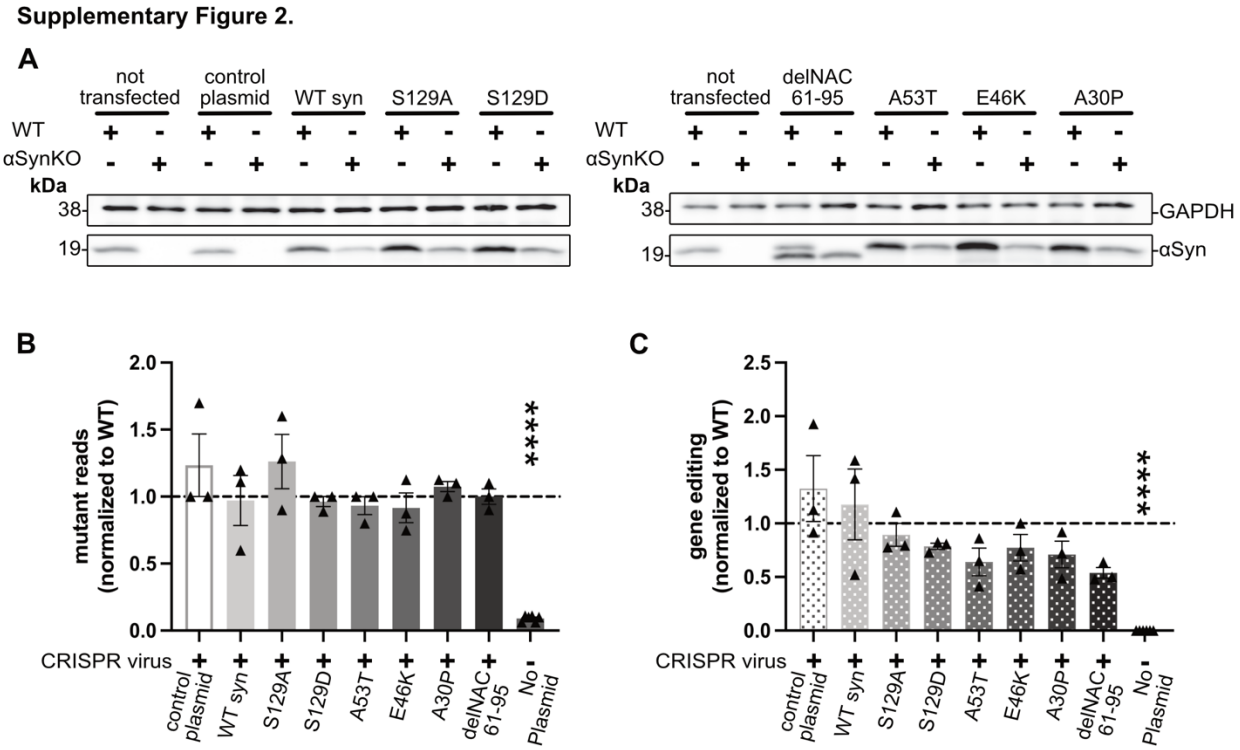

Supplementary Figure 2. Transient transfection cannot be used to assay DSB repair in αSyn KO HAP1 cells.

A) Western Blot post transfection confirming over-expression in WT HAP1 cells and full rescue in αSyn KO cells. Full rescue observed with WT syn, S129A syn, S129D syn, A53T syn, E46K syn, A30P syn, and delNAC 61-95 syn. B) Quantification of NGS of 288bp repair junction from αSyn KO cells with each synuclein construct condition normalized WT control plasmid. ANOVA summary p<0.0001. Post-hoc multiple comparisons show no significant differences. αSyn KO control plasmid (1.233 ±0.233) compared to WT control plasmid (p=0.5396). αSyn KO WT syn (0.9704±0.187)(p>0.9999). αSyn KO S129A (1.262 ±0.202)(p=0.4137). αSyn KO S129D (0.9630 ±0.037)(p>0.9999). αSyn KO A53T (0.9333 ±0.067)(p=0.9996). αSyn KO E46K (0.9167 ±0.110)(p-0.9977). αSyn KO A30P (1.075 ±0.038)(p=0.9990). αSyn KO delNAC 61-95 (1.000 ±0.058)(p>0.9999). αSyn KO Nontargeting virus (0.09120 ±0.009)(p<0.0001) N=3 biological replicates. One-way ANOVA. B) T7 Endonuclease I enzymatic assay quantification of percent gene editing of WT and αSyn KO cells

transfected with WT and mutant forms of synuclein. % Gene Editing = 100 x (1 – (1-fraction cleaved)$^{1/2}$). ANOVA summary $p<0.0001$. Post-hoc multiple comparisons show no significant differences. αSyn KO control plasmid (1.325 ±0.308) compared to WT control plasmid ($p=0.4784$). αSyn KO WT syn (1.177 ±0.107)($p=0.9451$). αSyn KO S129A (0.8936 ±0.107)($p=0.9982$). αSyn KO S129D (0.7871 ±0.029)($p=0.8634$). αSyn KO A53T (0.6414 ±0.129)($p=0.3716$). αSyn KO E46K (0.7729 ±0.124)($p=0.8215$). αSyn KO A30P (0.7102 ±0.125)($p=0.6015$). αSyn KO delNAC61-95 (0.5394 ±0.050)($p=0.1494$). αSyn KO Nontargeting virus (0.0 ±0.0)($p<0.0001$). N=3 biological replicates. One-way ANOVA.

Supplemental Figure 3.

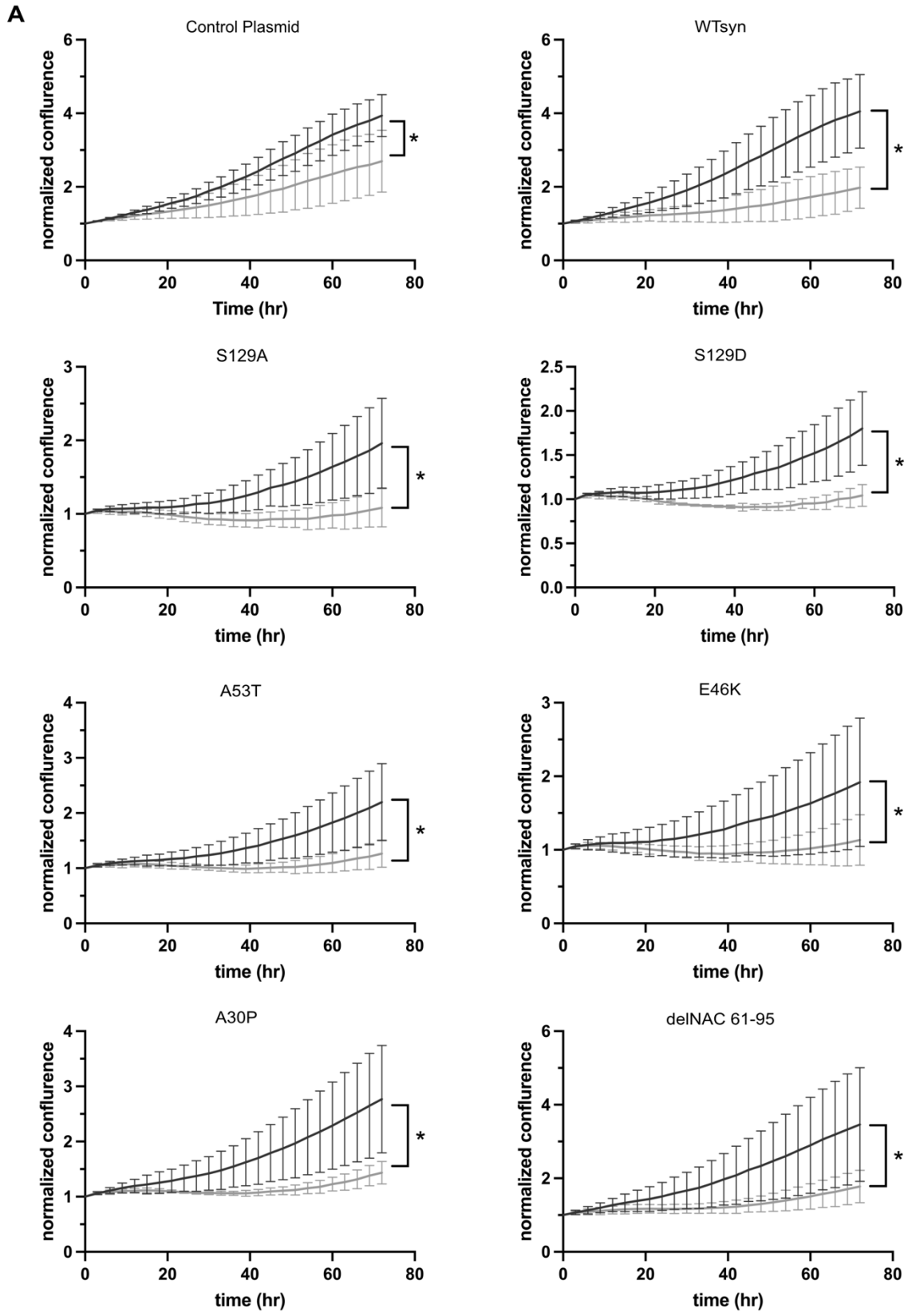

Supplementary Figure 3. Re-expression of WT and mutant forms of αSyn does not affect proliferation of HAP1 cells.

A) Proliferation assay of WT(black) and αSyn KO(gray) HAP1 cells transfected with WT and mutant forms of synuclein from Supplementary Figure 2. Significant differences between proliferative curves over 72 hours of cells transfected with control plasmids and mutants. WT control plasmid= 95% CI slope (0.03694-0.04849), KO control plasmid= 95% CI slope (0.01550- 0.03172). WT syn= 95% CI slope (0.03880-0.05068), KO WT syn= 95% CI slope (0.009200-0.01575). WT S129A= 95% CI slope (0.009390-0.01503), KO S129A= 95% CI slope (-0.001479-0.0009383). WT S129D= 95% CI slope (0.007822-0.01201), KO S129D= 95% CI slope (-0.001430– -0.0001155). WT A53T= 95% CI slope (0.01200-0.01867), KO A53T= 95% CI slope (0.0004279-0.002834). WT E46K= 95% CI slope (0.007699-0.01610), KO E46K= 95% CI slope (-0.001203-0.001774). WT A30P= 95% CI slope (0.01876-0.02842), KO A30P= 95% CI slope (0.002622-0.004776). WT delNAC61-95= 95% CI slope (0.02649-0.04193), KO delNAC61-95= 95% CI slope (0.006612-0.01099). N=3 biological replicates (6 technical replicates per biological replicate). Simple linear regression.

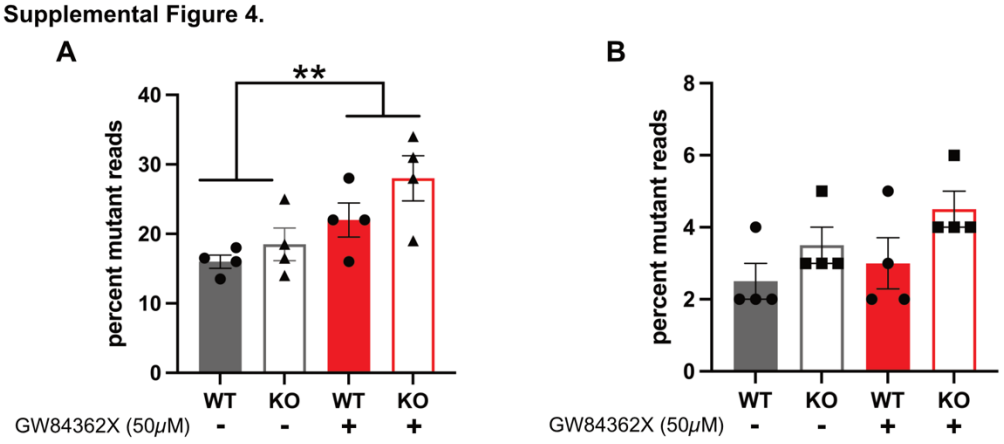

Supplementary Figure 4: PLK1/3 inhibition increases indel frequency in HAP1 cells, but not in mouse cortical neurons.

A) NGS of 288bp repair junction from WT and αSyn KO HAP1 cells transduced with CRISPR/Cas9 DSB inducing lentivirus and treated with 0.01% DMSO or PLK1/3 Inhibitor GW84362X 50μM for 72 hours. GW84362X treated cells show significantly increased mutant reads compared to DMSO treated cells. Row (Drug) Factor p=0.0071. Column (Cell Line) Factor p=0.1011. N=4 biological replicates (1-2 technical replicates per biological replicate). Two-way ANOVA. No post-hoc multiple comparisons. B) NGS of 272bp repair junction from WT and αSyn KO E18 mouse cortical neurons transduced with CRISPR/CAs9 DSB inducing lentivirus and treated with 0.01% DMSO or PLK1/3 Inhibitor GW84362X 50μM for 72 hours. Row (Drug) Factor p=0.2046. Column (Cell Line) Factor p=0.0451. N=4 biological replicates (1-2 technical replicates per biological replicate). Two-way ANOVA. No post-hoc multiple comparisons.

Raw Images of Electrophoretic Gels and Blots, uncropped, unprocessed

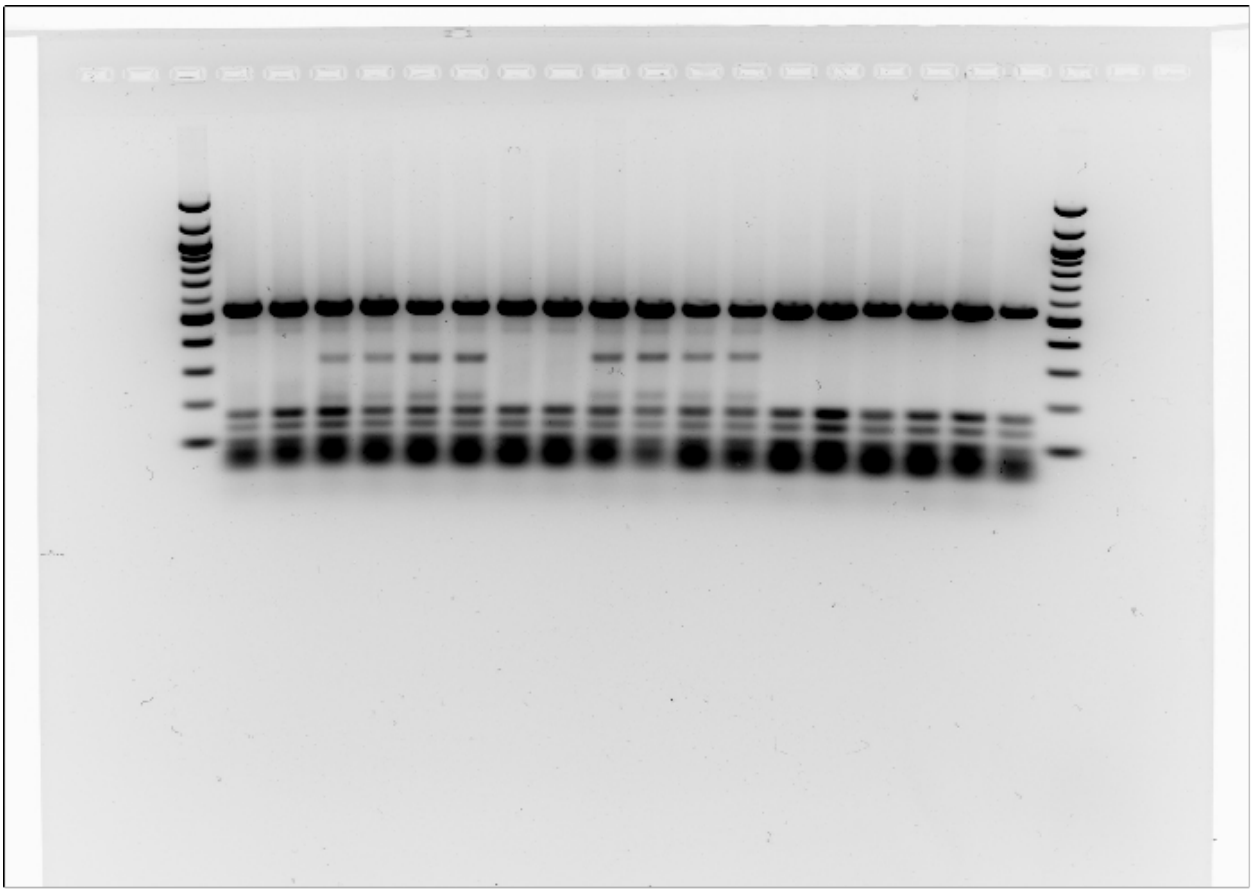

Electrophoretic Gel in Figure 2D. PCR amplicon from HAP1 cells. From left to right, Lane 1: NEB 100bp ladder, Lane 2-3: WT Non-targeting virus, Lane 4-5: WT CRISPR virus, Lane 6-7: WT under different experimental conditions (not comparable and not analyzed), Lane 8-9: αSyn KO Non-targeting virus, Lane 10-11: αSyn KO CRISPR virus, Lane 12-13: αSyn KO under different experimental conditions (not comparable and not analyzed), Lane 14-19: WT and αSyn KO samples not digested with T7E1, Lane 20: NEB 100bp ladder.

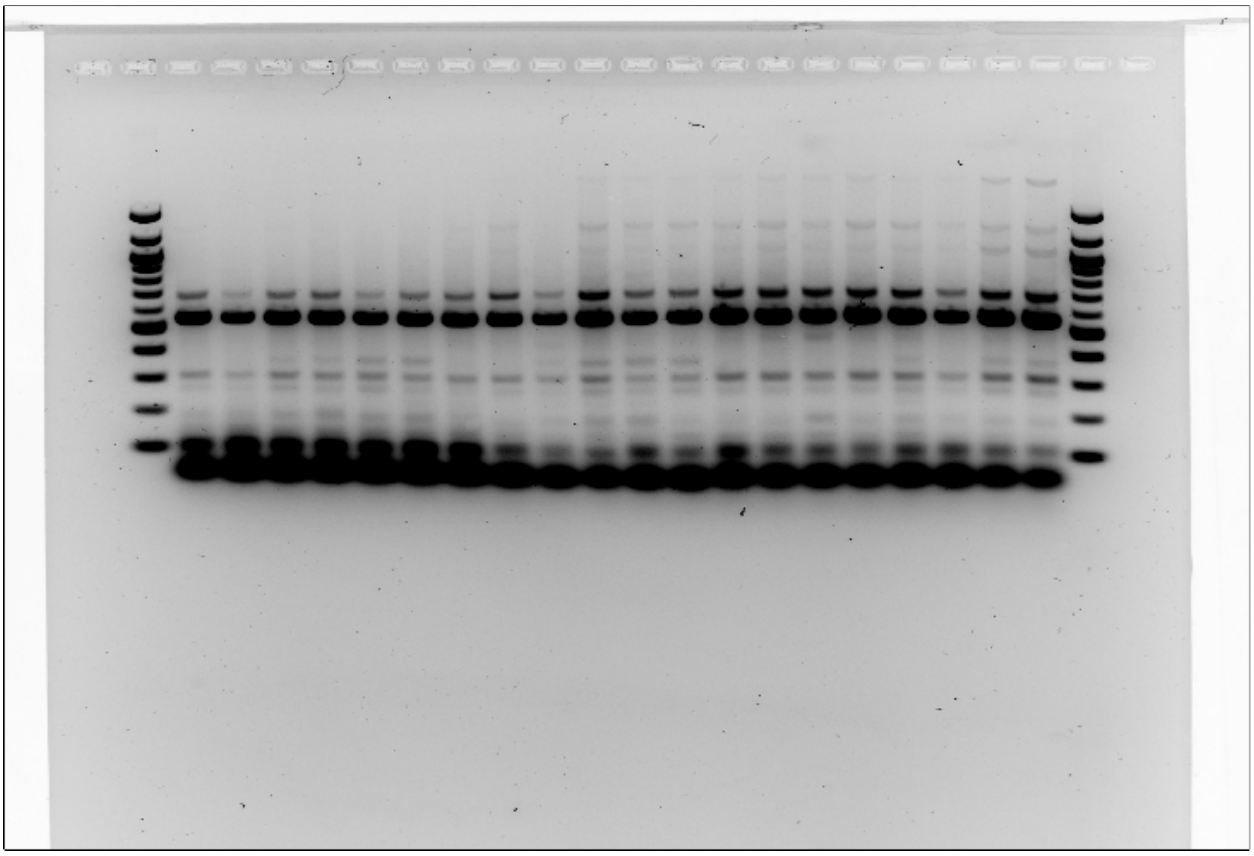

Electrophoretic Gel in Figure 3C. PCR amplicon from E18 cortical mouse neurons. From left to right, Lane 1: NEB 100bp ladder, Lane 2: WT Non-targeting virus, Lane 3: αSyn KO Non-targeting virus Lane 4-5: WT CRISPR virus, Lane 6-7: αSyn KO CRISPR virus. Lane 8-21: WT and αSyn KO samples under different experimental conditions (not comparable and not analyzed). Lane 22: NEB 100bp Ladder.

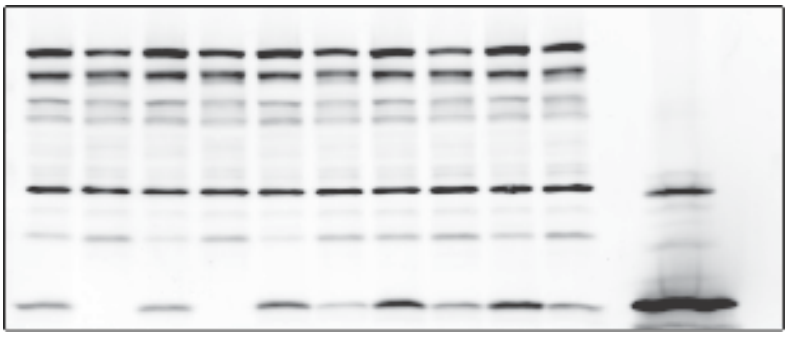

Western Blot in Supplemental Figure 2A (Left). HAP1 cell lysates stained with GAPDH loading control and αSyn antibodies. From left to right, Lane 1: WT HAP1 Not Transfected, Lane 2: αSyn KO HAP1 Not Transfected, Lane 3: WT HAP1 control plasmid, Lane 4: αSyn KO HAP1 control plasmid, Lane 5: WT HAP1 WT syn, Lane 6: αSyn KO HAP1 WT syn, Lane 7: WT HAP1 S129A, Lane 8: αSyn KO HAP1 S129A,

Lane 9: WT HAP1 S129D, Lane 10: αSyn KO HAP1 S129D, Lane 12: pSyn positive control.

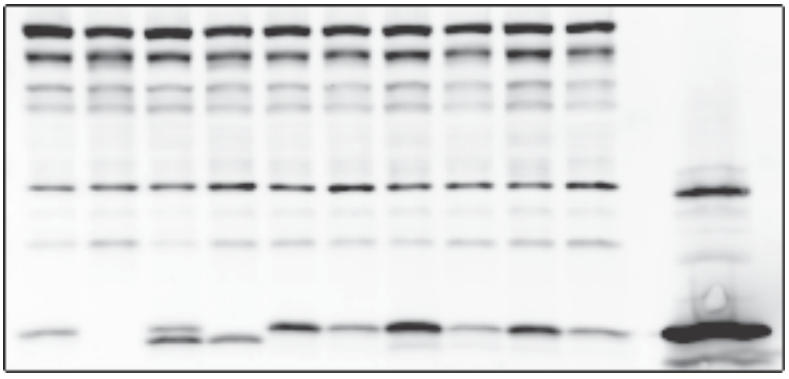

Western Blot in Supplemental Figure 2A (Right). HAP1 cell lysates stained with GAPDH loading control and αSyn antibodies. From left to right, Lane 1: WT HAP1 control plasmid, Lane 2: αSyn KO HAP1 control plasmid, Lane 3: WT HAP1 delNAC61-95, Lane 4: αSyn KO HAP1 delNAC61-95, Lane 5: WT HAP1 A53T, Lane 6: αSyn KO HAP1 A53T, Lane 7: WT HAP1 E46K, Lane 8: αSyn KO HAP1 E46K, Lane 9: WT HAP1 A30P, Lane 10: αSyn KO HAP1 A30P, Lane 12: pSyn positive control.

Chapter 3: αSyn and DNA Repair (Unpublished)

The data in Chapter 2 showed αSyn's modulation of DNA repair via a DNA-PK_{cs} regulated mechanism and an interesting connection between PLK inhibition, DSB histone modification levels and survival of inclusion-bearing neurons in a Lewy pathology mouse model. This project has undergone many iterations, redesigns, and changes based on where the data led us. Throughout the 5 years of this project, several other experiments have resulted in negative data or uninterpretable conclusions due to technical difficulties and therefore remain unpublished. These findings will be discussed here in chronological order, in which the most recent data will be presented last.

3.1 PARP inhibition decreases nuclear αSyn foci.

αSyn has not only been linked to DNA repair, but it has been associated with DNA damage, specifically with the DNA-damage response factor Poly ADP-Ribose (PAR). Nuclear αSyn foci co-localize with γH2AX and PAR in a human WT cell line and in mouse cortical neurons (Schaser et al., 2019). PAR has also been shown to promote pathologic αSyn formation and cell death, which is prevented by inhibition or genetic deletion of PAR Polymerase 1 (PARP1) (Kam et al., 2018). Because PAR and PARPs play an important role in DNA repair and cell death and are highly studied in the cancer field, many PARP inhibitors have been developed to kill tumors defective in BRCA1 or BRCA2 proteins through synthetic lethality. However, the PARP family has over 16 family members and PARP inhibitors can often target several members of the PARP family.

Since we have previously shown αSyn co-localizes with PAR, it would be useful to know which PARP is responsible for synthesizing the PAR that co-localizes with αSyn. Different PARPs have various roles in facilitating HR and NHEJ, and pinpointing the PARP that produces the specific PAR colocalizing with αSyn could help indicate which specific DNA repair mechanism αSyn is modulating. Here, we tested a panel of PARP inhibitors to investigate changes in levels of PAR, αSyn, and γH2AX and their co-localization.

Results

We quantified nuclear foci of PAR, αSyn, and γH2AX from human WT Hap1 cells treated with a panel of PARP inhibitors via IHC. We utilized 5 different PARP inhibitors: Veliparib (PARP1-2), Talazoparib (PARP1-2), G007 (PARP5a-5b), ITK413B (PARP1-2, 7), and RBN-pan (PARP6-8, 10-12, 14-16). All PARP inhibitors showed no significant effects on PAR production, but there was a trend of RBN-pan decreasing nuclear PAR foci (Figure 3.1.1). While it did not reach significance by a one-way ANOVA compared to other inhibitors, we do observe a significant decrease in PAR nuclear foci when conducting a dose response curve with RBN-pan (Figure 3.1.2). While other PARP inhibitors had widely different effects on αSyn and γH2AX levels, RBN-pan was the only inhibitor to both decrease αSyn levels and PAR levels (Figure 3.1.1), suggesting PARP6-8, 10-12, 14-16 may be involved in nuclear localization of αSyn. Reduction of PAR and αSyn foci via RBN-pan inhibition was also dose dependent (Figure 3.1.2). No changes in γH2AX levels or co-localization of PAR, αSyn, or γH2AX (not shown) after RBN-pan treatment were observed.

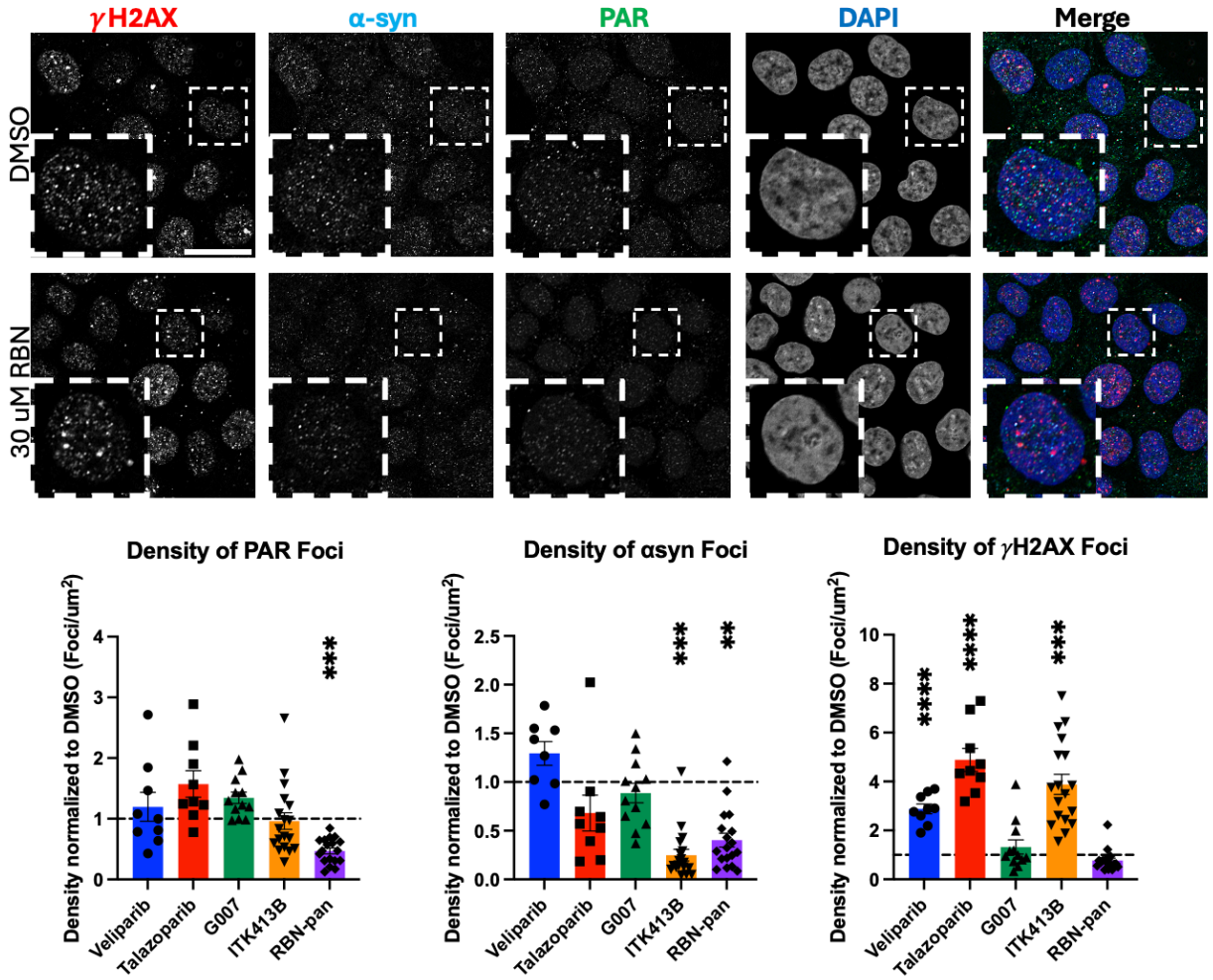

Figure 3.1.1. RBN-pan inhibition reduces PAR and αSyn levels in Hap1 cells via IHC. *Top:* IHC Representative images of RBN-treated Human Hap1 WT cells. *Bottom:* Quantification of nuclear PAR, αSyn, γH2AX after Veliparib, Talazoparib, G007, ITK413B, and RBN-pan treatment. Foci density normalized to DMSO condition. *Bottom Left:* Quantification of nuclear PAR foci. ANOVA summary p<0.0001. Post-hoc multiple comparisons show no significant differences between DMSO (1.000 ±0.22) and Veliparib (1.196 ±0.262) (p=0.9702), Talazoparib (1.573 ±0.309) (p=0.2165), G007 (1.345 ±0.203)(p=0.6938), and ITK413B (0.961 ±0.137)(p>0.9999), and RBN-pan conditions (0.470 ±0.049)(p=0.1759). Bottom *Center:* Quantification of nuclear αSyn foci. ANOVA summary p<0.0001. Post-hoc multiple comparisons show no significant difference between DMSO (1.000 ±0.228) and Veliparib (1.294 ±0.247) (p=0.6495), Talazoparib (0.682 ±0.172)(p=0.5402), and G007 (0.886 ±0.148)(p=0.9871). Significant decrease in αSyn foci with ITK413B (0.250 ±0.060) (p=0.0001) and RBN-pan (0.404 ±0.071) (p=0.0021). *Bottom Right*: Quantification of nuclear γH2AX foci. ANOVA summary p<0.0001. Significant increase of γH2AX foci between DMSO (1.000 ±0.224) with Veliparib (2.877 ±0.512) (p=0.0199), Talazoparib (4.886 ±0.898)(p<0.0001), and ITK413B (3.880 ±0.412)(p<0.0001). No significant difference observed with G007 (1.324 ±0.297) (p=0.9907) and RBN-pan (0.770 ±0.098)(p=0.9975). N=2-3 biological

replicates, 2 slides per biological replicate, 4-6 images per slide, 10-20 cells per image. One-way ANOVA. Post-hoc Tukey Multiple Comparisons.

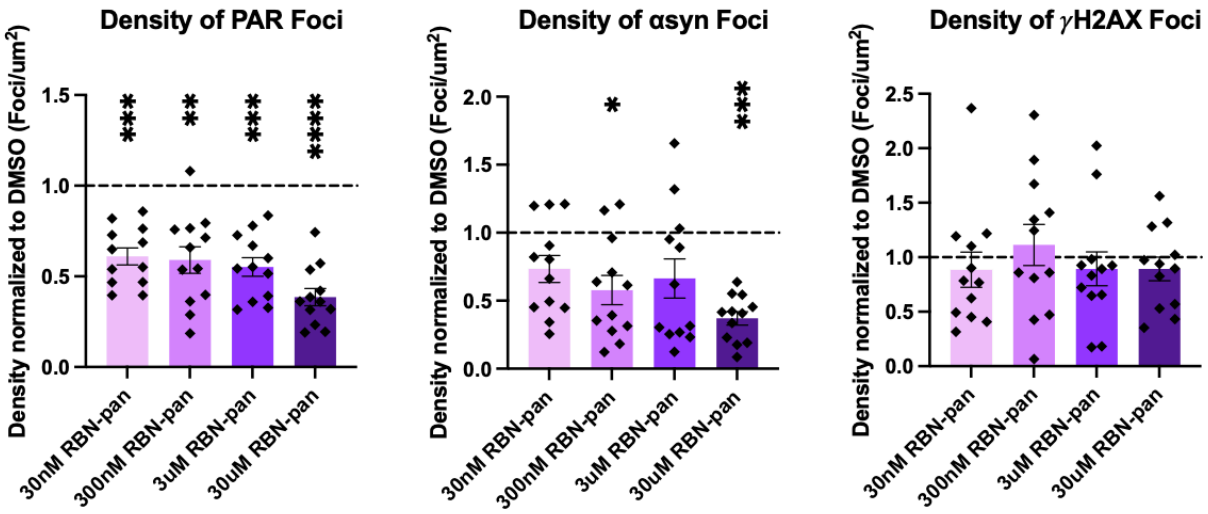

Figure 3.1.2. RBN-pan reduces PAR and αSyn foci in a dose dependent manner. IHC Quantification of nuclear PAR, αSyn, and γH2AX after 24-hour treatment of 30nM, 300nM, 3μM, and 30μM RBN-pan. *Left:* PAR foci density normalized to DMSO condition. ANOVA summary p<0.0001. Post-hoc multiple comparisons show RBN-pan significantly reduced nuclear PAR foci compared to DMSO (1.000 ±0.081) at 30nM (0.610 ±0.043) (p=0.0006), 300nM (0.590 ±0.067) (p=0.0003), 3μm (0.551 ±0.047) (p<0.0001), and 30μm (0.386 ±0.044) (p<0.0001) RBN-pan conditions. *Center:* αSyn foci density normalized to DMSO condition. ANOVA summary p=0.0047. Post-hoc multiple comparisons show no significant difference of αSyn foci density of DMSO treated cells (1.000 0.123) between 30nM (0.733 ±0.092) (p=0.4503), 300nM (0.578 ±0.099) (p=0.0717), and 3μm (0.664 ±0.133) (p=0.2238) RBN-pan conditions. RBN-pan significantly decreased nuclear αSyn foci at 30μm (0.0371 ±0.045) (p=0.0018). *Right:* γH2AX foci density normalized to DMSO condition. ANOVA summary p=0.5951. Post-hoc multiple comparisons show no significant difference of γH2AX foci density of DMSO treated cells (1.100 ±1.130) between 30nM (0.885 ±0.148) (p=0.7782), 300nM (1.113 ±0.174) (p>0.9999), 3μm (0.894 ±0.144) (p=0.7996), and 30μm (0.892 ±0.100) (p=0.7955) RBN-pan conditions. N=2 biological replicates, 2 slides per biological replicate, 6 images per slide, 10-20 cells per image. One-way ANOVA. Post-hoc Tukey Multiple Comparisons.

Discussion

Firstly, we found 1 out of 5 PARP inhibitors reduced the nuclear PAR foci staining. Additionally, the only PARP inhibitor to decrease PAR levels also reduced nuclear αSyn localization. This unpublished finding suggests that PARP6-8, 10-12, or 14-16 (inhibited by RBN-pan) is responsible for synthesizing the PAR that colocalizes with αSyn. This specific group of PARPs are more accurately named Mono ADP-ribose polymerases (MARPs) or MARylating enzymes because they covalently add a single molecule of ADP-ribose instead of polymeric chains. Once better inhibitors are developed in the future, narrowing down which of these MARylating enzymes could be modulating αSyn expression or localization could help indicate which DNA repair mechanism αSyn may be involved in.

Materials and Methods

Human Hap1 WT cells were maintained as previously described in Chapter 2 and seeded on PLL coated 1.5 coverslips. The next day, cells were treated with PARP inhibitors for 24 hours. 100μm Veliparib, 3μm Talazoparib, 1 μm G007, 30 μm ITK413B, and 30 μm RBN-pan were diluted in DMSO at 1000x stocks and stored at -80 °C. Cells were treated with PARP inhibitors at 1:1000 dilution in media. Cells were fixed, permeabilized, incubated in blocking buffer, and stained according to existing protocols (Schaser et al., 2019). Primary antibodies were used: anti-Syn1, 1:500 dilution, mouse monoclonal, BD Biosciences, cat. 610786; anti-Poly(ADP-Ribose) Polymer clone 10 H, 1:500 dilution, chicken polyclonal, Tulip BioLabs, cat. 1023; anti-Phospho-Histone H2A.X, 1:500 dilution, rabbit monoclonal, Cell Signaling, cat. 9718. Image analysis,

DAPI masking, nuclear volume calculation and nuclear foci quantification was performed on FIJI.

3.2 Whole genome sequencing of αSyn KO cells

Chapter 2 highlights the Next Generation Sequencing (NGS) work suggesting αSyn modulates DSB DNA repair, however other sequencing experiments have also been attempted. In the early stages of this project, we had hoped to use Whole Genome Sequencing (WGS) to investigate genome wide trends in mutations from mouse hippocampal brain regions with PFF induced αSyn pathology. It would be interesting to test if αSyn Lewy pathology leads to an increase in insertions/deletions (indels) as our overall hypothesis would suggest. As a preliminary experiment, we performed WGS on WT and αSyn KO human cells at baseline and after bleomycin treatment to induce widespread DNA DSBs throughout the genome.

Results

In order to test whether this WGS approach could comparing indel frequency across the genome in different samples, we submitted samples from WT and αSyn KO cells either treated with bleomycin (as a positive control to increase indel frequency) or water/vehicle (as the control). Our WGS confirmed that Hap1 cells are not fully haploid since portions of chromosomes 1 and 15 are diploid (Figure 3.2.1). It is believed that a fully haploid human cell line cannot survive in culture and specific genes found in these regions are required to be present at two copies for viability. It is important to note that Azenta formatted this data as default diploid samples, which is why the majority of the

WGS is shown at 2 copy numbers instead of 1 for haploid samples. Therefore, if all data is shifted down by 1 copy number, the orange portions of chromosome 1 and 15 are actually 2 and 3 copy number (Figure 3.2.1). When we compared indel percentage of samples treated with and without bleomycin, no obvious differences were observed, as we expected our positive control to show. Insertion and deletion percentages were exceptionally similar between all samples, suggesting this analysis of WGS was not suitable for detecting the low frequency of indel mutations at any one location that we are expecting (Table 3.2.2).

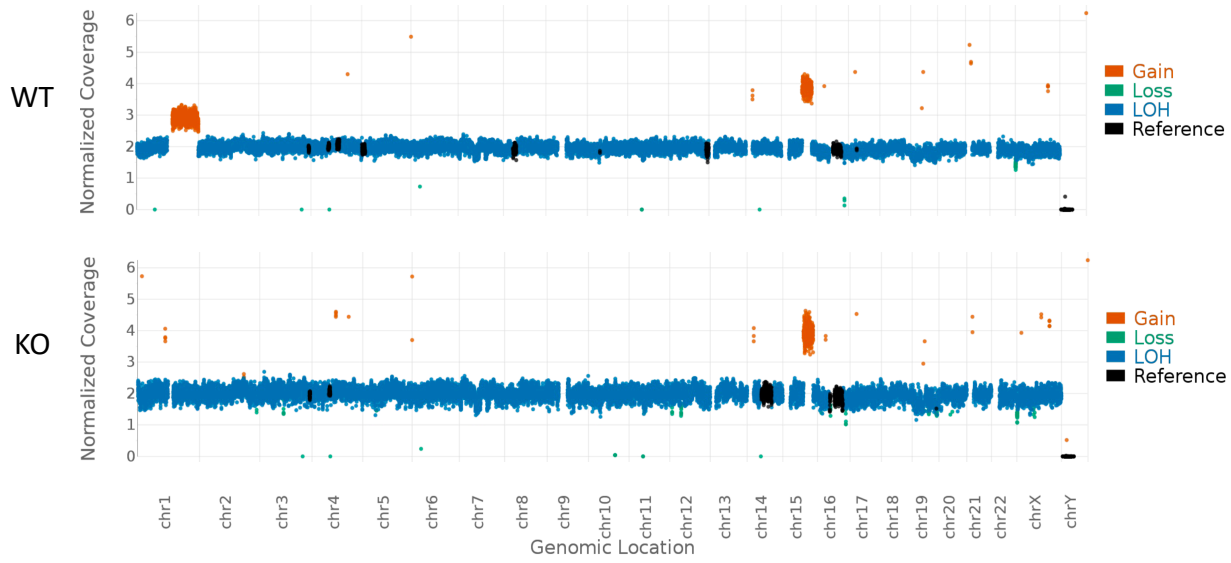

Figure 3.2.1. WGS of WT and αSyn KO Hap1 cells separated by chromosome. Copy number report from Azenta Life Sciences WGS from Human Hap1 WT and αSyn KO cells at baseline. Loss of Heterozygosity (LOH) indicating haploid status in blue, with genetic copy number gains (orange) and losses (green). The reference sequences (black) were used to align sequenced reads.

Table 3.2.2. Indel percent of WT and αSyn KO Hap1 cells treated with bleomycin.

Sample	Total Reads	Total Indels	Indel Percent (%)	Total Deletions	Deletion Percent (%)	Total Insertions	Insertion Percent (%)
WT CTL	355509094	721783	0.203	372204	0.105	349579	0.098
WT BLEO	356449322	719824	0.202	370556	0.104	349268	0.098
KO CTL	339939586	712460	0.210	368376	0.108	344084	0.101
KO BLEO	352369821	716658	0.203	369802	0.105	346856	0.098

Discussion

Because of difficulties in trying to validate this approach for comparing genome wide mutation profiles between samples even in our positive control samples, we concluded that WGS done in this way was not a viable experimental strategy for our purposes. We went through many rounds of working with Azenta representatives and several different analysis software packages to try to detect possible increases in indel frequency in our positive control condition, but no significant differences were detected. We confirmed the bleomycin treatment was causing an increase in DSB levels in cells via IHC (not shown); thus, we hypothesized that indel percentage was too low across the genome to detect changes between samples with these approaches and we decided to not pursue this line of inquiry.

Materials and Methods

Human Hap1 WT and αSyn KO cells were seeded to be ~70% confluent the following day. Cells were maintained according to protocols previously described in Chapter 2 and then treated either with water or Bleomcyin 10 μg/mL for 24 hours. Cells were lysed with the exact lysis buffer from CRISPR/Cas9 DSB repair assays. Cell lysates were harvested and submitted to Azenta Life Sciences on dry ice under the company's instructions.

3.3 Optimization of CRISPR/Cas9 DSB repair assay

Previously, our group has shown that αSyn modulates DNA DSB repair after damage induced by bleomycin. We have also shown that αSyn modulated DSB repair in a plasmid reporter system. However, to our knowledge, no one has ever investigated the role of αSyn in modulating repair after a single, predefined DSB has been introduced into the genome. Therefore, we developed a novel protocol using a CRISPR/Cas9 lentivirus to introduce a single DSB into the genome of human Hap1 cells. Because no protocol existed for doing this in our lab before, many preliminary experiments were conducted to optimize this protocol for my use and for the future. We compared different lentiviruses targeting the DNA Methyltransferase 3 Beta (DNMT3b) or Peptidylprolyl Isomerase B (PPIB) gene, encoding for a cyclosporine binding protein in the endoplasmic reticulum, as well as optimized different types of selection protocols post transduction. Furthermore, we determined the exact size of PCR product to amplify

around the repair region to detect the maximum differences in gene editing between samples. The unpublished data from these optimization experiments is presented here.

Results

We investigated two commercially available lentiviruses targeting the DNMT3b and PPIB gene to test how the DSB repair varied across the genome. We found that αSyn modulated DSB repair of the DNMT3b gene (Chapter 2, Figure 2), but the PPIB targeting virus data only showed a trend in this direction when indel frequency was tested with NGS, but the T7 Endonuclease I gel enzymatic assay suggested indel frequency was significantly increased in αSyn KO cells compared to WT cells at low multiplicities of infection (MOI) (Figure 3.3.1).

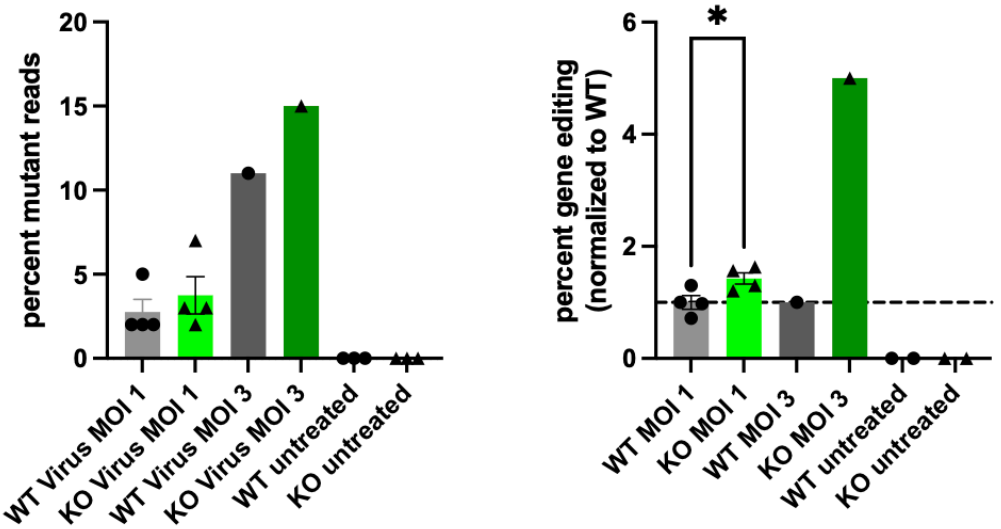

Figure 3.3.1. αSyn trends to modulate DSB repair after PPIB targeting lentiviral transduction. *Left:* NGS of 260 bp PCR product from WT and αSyn KO Hap1 cells transduced with PPIB targeting DSB inducing CRISPR/Cas9 lentivirus at multiplicity of infection (MOI) 1.0 or 3.0. No significant difference of percent of mutant reads between WT (2.750 ±0.750) and αSyn KO cells (3.750 ±1.109) (p=0.4832). *Right:* T7 Endonuclease 1 assay of 505bp PCR product from WT and αSyn KO Hap1 cells under exact conditions. αSyn KO percent gene editing normalized to WT corresponding condition. Percent gene editing significantly increased in αSyn KO cells (1.427±0.101)

compared to WT cells (1.000 ±0.120) (p=0.0345). N=1-2 biological replicates, 1-2 technical replicates per biological replicate. Two-tailed student's t-test.

All lentiviruses discussed so far also express GFP to collect data on transduction efficiency, however puromycin selective lentiviruses are also commercially available. Experiments with a puromycin selective lentivirus targeting the DNMT3b gene also showed a significant difference between DSBR gene editing between WT and αSyn KO samples, but only under certain lentiviral Multiplicity of Infection (MOI) conditions and only with NGS analysis and not the T7EI enzymatic assay, although consistent trends in this direction were seen (Figure 3.3.2).

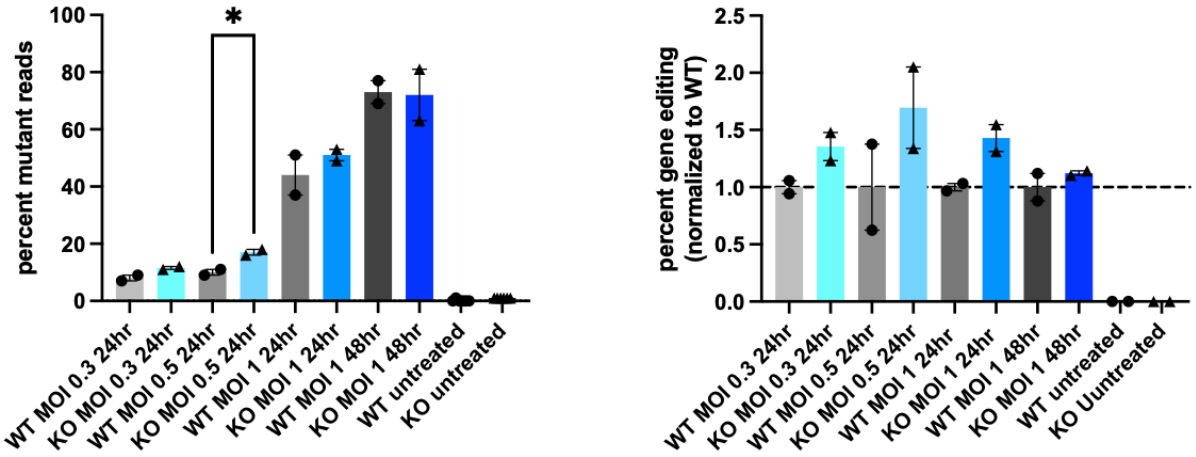

Figure 3.3.2. αSyn trends to modulate DSB repair after puromycin selective lentiviral transduction. *Left:* NGS of 288bp PCR product from WT and αSyn KO Hap1 cells transduced with Puromycin selective DSB inducing CRISPR/Cas9 lentivirus at MOI 0.3, 0.5, or 1.0. Puromycin selection at 1 µg/mL started at 24 or 48 hours post transduction. Percent mutant reads at MOI 0.5 significantly increased in αSyn KO cells (17.000 ±6.224) compared to WT cells (10.000 ±3.679) (p=0.0385). No significant difference of percent of mutant reads at MOI 0.3 between WT (8.000 ±2.955) and αSyn KO cells (11.500 ±4.205)(p=0.0887), at MOI 1.0 with 24 hour puromycin selection between WT cells (44.000 ±16.369) and αSyn KO cells (51.000 ±18.644)(p=0.4377), and at MOI 1.0 with 48 hour puromycin selection between WT cells (73.000 ±26.716) and αSyn KO cells (72.000 ±26.597)(p=0.9284). *Right:* T7 Endonuclease 1 assay of 544bp PCR product from WT and αSyn KO Hap1 cells under exact conditions. αSyn KO percent gene editing normalized to WT corresponding condition. No significant

difference of percent of gene editing at MOI 0.3 between WT (1.000 ±0.058) and αSyn KO cells (1.355 ±0.123) (p=0.1209), at MOI 0.5 between WT (1.000 ±0.376) and αSyn KO cells (1.694 ±0.357) (p=0.3122), at MOI 1.0 with 24 hour puromycin selection between WT cells (1.000 ±0.032) and αSyn KO cells (1.430 ±0.117) (p=0.0716), and at MOI 1.0 with 48 hour puromycin selection between WT cells (1.000 ±0.119) and αSyn KO cells (1.123 ±0.019) (p=0.4154). N=1-2 biological replicates, 1-2 technical replicates per biological replicate. Two-tailed student's t-test.

We not only optimized the transduction protocol with various lentiviruses, but also the PCR protocol for the length of the repair junction amplicon that was amplified for subsequent T7EI enzymatic assay. We tested 2 Kb and 8 Kb PCR product amplicons to investigate whether larger deletions that might occur after DSB repair could be detected between WT and αSyn cells. No significant differences were found between WT and αSyn KO cells with the 2 Kb or 8 Kb PCR products, although once again consistent trends were seen (Figure 3.3.3). NGS to sequence potential large deletions was not performed due to size limitations of NGS analysis.

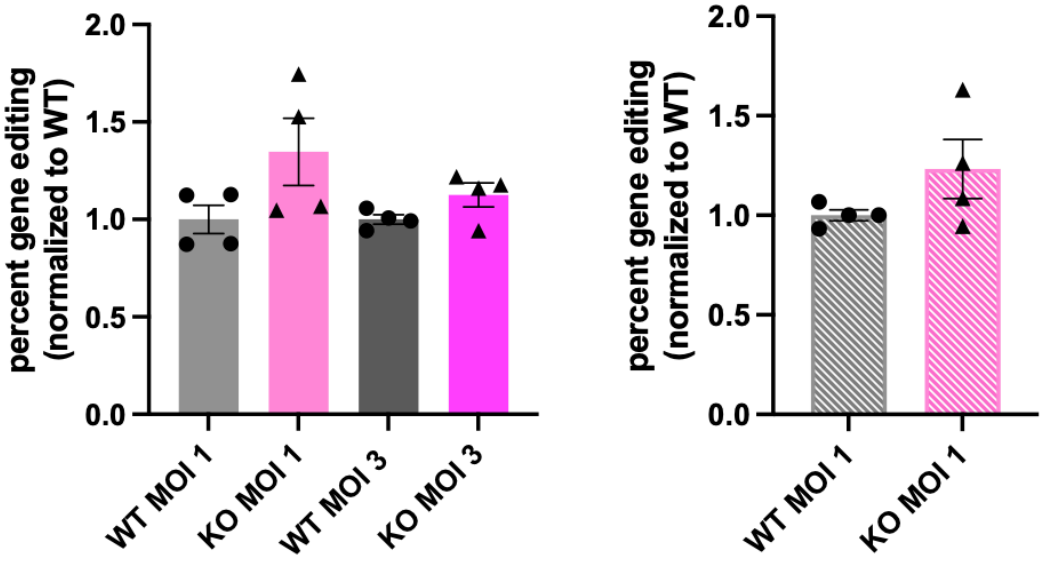

Figure 3.3.3. Trend of increased gene editing of αSyn KO cells with 2Kb and 8Kb PCR products. T7 Endonuclease 1 assay of 2 Kb and 8 Kb PCR products from WT and αSyn KO Hap1 cells transduced with DNMT3b targeting DSB inducing lentivirus at MOI 1.0 or 3.0. *Left:* 2Kb PCR Product. No significant differences of percent gene editing at MOI 1.0 between WT (1.000 ±0.072) and αSyn KO cells (1.347 ±0.173)

(p=0.1141) and at MOI 3.0 between WT (1.000 ±0.023) and αSyn KO cells (1.125 ±0.062)(p=0.1075). *Right:* 8Kb PCR Product. No significant differences of percent gene editing at MOI 1.0 between WT (1.000 ±0.028) and αSyn KO cells (1.232 ±0.148) (p=0.1749). N=2 biological replicates, 2 technical replicates per biological replicate. Two-tailed student's t-test.

Discussion

When finalizing the protocol for the CRISPR lentiviral DSB repair assay, we selected the EGFP DNMT3B lentivirus and 544bp PCR product to conduct experiments discussed in Chapter 2. We did this because our optimization experiments with puromycin selective lentivirus, PPIB targeting lentivirus, and 2 Kb and 8 Kb amplicons all appeared less sensitive at detecting differences between groups. The T7EI gel enzymatic assay with 2 Kb and 8 Kb repair junction amplicons also technically more difficult, which we could not prevent even after altering primer concentration, PCR protocol, or storage or thermal cycler settings. Due to these roadblocks, we did not continue experiments with 2 Kb and 8 Kb products and did not proceed with sequencing experiments to attempt to detect larger range deletions after DSB repair. This could be an interesting avenue in the future once further optimization to amplify larger PCR products is performed.

Materials and Methods

All DSB repair CRISPR/Cas9 lentiviral experiments were conducted following protocols from Chapter 2 (Rose et al., 2024). PPIB targeting EGFP lentivirus was commercially purchased from Horizon Discover (#VSGH12107) as well as *DNMT3b* targeting puromycin selective lentivirus (#VSGH11974). Puromycin selection at 1 µg/mL either began 24 hours or 28 hours after lentiviral transduction and was diluted 1:1000 in

cell culture media. Volume of lentivirus was calculated by V=MOI x CN ÷ VT x 1000, where CN is the cell number in the well at transduction and VT is the viral titer in transduction units/mL. After cells lysis, repair junctions of 544 bp, 2 Kb, or 8 Kb amplicons were amplified via PCR for subsequent T7EI gel enzymatic assay. A separate 288bp amplicon was amplified for NGS (see Chapter 2 methods). 544 bp primers (see Chapter 2 methods). 2 Kb primers: Forward: TCAAGTGATTCTCTCCTCAGCCT. Reverse: GGAGGAAATGAGCTGCTGTG. 8 Kb primers: Forward: CATGCCCCAATTGCAGCTG. Reverse: CACACTTCACTAAGTGGCAGA.

3.4 Inhibition of Pol θ and PLK do not affect αSyn's modulation of DSB repair.

In Chapter 2, we displayed several CRISPR lentiviral DSB repair experiments with the addition of pharmacological inhibitors. We showed that αSyn's modulation of DSB repair was not affected by Pol θ inhibition (Chapter 2, Figure 4), and our data on the effects of PLK 1/3 inhibition on WT and αSyn KO cells was inconclusive (Chapter 2, Supplementary Figure 4). We also performed further experiments with several other Pol θ and PLK family inhibitors in order to fully investigate their roles. Discovering that αSyn's modulation of DSB repair is affected by Pol θ or PLK inhibition would give insight into the mechanism of how αSyn is modulating DSB repair, which motivated these experiments.

Results

It is important to determine which pathway of DSB repair αSyn could be modulating. Pol θ is the DNA polymerase responsible for alt-NHEJ, which makes it an attractive target for blocking the alt-NHEJ pathway. Therefore, we tested if Pol θ inhibition via Novobiocin would alter or prevent the increase in indel frequency seen in αSyn KO cells. We found that the addition of Novobiocin did not change the previously seen effect on indel frequency in αSyn KO cells (Figure 3.4.1). We did not see a significant difference between WT and αSyn KO cells treated with DMSO, but this effect was trending.

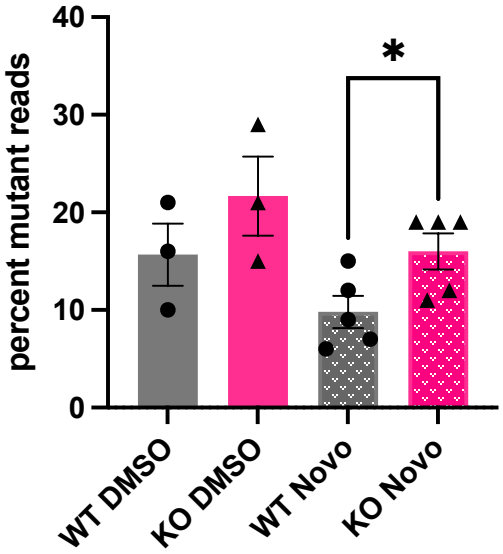

Figure 3.4.1. Inhibition of Pol θ does not affect αSyn's modulation of DSB repair. NGS of 288bp PCR product from WT and αSyn KO Hap1 cells transduced with DSB inducing CRISPR/Cas9 lentivirus and treated with Pol θ Inhibitor Novobiocin at 100μM or DMSO. Percent mutant reads significantly increased in αSyn KO cells treated with Novobiocin (16.000 ±1.844) compared to WT cells (9.800 ±1.655) ($p=0.0368$). No significant difference of percent of mutant reads DMSO treated WT (21.667 ±5.753) and

αSyn KO cells (15.667 ±4.214) (p=0.3090). N=3 biological replicates, 1-2 technical replicates per biological replicate. Two-tailed student's t-test.

The PLK family is thought to be the most important kinase that phosphorylates αSyn at S129. Investigating whether PLK inhibition would prevent the increase in indel frequency seen in αSyn KO cells would reveal that S129 phosphorylation could be involved mechanistically in how αSyn modulates DSB repair. PLK family (PLK 1, 2, 3 and 4) inhibition via BI2536 did not significantly increase indel frequency in αSyn KO cells, although a trend was observed when compared to WT cells (Figure 3.4.2). This was observed both in NGS analysis and T7EI gel enzymatic assays. Unfortunately, however, BI2536 was toxic to cells at the concentration needed to inhibit all 4 PLK family members. This roadblock made results difficult to interpret, so we transitioned to testing inhibition of individual PLKs, 1, 2, 3, and 4, with Tak960, TC-S-7005, GW84362X, and Centrinone, respectively. No significant differences were detected (Figure 3.4.3).

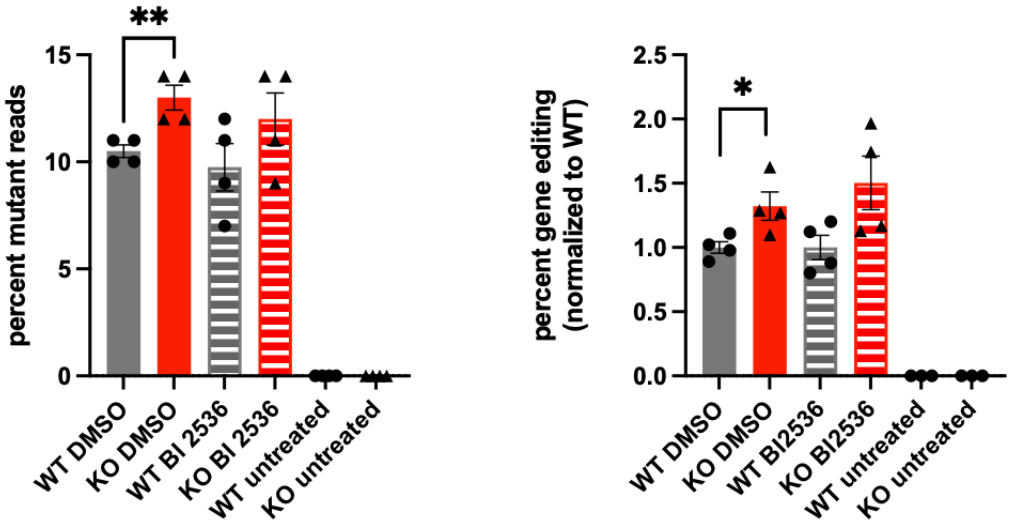

Figure 3.4.2. Inhibition of PLK Family does not affect αSyn's modulation of DSB

repair. *Left:* NGS of 288bp PCR product from WT and αSyn KO Hap1 cells transduced with DSB inducing CRISPR/Cas9 lentivirus and treated with PLK family inhibitor BI2536 at 1nM or DMSO. Percent mutant reads significantly increased in DSMO treated αSyn KO cells (13.000 ±0.577) compared to WT cells (10.500 ±0.289) (p=0.0082). Trending, but no significant difference of percent of mutant reads BI2536 treated WT (9.750 ±1.109) and αSyn KO cells (12.000 ±1.225) (p=0.2221). *Right:* T7 Endonuclease 1 assay of 544bp PCR product from WT and αSyn KO Hap1 cells treated with BI2536 or DMSO. αSyn KO percent gene editing normalized to each WT corresponding condition. Percent gene editing significantly increased in DSMO treated αSyn KO cells (1.321 ±0.110) compared to WT cells (1.000 ±0.045) (p=0.0359). Trending, but no significant difference of percent of gene editing of BI2536 treated WT (1.000 ±0.096) and αSyn KO cells (1.503 ±0.209) (p=0.0711). N=2 biological replicates, 2 technical replicates per biological replicate. Two-tailed student's t-test.

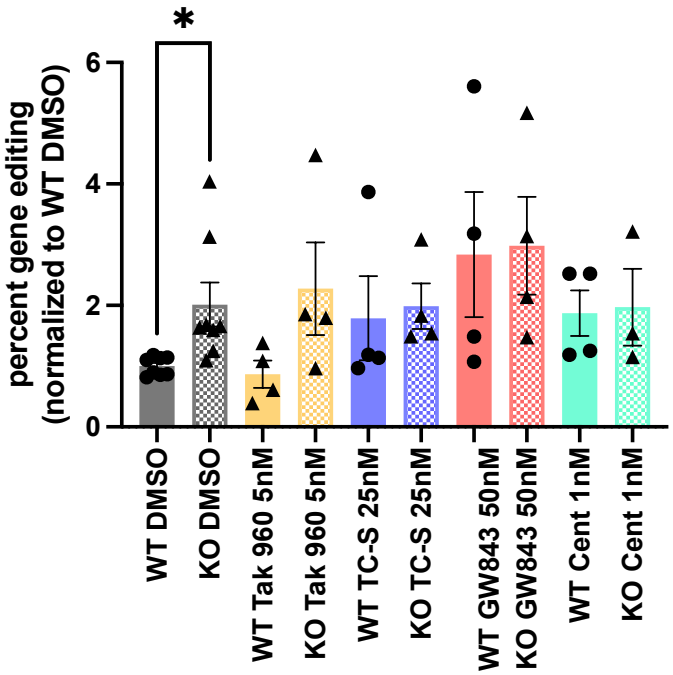

Figure 3.4.3. Individual inhibition of PLK 2, 3, and 4 prevents increased indel frequency previously seen in αSyn KO cells. T7EI Gel Enzymatic Assay of 544bp PCR product from WT and αSyn KO Hap1 cells transduced with DSB inducing CRISPR/Cas9 lentivirus and treated with PLK 1 Inhibitor Tak-960, PLK 2 Inhibitor TC-S-7005, PLK 1/3 Inhibitor GW84362X, PLK 4 Inhibitor Centrinone or DMSO. Samples normalized to WT DMSO condition. Percent gene editing significantly increased in DMSO treated αSyn KO cells (2.014 ±0.362) compared to WT cells (1.000 ±0.054) (p=0.0150). No significant difference of percent gene editing of Tak-960 treated WT (0.869 ±0.275) and αSyn KO cells (2.276 ±0.787) (p=0.1268), TC-S-7005 treated WT (1.790 ±0.660) and αSyn KO cells (1.988 ±0.585) (p=0.8098), GW84362X treated WT

cells (2.836 ±0.1015) and αSyn KO cells (2.983 ±0.956) (p=0.9147), or Centrinone treated WT cells (1.872 ±0.558) and αSyn KO cells (1.970 ±0.679) (p=0.8923). N=4 biological replicates, 2 technical replicates per biological replicate. Two-tailed student's t-test.

Discussion

Adding specific pharmacological manipulations to our established CRISPR/Cas9 DSB repair assay was attempted in order to provide insight into the mechanism of these effect. Unfortunately, some of these results were difficult to interpret. This was the case for Pol θ inhibition experiments in which NGS data suggested that Novobiocin did not prevent αSyn's modulation of DSB repair (Figure 3.4.1). However, we received feedback from others in the field that more selective compounds for inhibiting Pol θ exist compared to Novobiocin, and also that Novobiocin can alter other pathways, like single stranded DNA binding and translocation (Pismataro et al., 2023). This is why we attempted this experiment again with another Pol θ inhibitor, ART558, as shown in Chapter 2, Figure 4.

Manipulation of the DSB repair assay system with PLK inhibitors was also difficult to interpret. While the increase in indel frequency associated with αSyn KO cells disappeared under pan-PLK inhibition (BI2536, Figure 3.4.2) and specific PLK 2, 3, and 4 inhibitor treatment (Figure 3.4.3), these were small effects. BI2536 treated αSyn KO cells did not reach statistical significance, but there was a clear trend. This signaled to us that BI2536 had no effect on this system. Also, the data from PLK 1, 2, 3, and 4 individual inhibition was highly variable. We were hesitant to make firm claims on this data, as several more experiments would be needed to confirm that the small trends seen could be interpreted as these drugs having no effect on this system. We continued experiments with the PLK 1/3 inhibitor GW84362X because it was the most promising

inhibitor in terms of detecting changes in indel frequency in both WT and αSyn KO cells. We extended this experiment by testing PLK 1/3 inhibition in E18 primary cortical cultured neurons but found inconsistent results with this system as well (Chapter 2, Supplementary Figure 4). In the future, it would be of great interest to implement a cocktail of individual PLK inhibitors to avoid toxic effects of BI2536 or use non-pharmacologic approaches to genetically knockout PLK. It would also be interesting to repeat these CRISPR DSB repair assays in commercially available PLK 2 or PLK 3 KO Hap1 cell lines to answer this question more precisely.

Materials and Methods

All CRISPR/Cas9 lentiviral DSB repair assay methods were performed following exact protocols described in Chapter 2 (Rose et al., 2024). Deviations from this protocol include the addition of 100 uM Novobiocin Sodium (selleckchem #S2492), 1 nM BI2536 (selleckchem #S1109), 5 nM Tak-960 (selleckchem #S1239), 25nM TC-S-7005 (MedChemExpress #HY-108597), 50 nM GW84362X (selleckchem #S2880), 1 nM Centrinone (selleckchem #S7837) all diluted in DMSO and added to cell culture media at 1:1000 for 72 hours at start of transduction.

3.5 PLK family inhibition does not affect αSyn inclusion formation nor minimum average life span.

In Chapter 2, we provided evidence suggesting PLK family inhibition led to increased survival rate of cells bearing αSyn inclusions. This data was only including cells that already present and bearing αSyn inclusions at the start of the *in vivo* imaging

experiment. In order to test survival curves from comparable groups of cells (Chapter 2, Figure 5), we excluded cells that formed new inclusions after the start of the longitudinal imaging. These cells' formation rate and lifespan are analyzed and discussed below.

Results

Cortical regions of PFF injected mice were imaged *in vivo*, longitudinally tracking when αSyn spread to new cells and those cells' lifespans. In order to test the effects of PLK family inhibition, we imaged cortical mouse brain at baseline and continued imaging during a 2-week BI2536 or saline IP injection treatment. We found no significant differences between the formation of neuritic inclusions between saline and BI2536 treated groups before or after drug treatment (Figure 3.5.1). We also detected no difference in average minimum lifespan of these cells bearing newly formed inclusions overall (data not shown) or when binned into separate categories based on formation time and cell death time in relation to the drug treatment start (Figure 3.5.2). This lifespan is displayed as "minimum" because this data set includes cells bearing inclusions that did not die during the imaging window. These cells' death point is unknown and therefore their life spans are deemed as their minimum life spans. 31 out of 84 cells bearing inclusions were still living on the last day of *in vivo* imaging, but results and statistical significance remains unchanged if excluded (not shown).

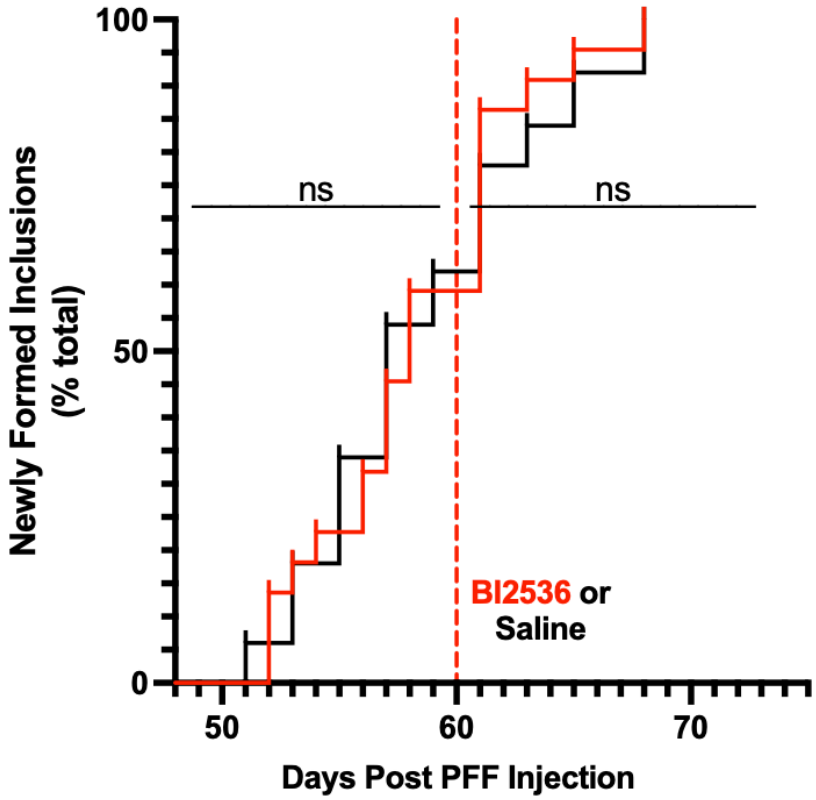

Figure 3.5.1. PLK family inhibition does not affect formation of αSyn inclusions. αSyn inclusion formation analysis across 25 days of longitudinal *in vivo* imaging of cortical regions in mice treated with saline (black) or PLK 1/2/3/4 Inhibitor BI2536 (red) (15 mg/kg) IP injections for 2 weeks starting day 60 post PFF injection. No significant difference between saline or BI2536 treated groups. Overall, Mantel-cox test p=0.7112. Pre BI2536/saline treatment p=0.8788. Post BI2536/saline treatment p=6311. Saline treated group N= 4 animals. BI2536 treated group N=4 animals. 69 neuritic inclusions counted. Mantel-cox test.

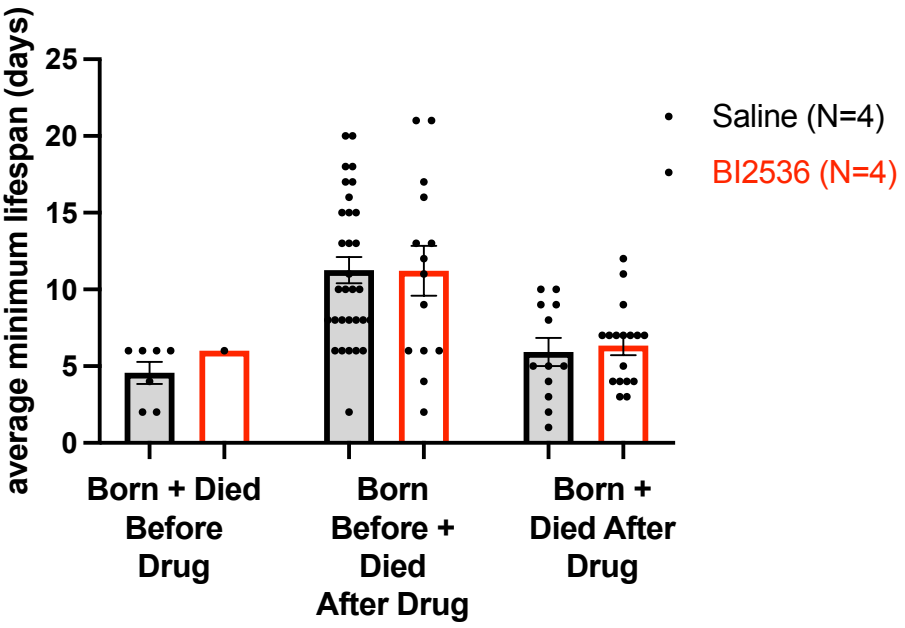

Figure 3.5.2. PLK family inhibition does not affect average minimum lifespan of cells with somatic inclusions. αSyn inclusion analysis of mouse cortex longitudinally imaged *in vivo* across 25 days in mice treated with saline or PLK 1/2/3/4 Inhibitor BI2536 (15 mg/kg) IP injections starting day 60 post PFF injection for 2 weeks, twice per week. Inclusions sorted into 3 categories if inclusions were formed "born" and cells bearing these inclusions died before drug treatment began, if inclusions were born before drug treatment and cells died after drug treatment, and if inclusions were born and cells died after drug treatment began. No significant differences of average minimum lifespan observed in inclusions born and died before treatment between saline (4.571 ±0.719) and BI2536 treated mice (6.000 ±0.000) (p=0.5087), in inclusions born and died after treatment between saline (11.258 ±0.860) and BI2536 treated mice (11.214 ±1.621) (p=0.9793), or in inclusions born and died after treatment between saline (5.917 ±0.917) and BI2536 mice (6.353 ±0.636) (p=0.6889). N=4 mice per group, 84 inclusions counted. Two-tailed student's t-test.

Discussion

As we are most interested in the connection between αSyn inclusions and cell death, cell survival analysis (Chapter 2, Figure 5) is the way we chose to investigate this question. We concluded that PLK inhibition led to an increase of survival rate in cells bearing αSyn inclusions that were present at the start of imaging. However, αSyn

inclusion formation and average life span are factors that can be measured from the cells that formed new inclusions after the start of imaging. Here, we described that PLK inhibition caused no observable changes to inclusion formation or average minimum life span (Figure 3.5.1 and Figure 3.5.2). It is curious how PLK inhibition led to a significant increase in survival rate but not minimum life span. It is possible that newly born inclusions are physiologically different from older established inclusions and that PLK inhibition affects these cells differently. One theory is that older established inclusions may be more dense of an aggregate with αSyn and other organelle and debris accumulation that it changes the biology of how PLK interacts with αSyn. In order to answer this question more directly, imaging for a longer period of time may be helpful to parse apart newer inclusions from older ones and study them separately. It will never be a perfect experiment where you can track the full lifespan of every cell because some inclusions will be born before imaging and not all of them will die before the imaging window ends. We have performed an extended longitudinal imaging experiment up to 180 days in WT and PLK2 KO mice and found similar neuroprotection (Weston et al., 2021), but this extended timeframe was deemed not necessary to test the short-term effects of PLK inhibition.

The question still remains of how S129 phosphorylation plays a role in this mechanism. As earlier stated, PLK inhibition did not lead to decreased S129 phosphorylation as predicted and instead caused an increase in total αSyn levels, which we interpreted as due to a decrease in αSyn degradation given previous work done in the field (Oueslati et al., 2013). This change in αSyn levels is associated with increased survival rate of cells bearing αSyn inclusions, yet no change in inclusion formation and

minimum life span. It also remains unclear how these effects are also associated with increased nuclear DSB levels (Chapter 2, Figure 6). Further investigation is needed to parse apart how these effects are mechanistically related and whether increased DSB levels is downstream or upstream of decreased αSyn degradation.

Materials and Methods

The PFF cortical injection protocol and *in vivo* imaging protocol was performed exactly the same as previously described in Chapter 2 (Rose et al., 2024). Figures from Chapter 3.5 were graphed and statistically analyzed with Prism Graphpad 10.0 software with inclusion formation graphs plotted as the inverse of survival curves.

Chapter 4: Discussion and Future Directions

4.1 Plasmid reporter and CRISPR/Cas9 lentiviral system

In this dissertation, we report that DNA DSB repair is altered in the absence of αSyn. In a loss-of-function plasmid GFP reporter system, αSyn KO Hap1 cells repair DSBs using NHEJ less efficiently than WT cells (Chapter 2, Figure 1). This impairment of NHEJ in αSyn KO cells was not seen using a plasmid GFP HR reporter, giving us our first indication that αSyn could be modulating or shifting repair towards NHEJ rather than HR. We expanded upon this work by testing whether genomic DNA DSB repair is also affected by the loss of αSyn. After introducing a single DSB into the genome using a CRISPR/Cas9-expressing lentivirus, we found that indel frequency is increased in the absence of αSyn in human cells and mouse primary cultured cortical neurons (Chapter 2, Figure 2-3). NHEJ can either happen faithfully, or with substitutions, insertions, or deletions. This increased indel frequency indicates that cells are not repairing DSBs efficiently and faithfully. We cannot detect faithful repair events with this approach because it is masked by un-repaired DNA, but the repair events that create mutations are important to fully understand as the health of the cell can depend on the prevention of consecutive mutations, ultimately leading to detrimental consequences. Although it is possible that αSyn functions as part of the molecular machinery of NHEJ, our data is more consistent with a function that shifts DSB repair towards sub-forms of c-NHEJ that have a lower frequency of small indels. The deletion spectrum we see in WT and αSyn KO cells looks identical (Figure 2-3), suggesting αSyn is not involved in the specific machinery of NHEJ. We would expect the deletion spectrum to change if this was the

case, but instead we see differences in the fraction of repair products with indels, implicating αSyn in an upstream choice of the cell to shift DSB repair towards c-NHEJ.

One caveat of the CRISPR DSB repair assays is that all reported significant differences between αSyn KO and WT cells were after an introduction of DSB into the DNMT3b gene which encodes for a DNA methyltransferase that can function in DNA repair to remove premutagenic DNA lesions (Sekiguchi & Sakumi, 1997). The DNA methyltransferase family, specifically DNMT1, has been implicated in microsatellite instability and mismatch repair (Jin & Robertson, 2013). While DNMTs, which catalyze DNA methylation, are linked to other types of DNA repair, no direct effect on DSB repair machinery exists currently (Jin & Robertson, 2013). Disrupting the DNMT3b gene with a DSB could cause abnormalities, however several instances of methyltransferase compensation have been documented, so compensation could also be at play here (Elliott et al., 2016; Scelfo et al., 2024). Furthermore, genetic deletion of DNMT3b can lead to increased rates of NHEJ and decreased rates of HR (Steinberg et al., 2023). While one DSB in DNMT3b is unlikely to cause dramatic changes in DSB repair pathway rates, nonetheless, it is vital to test whether this effect of αSyn loss increasing indel frequency will hold when the DSB is occurring in other genes. Preliminary optimization experiments in the PPIB gene were performed and showed similar trends, but were not continued as larger effects were seen with the DNMT3b targeting lentivirus (Figure 3.3.1). In the future, using lentiviruses to target other genes throughout the genome will be important to test the generalizability of the effects we have detected. Previous work from the Unni Lab has shown that there are hotspots in the genome where DSBs are programmed to upregulate transcription of immediate early genes and

this can alter synaptic plasticity and learning and memory (Weber Boutros et al., 2022). Targeting these genes in the future could provide insight into how αSyn could be connected to adaptive DSBs and aging.

Methodological Limitations

The plasmid reporter experiments have several limitations that are important to note. In the first experiment we detected NHEJ efficiency was impaired in αSyn KO cells, but HR rates were not altered (Chapter 2, Figure 1A). As the HR GFP reporter and NHEJ GFP reporter are separate plasmids, this approach does not detect HR and NHEJ rates within the same population of cells. Determining the ratio of HR/NHEJ within one sample is more complicated but would be interesting to know. Utilizing a novel fluorescence switching reporter, called RepairSwitch, could be useful in this situation to measure rates of the two main DSB repair pathways via flow cytometry. This would allow us to measure HR and NHEJ rates simultaneously, although would still not allow us to distinguish c-NHEJ and alt-NHEJ concurrently. In the second plasmid reporter experiment we found increased deletions after DSB repair in αSyn KO compared to WT cells transfected with the NHEJ plasmid reporter (Chapter 2, Figure 1B). While it is true this experiment does not allow us to collect any information on the difference between rate of repair in these cell lines, we are able to analyze indel frequency which was not possible during the GFP reporter flow cytometry experiment. These experiments individually are somewhat limited, but when taken together they can complement each other, showcasing the experimental details the other one lacks.

Limitations also existed for CRISPR DSB repair assays in human cells and mouse neurons. Despite many efforts, the lentiviruses used only transduced about 30%

of cells. Several optimization experiments were conducted, but none increased the transduction rate significantly, including the use of polybrene (Chaney et al., 1986; Jacobsen et al., 2006). This limited us to performing all DSB repair assay in a 96 well format to conserve lentiviral use. Additionally, primary cultured neurons were sensitive and susceptible to detrimental effects when manipulated at low cell densities. To combat this, we tried seeding neurons at higher density in order to improve their resilience to subsequent lentiviral transduction. At this density, however, flow cytometry was not possible to detect lentiviral transduction rate. To get around this problem we used fluorescence imaging microscopy to measure transduction efficiency. Although we used different methods for measuring transduction efficiency between human cells and mouse neurons, it was important to compare our results from human cell lines to neurons which strengthened our evidence that αSyn modulates DSB repair in multiple systems.

4.2 DSB repair pathways and pharmacological inhibitors

Pharmacological inhibitors are one tool to use to block different DSB repair pathways to learn more about αSyn's effect on this system. At baseline, we established that increased indel frequencies are associated with loss of αSyn. Blocking HR by inhibiting MRE11 and blocking alt-NHEJ by inhibiting Pol θ did not change this baseline (Chapter 2, Figure 4). This suggests that the absence of αSyn does not affect HR or alt-NHEJ. We also confirmed that alt-NHEJ is not directly altered by genetic deletion of αSyn with another inhibitor, novobiocin (Figure 3.4.1). We did, however, find changes to the

baseline effect when inhibiting the 3 kinases that phosphorylate H2AX: ATM, ATR, and DNA-PK$_{cs}$. All three prevented the increase of indel frequency seen in αSyn KO cells and under DNA-PK$_{cs}$ inhibition, a decrease of indel frequency was observed in αSyn KO cells compared to WT, the opposite effect to what we see under baseline conditions. Since the effect was the most striking under DNA-PK$_{cs}$ inhibition, we decided to investigate the regulation of DNA-PK$_{cs}$ in the absence of αSyn. We treated WT and αSyn KO HAP1 human cells with DMSO or DNA-PK$_{cs}$i (AZD7648) at the same concentration that decreased gene editing after DSB repair in αSyn KO cells compared to WT cells. We found that DNA-PK$_{cs}$ nuclear levels were significantly increased in αSyn KO cells with this inhibition, while WT cells showed no significant differences with DNA-PK$_{cs}$ inhibition (Figure 4.2.1).

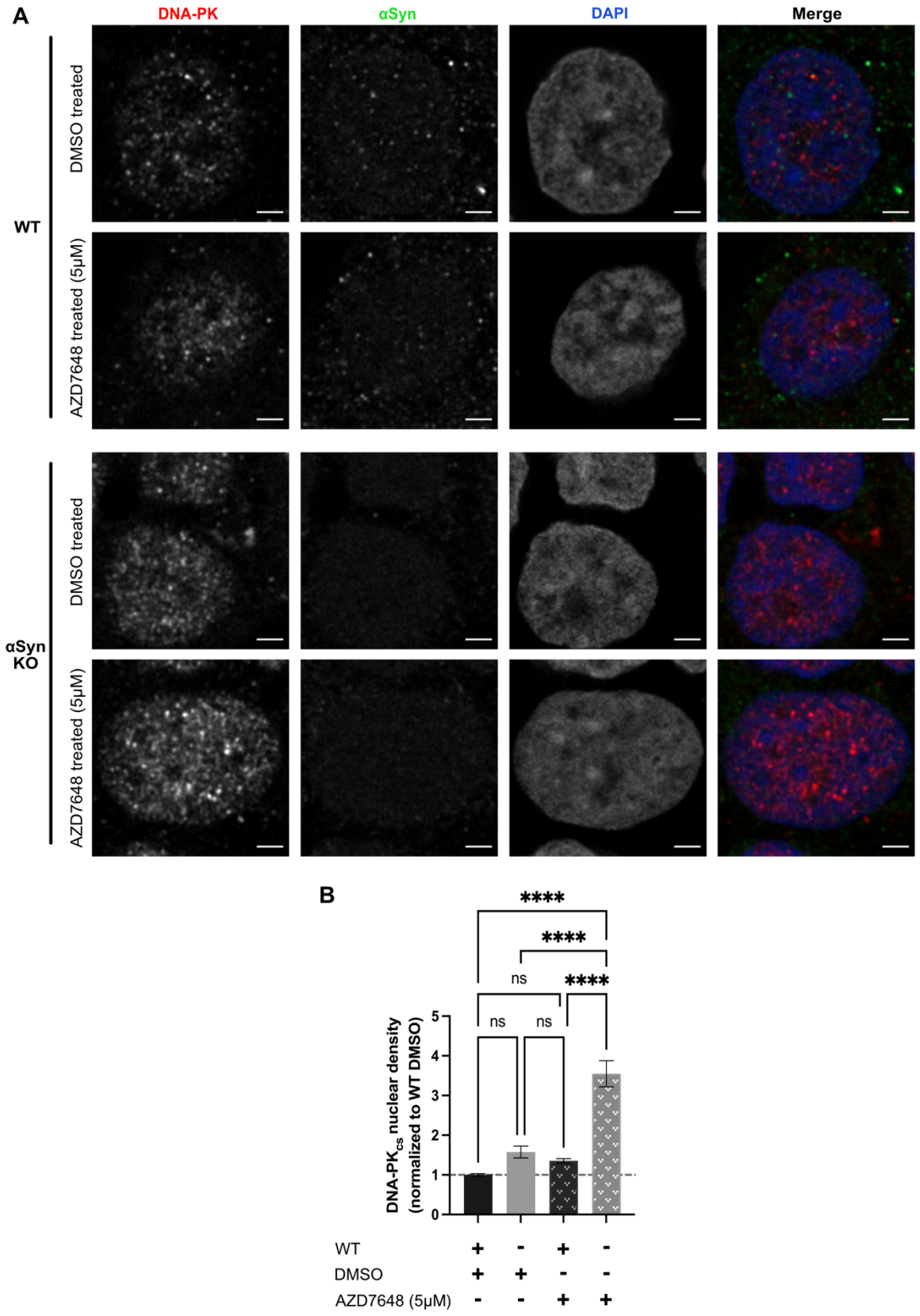
A
DNA-PK
αSyn
DAPI
Merge
WT
DMSO treated
AZD7648 treated (5μM)
αSyn KO
DMSO treated
AZD7648 treated (5μM)
B
****
****
ns
****
ns
ns
DNA-PKcs nuclear density (normalized to WT DMSO)
0
1
2
3
4
5
WT + - + -
DMSO + + - -
AZD7648 (5μM) - - + +

Figure 4.2.1. DNA-PK$_{cs}$ nuclear density is enhanced in αSyn KO HAP1 cells compared to WT cells under DNA-PK$_{cs}$ inhibition.

A) Representative images of WT and αSyn KO HAP1 human cells treated with either 0.01% DMSO or DNA-PK$_{cs}$i (AZD7648 5μM) for 72 hours *in vitro*. Scale bar 2 μm. B) Quantification of nuclear density of DNA-PK$_{cs}$ foci normalized to WT DMSO condition (Number of foci/volume). ANOVA summary $p<0.0001$. Post-hoc multiple comparisons: Significant increase of nuclear density DNA-PK$_{cs}$i treated αSyn KO cells (3.547 ±0.328) compared to DMSO treated WT cells (1.000 ±0.030) ($p<0.0001$), DMSO treated αSyn KO cells (1.578 ±0.151)($p<0.0001$), and DNA-PK$_{cs}$i WT cells (1.355 ±0.056) ($p<0.0001$). No significant differences observed between DMSO treated WT and αSyn KO cells ($p=0.0870$), between DNA-PK$_{cs}$i treated WT cells and DMSO treated WT cells ($p=0.4470$), or between DNA-PK$_{cs}$i treated WT cells and DMSO treated αSyn KO cells ($p=0.8051$). N= 3 biological replicates, ~50 nuclei imaged per condition. One-way ANOVA.

Because of this unexpected reversal of effect seen under DNA-PK$_{cs}$ inhibition (Chapter 2, Figure 4), we speculate that αSyn could act as a partial agonist for DNA-PK$_{cs}$, reducing Artemis endonuclease activity and reducing indels incorporated after repair as a way to explain this data. This proposed model is depicted in a cartoon graphical summary, created with Biorender (Figure 4.2.2). While DNA-PK$_{cs}$ is involved in c-NHEJ, other DSB repair proteins are also required for c-NHEJ repair. Repeating this experiment with pharmacological inhibitors for Ku70/80 and DNA ligase IV, to test if a decrease in indel frequency in αSyn KO cells is also seen as it was with DNA-PK$_{cs}$ inhibition, would be a useful future direction. As c-NHEJ cannot function without Ku70/80 and DNA ligase IV, this experiment, could potentially strengthen the evidence suggesting αSyn shifts DSB repair towards c-NHEJ.

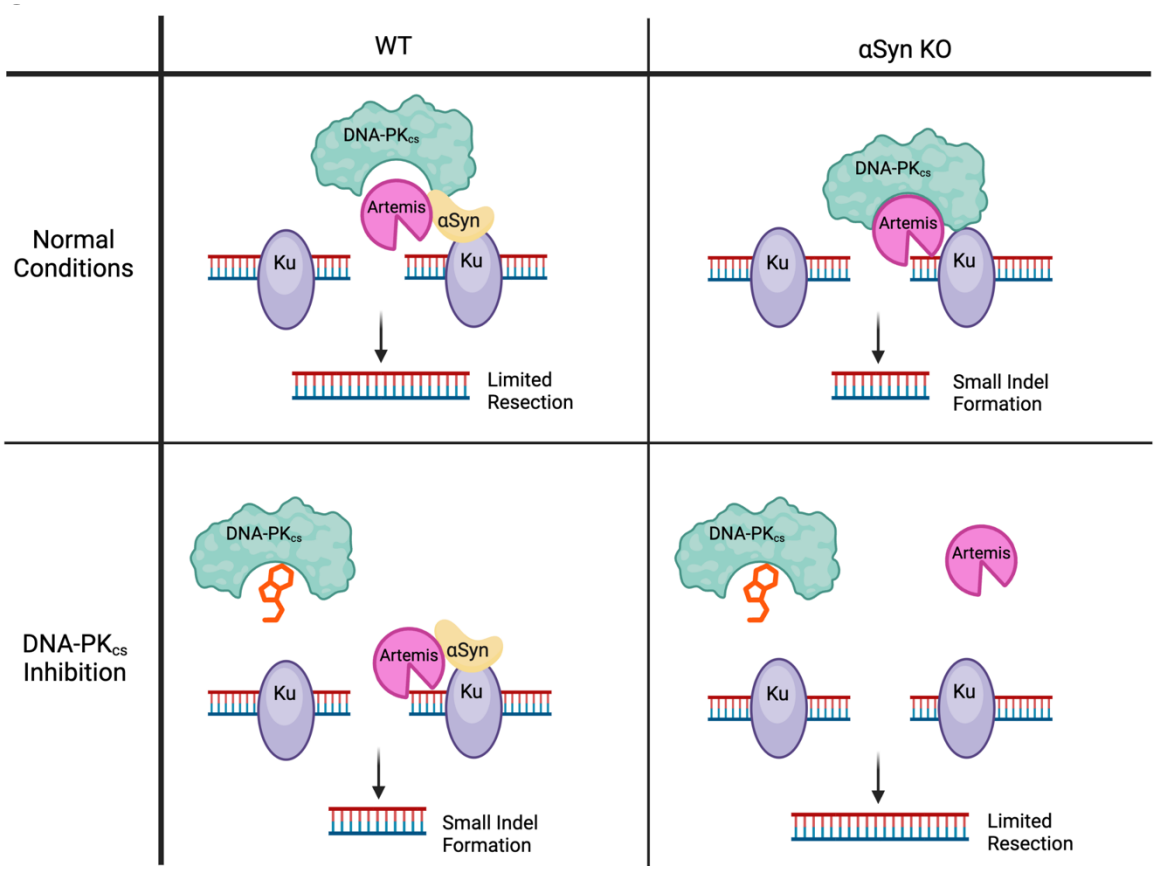

Figure 4.2.2. Proposed partial agonist model for how αSyn may regulate DNA-PK$_{cs}$ facilitated DSB repair.

Cartoon schematic visually summarizing one possible model of how αSyn may act as a partial agonist to reduce DNA-PK$_{cs}$ kinase activity or Artemis nuclease activity, which may limit resection and reduce indel formation after DSB repair. The bottom panel shows how under DNA-PK$_{cs}$ inhibition, αSyn partial agonism could enhance DNA-PK$_{cs}$/Artemis activity, leading to increased resection and deletions incorporated at the repair junction.

The ATM and ATR inhibition results showing that these kinases that phosphorylate γH2AX prevented the baseline effect of increased indel frequency in the absence of αSyn is also interesting. ATM has recently been shown to suppress c-NHEJ events and c-NHEJ factor recruitment (Balmus et al., 2019; Bennardo & Stark, 2010; Cisneros-Aguirre et al., 2022). One possibility is that αSyn is a partial agonist of ATM. In

the presence of ATM, αSyn could reduce the level of ATM activity, which in turn increases c-NHEJ rates or shifts DSB repair to c-NHEJ alternative pathways, resulting in a reduction of small indels incorporated after repair. Conversely, in the presence of ATM pharmacologic inhibition, αSyn partial agonism could facilitate ATM activity, suppressing c-NHEJ and increasing small indel formation. Several theories are possible, but this partial agonist hypothesis does fit the data presented in the current study (Chapter 2, Figure 4).

Similarly to ATM, ATR is one of the kinases that phosphorylates H2AX. Loss of H2AX can also increase c-NHEJ events (Feng et al., 2017) which could similarly explain how αSyn affects ATR, similar to the proposed mechanism for ATM above. While NHEJ can occur independently of ATR and a potential mechanism for how ATR and αSyn is more unclear, there is well-known redundancy between ATM, ATR, and DNA-PK_{cs}, therefore it is not necessarily surprising all 3 kinases showed a similar result when inhibited. ATM and ATR have hundreds of phosphorylation targets, so it will be interesting to learn in future experiments how these might be altered when αSyn is knocked out. It would also be interesting to simultaneously test a cocktail of inhibitors with ATR, ATM, and DNA-$PK_{cs,}$ as well as a group of c-NHEJ inhibitors in Ku60/70, DNA ligase IV, and DNA-PK_{cs} to ensure that c-NHEJ is abolished. These future directions could be integral to deciphering how exactly αSyn can shift DSB repair towards c-NHEJ.

Methodological Limitations

While pharmacological inhibitors can be effective at blocking certain targets, there are certainly limitations associated with this approach. Efficacy issues can arise if

high enough concentrations are not used to fully inhibit the target. For all pharmacological inhibition used in this project, a concentration was chosen at least twice the IC50 of any given drug. Additionally, partial inhibition, off target inhibition, and adverse downstream effects are all caveats and limitations with a pharmacological experimental design. For example, several of the PLK family individual inhibitors used in Figure 3.4.3 also inhibit other PLK family members at certain concentrations. This was at times unavoidable in order to ensure inhibition of the target of interest. One way to bypass this issue would be to implement bump and hole chemical genetics to attain specificity without affecting other members in the protein family by manipulating the sterics of protein-ligand interactions (Islam, 2018). These methods were outside of the scope of this project but could provide useful roadmaps for the future.

For DNA-PK$_{cs}$ inhibition, other methods could be utilized to further investigate the connection between αSyn and DNA-PK$_{cs}$. Performing a co-immunoprecipitation assay between αSyn and DNA-PK$_{cs}$ could reveal whether αSyn is directly binding to DNA-PK$_{cs}$ or, alternatively, it is indirectly affecting how DNA-PK$_{cs}$ functions in the DSB repair pathway choice. Furthermore, measuring a readout of Artemis endonuclease activity via western blot at baseline, in the absence of αSyn, and under DNA-PK inhibition could also elucidate this complex multi-protein system. Testing whether Artemis endonuclease activity reduces in WT condition via partial agonism of αSyn on DNA-PK$_{cs}$ could indicate a potential mechanism for this complex system. Discovering that Artemis endonuclease activity increases under DNA-PK$_{cs}$ inhibition and decreases in αSyn KO cells under DNA-PK$_{cs}$ inhibition would help to confirm this hypothesis. Overall,

pharmacological inhibition is just one way to scientifically manipulate a system but could be bolstered with additional alternative genetic and/or biochemical approaches.

4.3 Rescue of αSyn via transient transfection

After discovering the novel finding that increased indel frequency was associated with loss of αSyn, we immediately wanted to test whether reintroduction of αSyn would prevent this effect. This rescue experiment was prioritized in the current study yet suffered from many complications. We theorized that αSyn reintroduction would reduce indel frequencies to those seen in WT cells at baseline, but we were also interested if mutant αSyn forms would function similarly to WT αSyn at baseline or not. We utilized a transient transfection approach to reintroduce WT αSyn, αSyn lacking the NAC domain, phosphodeficient S129A and phosphomimic S129D mutants, and 3 familial PD associated mutant αSyn forms: A53T, E46K, and A30P. The NGS indel results after αSyn rescue were ultimately uninterpretable due to technical difficulties (Chapter 2, Supplementary Figure 2). If these obstacles were overcome, it would have been fascinating to learn if mutant αSyn forms are equally functional to shift DSB repair to c-NHEJ, like we hypothesize WT αSyn is able to accomplish.

Methodological Limitations

The technical limitations of this αSyn rescue experiment caused the results to be challenging to interpret because the established effect of increased indel frequency was not consistently observed when we were also transfecting a control plasmid. Based on this control not reproducing the baseline result, we concluded that the prior transient

transfection somehow disrupted the effect in seen in αSyn KO cells after lentiviral transduction. This transient transfection of WT αSyn and all mutant αSyn forms was performed on the same day as CRISPR/Cas9 lentiviral transduction. We were limited to this timeline because the transfection could not occur earlier due to concerns about over confluency in a 96-well plate format by 72 hours after transfection/transduction. Transfection was not attempted later out of concern that the rescue of αSyn expression would not high enough 24 hours after lentiviral transduction. We also tested four different transfection reagents: lipofectamine 3000, calPhos, X-tremeGene, and jetOPTIMUS, but similar results were found with each. We ultimately chose to use jetOPTIMUS because it showed the highest expression of αSyn, but due to proprietary restrictions it is still unclear what compounds are present in the transfection reagent and if these could potentially be disrupting subsequent lentiviral transduction.

Not only was the transient transfection limited, but other approaches were met with roadblocks as well. We attempted nucleofection in a 96-well plate format, but WB analysis showed that cells did not adequately express αSyn, suggesting nucleofection was not rescuing αSyn. We also considered creating stable cell lines with αSyn transgenically re-expressed for the rescue. However, with 6 mutant αSyn strains, WT αSyn and a negative control, creating 8 stable cell lines in this way was not feasible. Another possible downside of a stable cell line experiment is that once they are created and passaged, compensation can occur to minimize any detrimental effects from the genetic manipulations made. For these reasons, we chose the transient transfection route in this experimental design, which were ultimately unsuccessful. Although 8 stable cell lines may be technically and financially challenging to produce, it may be beneficial

to extend our results and further investigate the effect of αSyn disease-causing mutations on DSB repair.

4.4 PLK Inhibition leads to increased cell survival

In order to link the *in vitro* findings connecting αSyn to DSB repair to *in vivo* αSyn Lewy pathology, we investigated how PLK inhibition affected longitudinal cell survival of neurons bearing αSyn inclusions in mouse cortex. We found that PLK inhibition led to increased cell survival, but it is unclear if this was due to any changes in S129 phosphorylation (Chapter 2, Figure 5). We were surprised to find, after IHC analysis of mouse tissue, there were no changes to S129 pSyn levels and only an increase in total αSyn levels after PLK inhibition via BI2536 IP injections (Chapter 2, Figure 6). We had hoped to investigate how S129 phosphorylation is connected to αSyn and DSBs in the current study, but after this unexpected pSyn result, the technical limitations of S129A/D transient transfection *in vitro* (Chapter 2, Supplementary Figure 2), and the inconsistent results in human cells and mouse neurons *in vitro* after PLK 1/3 inhibition via GW84362X pharmacological inhibition (Chapter 2, Supplementary Figure 4) and BI2536 (Figure 3.4.2), we are unable to comment on how changes in S129 phosphorylation modulate this system.

Another unexpected result came from IHC analysis of BI2536 treated mice, in which higher γH2AX levels were associated with PLK family inhibition compared to saline controls (Chapter 2, Figure 6). At first, this finding was counterintuitive because one would assume that if cells bearing αSyn Lewy pathology survived at a higher rate

after BI2536 treatment, they would also have a lower insult of nuclear DSB levels. However, BI2536 treatment correlated to higher cell survival yet increased γH2AX levels. This could be due to PLK's many targets. PLK is involved in cell cycle regulation (Lee et al., 2014) and DNA damage response as it is upstream of ATM/ATR (Hyun et al., 2014; Li et al., 2017) which could explain why γH2AX levels increase after inhibition. Also, here we are using γH2AX staining to measure a snapshot of DSB levels which isn't a perfect correlate and could explain this result. Increased γH2AX levels could indicate more efficient DSB repair in which the cell is recruiting more γH2AX to break sites, which could in turn be associated with increased genome stability and cell survival. Expanding this experiment to include multiple time points of γH2AX staining may be useful. Additionally, an *in vitro* correlate with BI2536 treatment in primary cultured neurons and conducting neutral comet assays will be vital to testing whether DSB levels actually increase after PLK inhibition or whether recruitment of γH2AX could be associated with more efficient DSB repair.

It is possible that genomic stability is still linked to PLK inhibition. We determined that PLK inhibition led to an increase of total aggregated αSyn within the inclusion. From past work, we also learned that as αSyn inclusions aggregate and mature, the soluble synuclein in the nucleus decreases (Schaser et al., 2019). Perhaps the increase in somatic aggregated αSyn was also correlated with a small increase in soluble αSyn nuclear localization, which could facilitate error-free DSB repair by shifting repair towards c-NHEJ, leading to genomic stability. There is much more work to do to connect these ideas, but it is interesting to speculate if there could be genomic stability

facilitated by nuclear αSyn that is driving the protection against neurodegeneration observed after PLK inhibition treatment.

Linking αSyn to genomic stability is a challenging feat, but other experimental approaches may be better suited to this task. We attempted to perform WGS on mouse brains with and without hippocampal Lewy pathology to compare indel frequency and to look for hotspots in the genome where mutations or large indels may have been incorporated. This was an original aim for this project, but we were unable to identify a comparative WGS analysis tool that would detect changes in indel frequency across samples in preliminary experiments (Table 3.2.2). Another approach would be to replicate the pathology induced loss of nuclear soluble αSyn in primary cultured neurons *in vitro*. With this design, we could test whether the loss of nuclear soluble αSyn translates to changes in genomic instability by γH2AX staining via ICC, measure DSB levels directly with neutral comet assays, and even apply our CRISPR/Cas9 lentiviral DSB repair assay and performing NGS to detect changes in indel frequency. A more advanced future direction once these prior questions have been investigated would be to expand upon the PLK inhibition longitudinal multiphoton *in vivo* imaging experiment and test whether DNA-PK_{cs} inhibition results in protection against neurodegeneration as well. Based on the decrease in indel frequency seen with DNA-PK_{cs} inhibition (Chapter 2, Figure 4), we would expect to see similar neuroprotection of αSyn inclusion bearing cells if our speculation that αSyn is facilitating genomic stability and in turn promoting neuronal survival is correct. Although more questions about this mechanism still exist, the findings of this dissertation can be summarized in a graphical abstract (Figure 4.41).

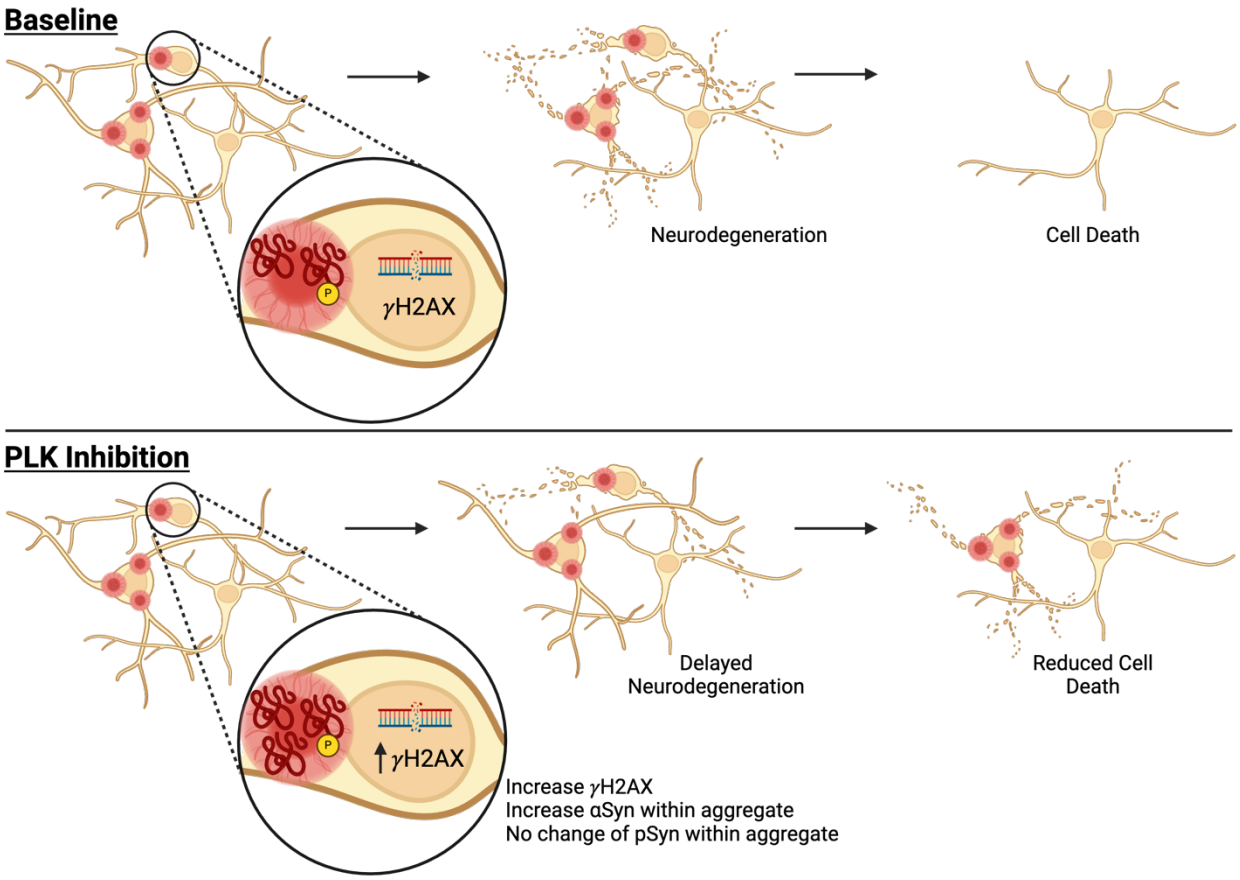

Figure 4.4.1. Graphical summary of the changes reflected in mouse cortical neurons *in vivo* after PLK inhibition.

Cartoon schematic visually summarizing how under PLK inhibition, neurodegeneration of neurons bearing αSyn inclusions is delayed. Additionally within the aggregate, total αSyn is increased and nuclear γH2AX levels are increased. The mechanism for how these changes lead to reduced cell death remail unclear.

Methodological Limitations

Longitudinal *in vivo* imaging experiments are challenging and do have several technical limitations. We are limited in that we can only analyze cells bearing inclusions present at the time of the start of imaging. Cells that form new inclusions can be analyzed separately but their life span are impossible to measure if the cells do not die

within the imaging time period (Figure 3.5.2). We were limited to imaging for a month-long period for a variety of technical reasons. Furthermore, there was a spread of αSyn pathology between individual animals. We tried to address this variability by ensuring both saline and BI2536 treated groups contained mice with relatively equivalent pathology loads. This issue is mitigated by baseline imaging before treatment with drug, since then each mouse can also act as its own control pre- and post-drug treatment.

Another experimental design limitation is that PLK has several cellular functions that when inhibited can lead to adverse effects. PLK was first discovered for its role in cell cycle regulation in which it functions to regulate centrosome maturation, checkpoint recovery, spindle assembly, cytokinesis, and apoptosis (Lee et al., 2014). Furthermore, PLK has been shown to contribute to DNA damage response by phosphorylating factors upstream of ATM/ATR and phosphorylates MRE11, regulating their DNA damage response functions (Li et al., 2017). With PLK playing a role in cell recognition of DNA damage, it can be difficult to parse a part whether an effect is only due to PLK manipulation or whether αSyn is driving changes observed. This challenge is exaggerated when studying this question in an *in vivo* system where variability and animal-to-animal differences are also at play. We attempted to address this in part by inhibiting PLK in human cells with BI2536 treatment *in vitro* (Figure 3.4.2), but unfortunately toxicity issues made this difficult. It would be interesting to try other PLK inhibitors to test whether DSB levels increase in WT and αSyn KO human cells via γH2AX staining and neutral comet assays. This could provide information on whether PLK is upstream or downstream of αSyn in its role to shift DSB repair towards c-NHEJ.

Lastly, we were limited by the available antibodies to successfully detect differences in pSyn levels after PLK inhibition via BI2536 in mouse brain IHC samples. pSyn antibodies can vary in their ability to detect pSyn based on other post-translational modifications that might be present such as truncation and/or aggregation into αSyn fibrils (Lashuel et al., 2022). In our hands, we have not identified a pSyn antibody that stains within the nucleus and is specific (as defined by validation in αSyn KO human cells). In the future, we would be interested in testing newer pSyn antibodies created by the Lashuel group to be able to detect whether PLK inhibition affects pSyn levels within αSyn inclusions.

4.5 Conclusions

The data presented here in this dissertation showcase the role of αSyn in DNA DSB repair that may be regulated by DNA-PK_{cs} and provide evidence that it may shift DSB repair towards c-NHEJ. We highlight how BI2536 treatment to inhibit PLK protects against neurodegeneration, showing its potential as a future therapeutic in PD. Questions remain about how αSyn affects genomic stability when αSyn pathology is present and how this may eventually contribute to death of dopaminergic neurons. While these questions persist, we have uncovered one piece of the puzzle. There is a long road ahead to solve these problems to ultimately discover a disease-altering therapeutic for PD. And yet, the journey will be filled with curiosity, novelty, and the joys of knowledge seeking to discover the vastness of what is left to uncover.

Appendix A: Supporting Data

A.1 DSB repair assay sanger sequencing

Preliminary sequencing results were conducted using sanger sequencing to compare indel frequency between WT and αSyn KO PCR products from the same cell lysates used in Chapter 2, Figure 2 that were transduced with a DSB inducing CRISPR/Cas9 lentivirus. The sanger sequencing confirmed our finding that indel frequency is increased in αSyn KO cells compared to WT cells (Figure A.1.1). These experiments were conducted as preliminary experiments before NGS was performed but were ultimately not continued due to finding more consistent and larger effects with the accuracy of NGS.

Materials and Methods

PCR products from the DSB repair junction were submitted to the Vollum DNA Sequencing Core for sanger sequencing. Applied Biosystems Sequence Trace files were analyzed with Tracking of Indels, Deletions, and Recombination events (TIDER) software from the Netherlands Cancer Institute (Brinkman et al., 2018).

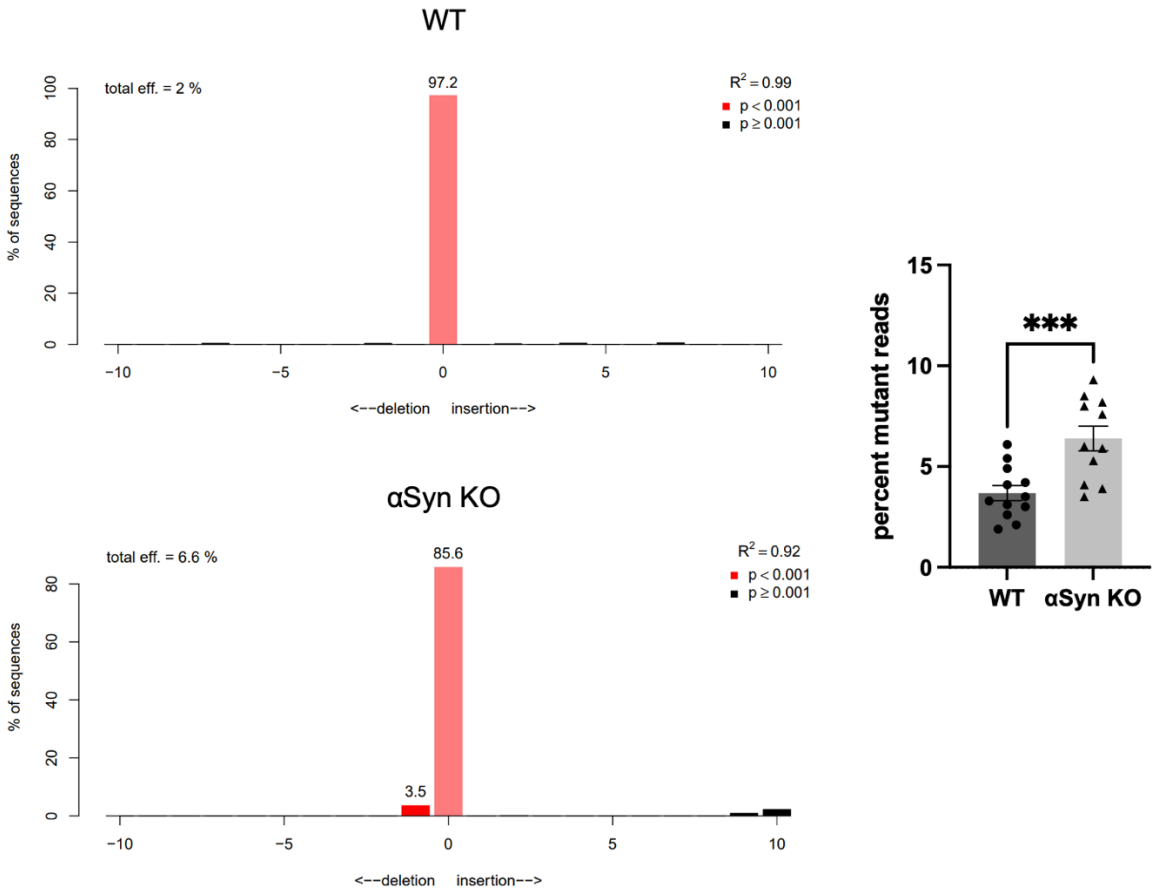

Figure A.1.1. Sanger sequencing confirms NGS result of DSB repair of WT and αSyn KO Cells. Sanger Sequencing of 544bp PCR product from WT and αSyn KO Hap1 cells transduced with DSB inducing CRISPR/Cas9 lentivirus. *Top:* Indel map from a representative WT sample with percent of sequences plotted against deletions (negative x axis) or insertions (positive x axis) by increments of 5 base pairs. Red bar at 0 indicates faithful repair. *Bottom*: Indel map from a representative αSyn KO sample. *Right:* Quantification of sanger sequencing with the equation: *percent mutant reads = (1 – percent sequences with faithful repair).* Significant increase of percent mutant reads of αSyn KO cells (6.391 ±0.615) compared to WT cells (3.683 ±0.375) (p=0.0010). N=4 biological replicates, 3 technical replicates per biological replicate. Two-tailed student's t-test.

A.2 Flow Cytometry

In order to confirm the transduction rates of the DSB-inducing GFP expressing lentivirus were affecting WT and αSyn Hap1 cells similarly, we performed flow cytometry to measure GFP positive transduced cells. Overall transduction rates of WT cells were not significantly different from αSyn KO cells (reported in Chapter 2, see Methods). Cell populations with gating on forward side scatter plots to exclude debris and doublet cells are represented here for non-transduced GFP negative cells (Figure A.2.1) and transduced cells (Figure A.2.2) with a subset GFP positive.

Materials and Methods

Protocols for flow cytometry were previously described in Chapter 2 (see Methods). GFP negative and positive events were analyzed in the OHSU Flow Cytometry Core using BD FACSDiva 9.0.

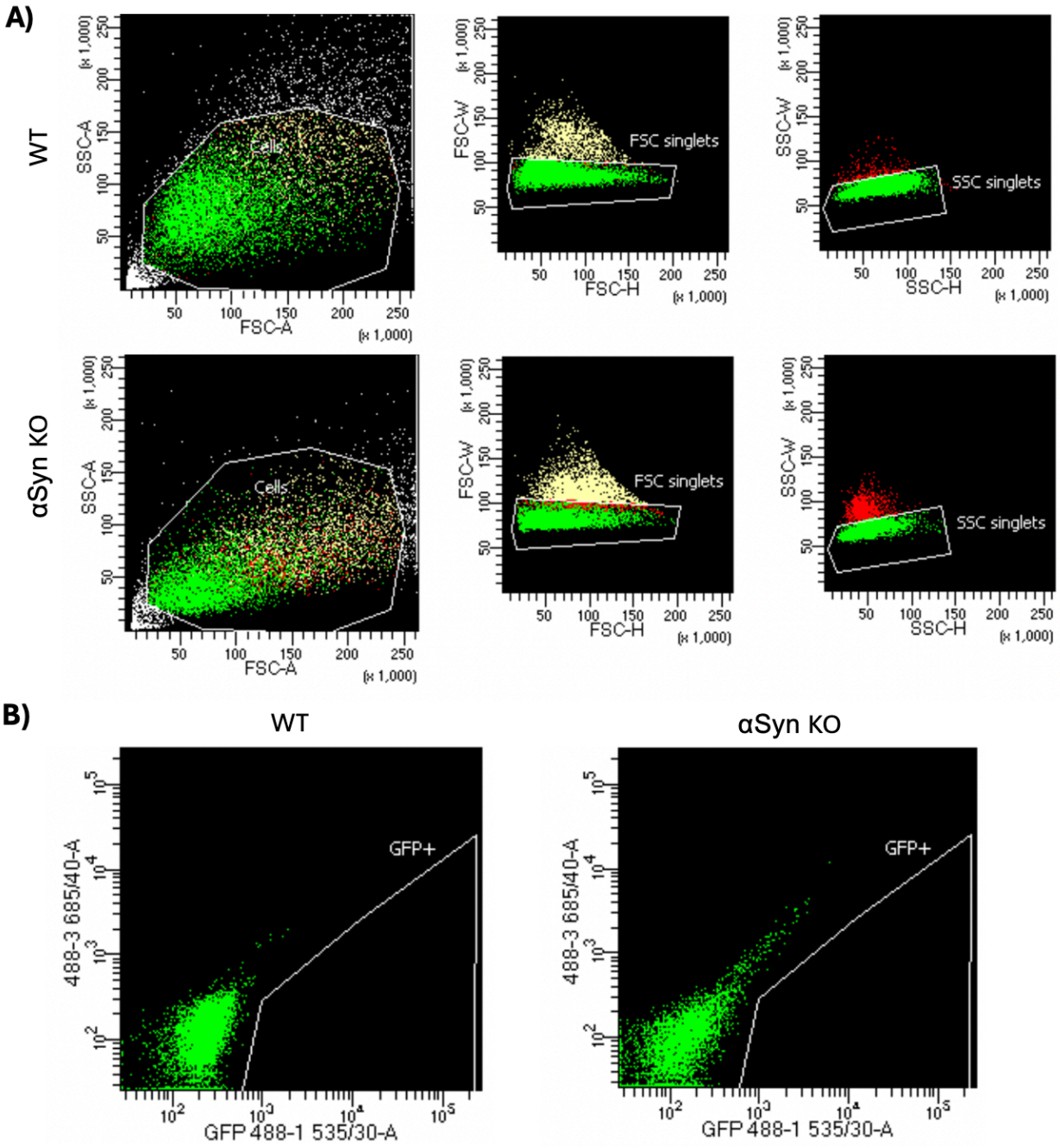

Figure A.2.1. Flow cytometry of non-transduced WT and αSyn KO Hap1 cells. 72 hours after seeding, cells were strained in FACS buffer (PBS + 1%FBS) and GFP positive singlet cells were measured on the BD Canto II machine in the OHSU Flow Cytometry core. A) Cell populations were selected to exclude debris (white) by gating cells on a forward side scatter and then by gating cells on forward side scatter height (FSC-H) by forward side scatter area (FSC-A) for doublet cell (yellow/red) discrimination in WT cells (*top*) and αSyn KO cells (*middle*). B) Green events represent singlet cells in the selected gated population with the GFP+ gate outlined in white text. 0.0% of singlet cells were GFP positive for WT (*left*) and 0.0% for αSyn KO cells (*right*).

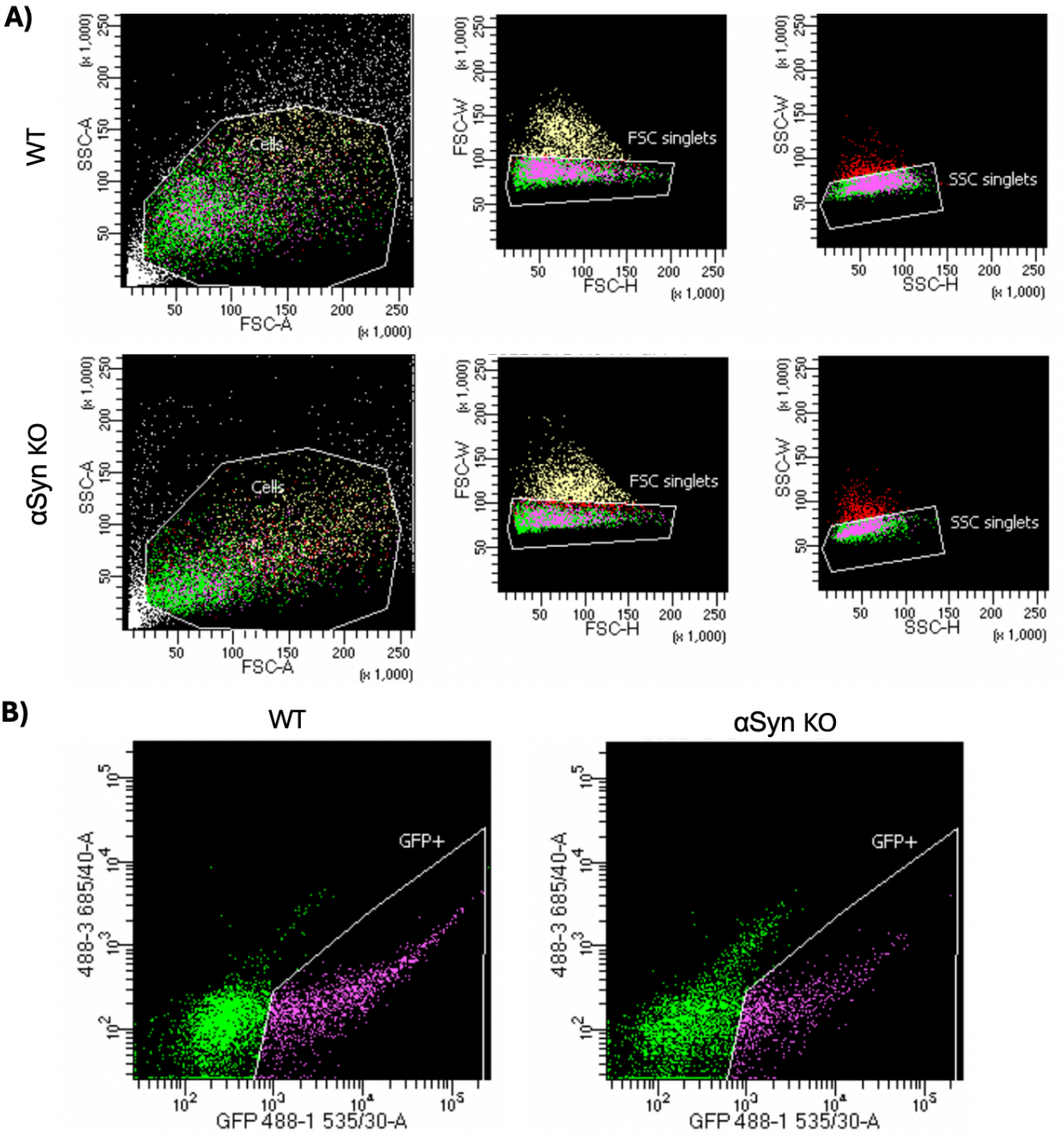

Figure A.2.2. Flow cytometry of GFP lentivirus transduced WT and αSyn KO Hap1 cells. 72 hours after lentiviral transduction, cells were strained in FACS buffer (PBS + 1%FBS) and GFP positive singlet cells were measured on the BD Canto II machine in the OHSU Flow Cytometry core. A) Cell populations were selected to exclude debris (white) by gating cells on a forward side scatter and then by gating cells on forward side scatter height (FSC-H) by forward side scatter area (FSC-A) for doublet cell (yellow/red) discrimination in WT cells (*top*) and αSyn KO cells (*middle*). B) Green puncta represent GFP negative singlet cells in the selected gated population with the GFP positive population (pink). 11.2% of singlet cells were GFP positive for WT (*left*) and 9.8% for αSyn KO cells (*right*).

Appendix B: Recipes

B.1 DSB Repair Assay

1. Lysis Buffer (For one well from 96-well plate)
    a. 20µL 5x Phusion HF buffer
    b. 5µL Proteinase K (20mg/mL)
    c. 5µL RNase A (10mg/mL)
    d. 70µL nuclease free water
2. PCR Reaction (For one well from 96-well plate)
    a. 25µL 2x Phusion HF buffer (dNTPs included)
    b. FWD primer 500nM final concentration
    c. REV primer 500nM final concentration
    d. 1µL Phusion Hot Start II HF DNA Polymerase (2 U/µL)
    e. 5µL cell lysate
3. T7 Endonuclease I Reaction (For one well from 96-well plate)
    a. 10µL PCR reaction from gDNA
    b. 3µL nuclease free water
    c. 1.5µL NEBufer (10x)
    d. 0.5µL T7 Endonuclease I (10 U/µL)

B.2 Primary Cultured Neurons

4. Plating Medium
    a. Neurobasal Medium
    b. 10% FBS
    c. 1% GlutaMAX (100x)
    d. 1% sodium pyruvate
    e. 1% penicillin streptomycin (100x)

5. Culture Medium
    a. Neurobasal medium
    b. 2% B27 supplement
    c. 0.5% GlutaMAX (100x)

B.3 Western Blot

1. RIPA lysing buffer
    a. Add the following to 1358µL nuclease free water for a final volume of 2mL
    b. 100µL 1M Tris HCL
    c. 300µL 1M NaCl
    d. 200µL 10% TX-100
    e. 20µL SDS
    f. 20µL 100X protease inhibitor
    g. 2µL 1000X phosphatase inhibitor cocktail
2. Running Buffer
    a. 720mL DI water
    b. 80mL 10X Tris-Glycine SDS Running Buffer (Li-Cor)
3. Transfer Buffer
    a. 100mL methanol
    b. 960mL DI water
    c. 40mL 25X Tris-Glycine Transfer Buffer (Li-Cor)
4. Fixation Solution
    a. 7.5mL PBS
    b. 2.5mL 16% PFA
    c. 12.5µL 7% glutaraldehyde

B.4 Immunohistochemistry

1. Blocking Buffer
    a. PBS
    b. 0.1% Triton-X 100
    c. 10% goat serum
2. Permeabilization Buffer
    a. PBS
    b. 0.25% Triton-X 100
3. Incubation Buffer
    a. 1:5 dilution Blocking Buffer in PBS
    b. Primary/secondary antibodies at denoted dilution

References

Agamanolis, D. P., & Greenstein, J. I. (1979). Ataxia-Telangiectasia: Report of a Case With Lewy Bodies and Vascular Abnormalities within Cerebral Tissue. *Journal of Neuropathology & Experimental Neurology*, *38*(5), 475–489. https://doi.org/10.1097/00005072-197909000-00003

Ahmad, K. A., Wang, G., Unger, G., Slaton, J., & Ahmed, K. (2008). Protein kinase CK2 – A key suppressor of apoptosis. *Advances in Enzyme Regulation*, *48*(1), 179–187. https://doi.org/10.1016/j.advenzreg.2008.04.002

Anderson, J. P., Walker, D. E., Goldstein, J. M., Laat, R. de, Banducci, K., Caccavello, R. J., Barbour, R., Huang, J., Kling, K., Lee, M., Diep, L., Keim, P. S., Shen, X., Chataway, T., Schlossmacher, M. G., Seubert, P., Schenk, D., Sinha, S., Gai, W. P., & Chilcote, T. J. (2006). Phosphorylation of Ser-129 Is the Dominant Pathological Modification of α-Synuclein in Familial and Sporadic Lewy Body Disease. *Journal of Biological Chemistry*, *281*(40), 29739–29752. https://doi.org/10.1074/jbc.M600933200

Anwar, S., Peters, O., Millership, S., Ninkina, N., Doig, N., Connor-Robson, N., Threlfell, S., Kooner, G., Deacon, R. M., Bannerman, D. M., Bolam, J. P., Chandra, S. S., Cragg, S. J., Wade-Martins, R., & Buchman, V. L. (2011). Functional Alterations to the Nigrostriatal System in Mice Lacking All Three Members of the Synuclein Family. *Journal of Neuroscience*, *31*(20), 7264–7274. https://doi.org/10.1523/JNEUROSCI.6194-10.2011

Arnold, M. R., Cohn, G. M., Oxe, K. C., Elliott, S. N., Moore, C., Laraia, P. V., Shekoohi, S., Brownell, D., Meshul, C. K., Witt, S. N., Larsen, D. H., & Unni, V. K. (2024). *Alpha-synuclein*

regulates nucleolar DNA double-strand break repair in melanoma (p. 2024.01.13.575526). bioRxiv. https://doi.org/10.1101/2024.01.13.575526

Aubele, D. L., Hom, R. K., Adler, M., Galemmo, R. A., Bowers, S., Truong, A. P., Pan, H., Beroza, P., Neitz, R. J., Yao, N., Lin, M., Tonn, G., Zhang, H., Bova, M. P., Ren, Z., Tam, D., Ruslim, L., Baker, J., Diep, L., … Artis, D. R. (2013). Selective and brain-permeable polo-like kinase-2 (Plk-2) inhibitors that reduce α-synuclein phosphorylation in rat brain. *ChemMedChem*, *8*(8), 1295–1313. https://doi.org/10.1002/cmdc.201300166

Azeredo da Silveira, S., Schneider, B. L., Cifuentes-Diaz, C., Sage, D., Abbas-Terki, T., Iwatsubo, T., Unser, M., & Aebischer, P. (2009). Phosphorylation does not prompt, nor prevent, the formation of alpha-synuclein toxic species in a rat model of Parkinson's disease. *Human Molecular Genetics*, *18*(5), 872–887. https://doi.org/10.1093/hmg/ddn417

Baldi, I., Cantagrel, A., Lebailly, P., Tison, F., Dubroca, B., Chrysostome, V., Dartigues, J.-F., & Brochard, P. (2003). Association between Parkinson's disease and exposure to pesticides in southwestern France. *Neuroepidemiology*, *22*(5), 305–310. https://doi.org/10.1159/000071194

Balmus, G., Pilger, D., Coates, J., Demir, M., Sczaniecka-Clift, M., Barros, A. C., Woods, M., Fu, B., Yang, F., Chen, E., Ostermaier, M., Stankovic, T., Ponstingl, H., Herzog, M., Yusa, K., Martinez, F. M., Durant, S. T., Galanty, Y., Beli, P., … Jackson, S. P. (2019). ATM orchestrates the DNA-damage response to counter toxic non-homologous end-joining at broken replication forks. *Nature Communications*, *10*(1), 87. https://doi.org/10.1038/s41467-018-07729-2

Bartels, T., Choi, J. G., & Selkoe, D. J. (2011). α-Synuclein occurs physiologically as a helically folded tetramer that resists aggregation. *Nature*, *477*(7362), 107–110. https://doi.org/10.1038/nature10324

Barton, O., Naumann, S. C., Diemer-Biehs, R., Künzel, J., Steinlage, M., Conrad, S., Makharashvili, N., Wang, J., Feng, L., Lopez, B. S., Paull, T. T., Chen, J., Jeggo, P. A., & Löbrich, M. (2014). Polo-like kinase 3 regulates CtIP during DNA double-strand break repair in G1. *Journal of Cell Biology*, *206*(7), 877–894. https://doi.org/10.1083/jcb.201401146

Basso, E., Antas, P., Marijanovic, Z., Gonçalves, S., Tenreiro, S., & Outeiro, T. F. (2013). PLK2 modulates α-synuclein aggregation in yeast and mammalian cells. *Molecular Neurobiology*, *48*(3), 854–862. https://doi.org/10.1007/s12035-013-8473-z

Bennardo, N., & Stark, J. M. (2010). ATM Limits Incorrect End Utilization during Non-Homologous End Joining of Multiple Chromosome Breaks. *PLOS Genetics*, *6*(11), e1001194. https://doi.org/10.1371/journal.pgen.1001194

Benskey, M. J., Sellnow, R. C., Sandoval, I. M., Sortwell, C. E., Lipton, J. W., & Manfredsson, F. P. (2018). Silencing Alpha Synuclein in Mature Nigral Neurons Results in Rapid Neuroinflammation and Subsequent Toxicity. *Frontiers in Molecular Neuroscience*, *11*, 36. https://doi.org/10.3389/fnmol.2018.00036

Bergeron, M., Motter, R., Tanaka, P., Fauss, D., Babcock, M., Chiou, S.-S., Nelson, S., San Pablo, F., & Anderson, J. P. (2014). In vivo modulation of polo-like kinases supports a key role for PLK2 in Ser129 α-synuclein phosphorylation in mouse brain. *Neuroscience*, *256*, 72–82. https://doi.org/10.1016/j.neuroscience.2013.09.061

Betarbet, R., Sherer, T. B., MacKenzie, G., Garcia-Osuna, M., Panov, A. V., & Greenamyre, J. T. (2000). Chronic systemic pesticide exposure reproduces features of Parkinson's disease. *Nature Neuroscience*, *3*(12), 1301–1306. https://doi.org/10.1038/81834

Bétermier, M., Bertrand, P., & Lopez, B. S. (2014). Is non-homologous end-joining really an inherently error-prone process? *PLoS Genetics*, *10*(1), e1004086. https://doi.org/10.1371/journal.pgen.1004086

Bisi, N., Feni, L., Peqini, K., Pérez-Peña, H., Ongeri, S., Pieraccini, S., & Pellegrino, S. (2021). α-Synuclein: An All-Inclusive Trip Around its Structure, Influencing Factors and Applied Techniques. *Frontiers in Chemistry*, *9*. https://doi.org/10.3389/fchem.2021.666585

Blandini, F., Armentero, M.-T., & Martignoni, E. (2008). The 6-hydroxydopamine model: News from the past. *Parkinsonism & Related Disorders*, *14 Suppl 2*, S124-129. https://doi.org/10.1016/j.parkreldis.2008.04.015

Blauwendraat, C., Reed, X., Krohn, L., Heilbron, K., Bandres-Ciga, S., Tan, M., Gibbs, J. R., Hernandez, D. G., Kumaran, R., Langston, R., Bonet-Ponce, L., Alcalay, R. N., Hassin-Baer, S., Greenbaum, L., Iwaki, H., Leonard, H. L., Grenn, F. P., Ruskey, J. A., Sabir, M., … on behalf of the International Parkinson's Disease Genomics Consortium (IPDGC). (2020). Genetic modifiers of risk and age at onset in GBA associated Parkinson's disease and Lewy body dementia. *Brain*, *143*(1), 234–248. https://doi.org/10.1093/brain/awz350

Bodner, R. A., Outeiro, T. F., Altmann, S., Maxwell, M. M., Cho, S. H., Hyman, B. T., McLean, P. J., Young, A. B., Housman, D. E., & Kazantsev, A. G. (2006). Pharmacological promotion of inclusion formation: A therapeutic approach for Huntington's and Parkinson's diseases.

Proceedings of the National Academy of Sciences, *103*(11), 4246–4251. https://doi.org/10.1073/pnas.0511256103

Bonifati, V., Rizzu, P., Squitieri, F., Krieger, E., Vanacore, N., van Swieten, J. C., Brice, A., van Duijn, C. M., Oostra, B., Meco, G., & Heutink, P. (2003). DJ-1(PARK7), a novel gene for autosomal recessive, early onset parkinsonism. *Neurological Sciences: Official Journal of the Italian Neurological Society and of the Italian Society of Clinical Neurophysiology*, *24*(3), 159–160. https://doi.org/10.1007/s10072-003-0108-0

Book, A., Guella, I., Candido, T., Brice, A., Hattori, N., Jeon, B., & Farrer, M. J. (2018). A Meta-Analysis of α-Synuclein Multiplication in Familial Parkinsonism. *Frontiers in Neurology*, *9*, 1021. https://doi.org/10.3389/fneur.2018.01021

Brinkman, E. K., Kousholt, A. N., Harmsen, T., Leemans, C., Chen, T., Jonkers, J., & van Steensel, B. (2018). Easy quantification of template-directed CRISPR/Cas9 editing. *Nucleic Acids Research*, *46*(10), e58. https://doi.org/10.1093/nar/gky164

Brundin, P., & Melki, R. (2017). Prying into the Prion Hypothesis for Parkinson's Disease. *Journal of Neuroscience*, *37*(41), 9808–9818. https://doi.org/10.1523/JNEUROSCI.1788-16.2017

Burré, J., Sharma, M., & Südhof, T. C. (2018). Cell Biology and Pathophysiology of α-Synuclein. *Cold Spring Harbor Perspectives in Medicine*, *8*(3), a024091. https://doi.org/10.1101/cshperspect.a024091

Bussell, R., & Eliezer, D. (2001). Residual Structure and Dynamics in Parkinson's Disease-associated Mutants of α-Synuclein *. *Journal of Biological Chemistry*, *276*(49), 45996–46003. https://doi.org/10.1074/jbc.M106777200

Caporossi, D., Ciafrè, S. A., Pittaluga, M., Savini, I., & Farace, M. G. (2003). Cellular responses to H2O2 and bleomycin-induced oxidative stress in L6C5 rat myoblasts. *Free Radical Biology and Medicine*, *35*(11), 1355–1364. https://doi.org/10.1016/j.freeradbiomed.2003.08.008

Carlsson, A., Lindqvist, M., & Magnusson, T. (1957). 3,4-Dihydroxyphenylalanine and 5-hydroxytryptophan as reserpine antagonists. *Nature*, *180*(4596), 1200. https://doi.org/10.1038/1801200a0

Cerri, S., Mus, L., & Blandini, F. (n.d.). Parkinson's Disease in Women and Men: What's the Difference? *Journal of Parkinson's Disease*, *9*(3), 501–515. https://doi.org/10.3233/JPD-191683

Cerri, S., Mus, L., & Blandini, F. (2019). Parkinson's Disease in Women and Men: What's the Difference? *Journal of Parkinson's Disease*, *9*(3), 501–515. https://doi.org/10.3233/JPD-191683

Chang, H. H. Y., Pannunzio, N. R., Adachi, N., & Lieber, M. R. (2017). Non-homologous DNA end joining and alternative pathways to double-strand break repair. *Nature Reviews. Molecular Cell Biology*, *18*(8), 495–506. https://doi.org/10.1038/nrm.2017.48

Chartier-Harlin, M.-C., Kachergus, J., Roumier, C., Mouroux, V., Douay, X., Lincoln, S., Levecque, C., Larvor, L., Andrieux, J., Hulihan, M., Waucquier, N., Defebvre, L., Amouyel, P., Farrer, M., & Destée, A. (2004). α-synuclein locus duplication as a cause of familial Parkinson's disease. *The Lancet*, *364*(9440), 1167–1169. https://doi.org/10.1016/S0140-6736(04)17103-1

Chen, L., & Feany, M. B. (2005). α-Synuclein phosphorylation controls neurotoxicity and inclusion formation in a Drosophila model of Parkinson disease. *Nature Neuroscience*, *8*(5), Article 5. https://doi.org/10.1038/nn1443

Choi, D.-Y., Zhang, J., & Bing, G. (2010). Aging enhances the neuroinflammatory response and alpha-synuclein nitration in rats. *Neurobiology of Aging*, *31*(9), 1649–1653. https://doi.org/10.1016/j.neurobiolaging.2008.09.010

Cicchetti, F., Lapointe, N., Roberge-Tremblay, A., Saint-Pierre, M., Jimenez, L., Ficke, B. W., & Gross, R. E. (2005). Systemic exposure to paraquat and maneb models early Parkinson's disease in young adult rats. *Neurobiology of Disease*, *20*(2), 360–371. https://doi.org/10.1016/j.nbd.2005.03.018

Cisneros-Aguirre, M., Ping, X., & Stark, J. M. (2022). To indel or not to indel: Factors influencing mutagenesis during chromosomal break end joining. *DNA Repair*, *118*, 103380. https://doi.org/10.1016/j.dnarep.2022.103380

Coskuner, O., & Wise-Scira, O. (2013). Structures and Free Energy Landscapes of the A53T Mutant-Type α-Synuclein Protein and Impact of A53T Mutation on the Structures of the Wild-Type α-Synuclein Protein with Dynamics. *ACS Chemical Neuroscience*, *4*(7), 1101–1113. https://doi.org/10.1021/cn400041j

Costello, S., Cockburn, M., Bronstein, J., Zhang, X., & Ritz, B. (2009). Parkinson's disease and residential exposure to maneb and paraquat from agricultural applications in the central valley of California. *American Journal of Epidemiology*, *169*(8), 919–926. https://doi.org/10.1093/aje/kwp006

Cuervo, A. M., Stefanis, L., Fredenburg, R., Lansbury, P. T., & Sulzer, D. (2004). Impaired degradation of mutant alpha-synuclein by chaperone-mediated autophagy. *Science (New York, N.Y.)*, *305*(5688), 1292–1295. https://doi.org/10.1126/science.1101738

Decressac, M., Mattsson, B., Lundblad, M., Weikop, P., & Björklund, A. (2012). Progressive neurodegenerative and behavioural changes induced by AAV-mediated overexpression of α-synuclein in midbrain dopamine neurons. *Neurobiology of Disease*, *45*(3), 939–953. https://doi.org/10.1016/j.nbd.2011.12.013

Dent, S. E., King, D. P., Osterberg, V. R., Adams, E. K., Mackiewicz, M. R., Weissman, T. A., & Unni, V. K. (2022). Phosphorylation of the aggregate-forming protein alpha-synuclein on serine-129 inhibits its DNA-bending properties. *Journal of Biological Chemistry*, *298*(2). https://doi.org/10.1016/j.jbc.2021.101552

Dexter, D. T., & Jenner, P. (2013). Parkinson disease: From pathology to molecular disease mechanisms. *Free Radical Biology and Medicine*, *62*, 132–144. https://doi.org/10.1016/j.freeradbiomed.2013.01.018

Dileep, V., Boix, C. A., Mathys, H., Marco, A., Welch, G. M., Meharena, H. S., Loon, A., Jeloka, R., Peng, Z., Bennett, D. A., Kellis, M., & Tsai, L.-H. (2023). Neuronal DNA double-strand breaks lead to genome structural variations and 3D genome disruption in neurodegeneration. *Cell*, *186*(20), 4404-4421.e20. https://doi.org/10.1016/j.cell.2023.08.038

Ding, F., Luan, L., Ai, Y., Walton, A., Gerhardt, G. A., Gash, D. M., Grondin, R., & Zhang, Z. (2008). Development of a stable, early stage unilateral model of Parkinson's disease in middle-

aged rhesus monkeys. *Experimental Neurology*, *212*(2), 431–439. https://doi.org/10.1016/j.expneurol.2008.04.027

Donadio, V., Incensi, A., Leta, V., Giannoccaro, M. P., Scaglione, C., Martinelli, P., Capellari, S., Avoni, P., Baruzzi, A., & Liguori, R. (2014). Skin nerve α-synuclein deposits: A biomarker for idiopathic Parkinson disease. *Neurology*, *82*(15), 1362–1369. https://doi.org/10.1212/WNL.0000000000000316

Doppler, K., Ebert, S., Uçeyler, N., Trenkwalder, C., Ebentheuer, J., Volkmann, J., & Sommer, C. (2014). Cutaneous neuropathy in Parkinson's disease: A window into brain pathology. *Acta Neuropathologica*, *128*(1), 99–109. https://doi.org/10.1007/s00401-014-1284-0

Dovonou, A., Bolduc, C., Soto Linan, V., Gora, C., Peralta III, M. R., & Lévesque, M. (2023). Animal models of Parkinson's disease: Bridging the gap between disease hallmarks and research questions. *Translational Neurodegeneration*, *12*(1), 36. https://doi.org/10.1186/s40035-023-00368-8

Duvoisin, R. C., Eldridge, R., Williams, A., Nutt, J., & Calne, D. (1981). Twin study of Parkinson disease. *Neurology*, *31*(1), 77–80. https://doi.org/10.1212/wnl.31.1.77

Eilam, R., Peter, Y., Groner, Y., & Segal, M. (2003). Late degeneration of nigro-striatal neurons in ATM−/− mice. *Neuroscience*, *121*(1), 83–98. https://doi.org/10.1016/S0306-4522(03)00322-1

Ekmark-Lewén, S., Lindström, V., Gumucio, A., Ihse, E., Behere, A., Kahle, P. J., Nordström, E., Eriksson, M., Erlandsson, A., Bergström, J., & Ingelsson, M. (2018). Early fine motor impairment and behavioral dysfunction in (Thy-1)-h[A30P] alpha-synuclein mice. *Brain and Behavior*, *8*(3), e00915. https://doi.org/10.1002/brb3.915

El-Agnaf, O. M. A., Salem, S. A., Paleologou, K. E., Cooper, L. J., Fullwood, N. J., Gibson, M. J., Curran, M. D., Court, J. A., Mann, D. M. A., Ikeda, S.-I., Cookson, M. R., Hardy, J., & Allsop, D. (2003). α-Synuclein implicated in Parkinson's disease is present in extracellular biological fluids, including human plasma. *The FASEB Journal*, *17*(13), 1–16. https://doi.org/10.1096/fj.03-0098fje

Emmer, K. L., Waxman, E. A., Covy, J. P., & Giasson, B. I. (2011). E46K Human α-Synuclein Transgenic Mice Develop Lewy-like and Tau Pathology Associated with Age-dependent, Detrimental Motor Impairment *. *Journal of Biological Chemistry*, *286*(40), 35104–35118. https://doi.org/10.1074/jbc.M111.247965

Fattah, F., Lee, E. H., Weisensel, N., Wang, Y., Lichter, N., & Hendrickson, E. A. (2010). Ku regulates the non-homologous end joining pathway choice of DNA double-strand break repair in human somatic cells. *PLoS Genetics*, *6*(2), e1000855. https://doi.org/10.1371/journal.pgen.1000855

Fearnley, J. M., & Lees, A. J. (1991). Ageing and Parkinson's disease: Substantia nigra regional selectivity. *Brain: A Journal of Neurology*, *114 (Pt 5)*, 2283–2301. https://doi.org/10.1093/brain/114.5.2283

Feng, Y.-L., Xiang, J.-F., Liu, S.-C., Guo, T., Yan, G.-F., Feng, Y., Kong, N., Li, H.-D., Huang, Y., Lin, H., Cai, X.-J., & Xie, A.-Y. (2017). H2AX facilitates classical non-homologous end joining at the expense of limited nucleotide loss at repair junctions. *Nucleic Acids Research*, *45*(18), 10614–10633. https://doi.org/10.1093/nar/gkx715

Fernandes, V. S., Santos, J. R., Leão, A. H. F. F., Medeiros, A. M., Melo, T. G., Izídio, G. S., Cabral, A., Ribeiro, R. A., Abílio, V. C., Ribeiro, A. M., & Silva, R. H. (2012). Repeated treatment

with a low dose of reserpine as a progressive model of Parkinson's disease. *Behavioural Brain Research*, *231*(1), 154–163. https://doi.org/10.1016/j.bbr.2012.03.008

Fleming, S. M., Zhu, C., Fernagut, P.-O., Mehta, A., DiCarlo, C. D., Seaman, R. L., & Chesselet, M.-F. (2004). Behavioral and immunohistochemical effects of chronic intravenous and subcutaneous infusions of varying doses of rotenone. *Experimental Neurology*, *187*(2), 418–429. https://doi.org/10.1016/j.expneurol.2004.01.023

Foulds, P. G., Yokota, O., Thurston, A., Davidson, Y., Ahmed, Z., Holton, J., Thompson, J. C., Akiyama, H., Arai, T., Hasegawa, M., Gerhard, A., Allsop, D., & Mann, D. M. A. (2012). Post mortem cerebrospinal fluid α-synuclein levels are raised in multiple system atrophy and distinguish this from the other α-synucleinopathies, Parkinson's disease and Dementia with Lewy bodies. *Neurobiology of Disease*, *45*(1), 188–195. https://doi.org/10.1016/j.nbd.2011.08.003

Fujiwara, H., Hasegawa, M., Dohmae, N., Kawashima, A., Masliah, E., Goldberg, M. S., Shen, J., Takio, K., & Iwatsubo, T. (2002). Alpha-Synuclein is phosphorylated in synucleinopathy lesions. *Nature Cell Biology*, *4*(2), 160–164. https://doi.org/10.1038/ncb748

Garcia-Reitboeck, P., Anichtchik, O., Dalley, J. W., Ninkina, N., Tofaris, G. K., Buchman, V. L., & Spillantini, M. G. (2013). Endogenous alpha-synuclein influences the number of dopaminergic neurons in mouse substantia nigra. *Experimental Neurology*, *248*, 541–545. https://doi.org/10.1016/j.expneurol.2013.07.015

GBD 2015 Neurological Disorders Collaborator Group. (2017). Global, regional, and national burden of neurological disorders during 1990-2015: A systematic analysis for the Global

Burden of Disease Study 2015. *The Lancet. Neurology*, *16*(11), 877–897. https://doi.org/10.1016/S1474-4422(17)30299-5

Geertsma, H. M., Suk, T. R., Ricke, K. M., Horsthuis, K., Parmasad, J.-L. A., Fisk, Z. A., Callaghan, S. M., & Rousseaux, M. W. C. (2022). Constitutive nuclear accumulation of endogenous alpha-synuclein in mice causes motor impairment and cortical dysfunction, independent of protein aggregation. *Human Molecular Genetics*, *31*(21), 3613–3628. https://doi.org/10.1093/hmg/ddac035

Gertz, H. J., Siegers, A., & Kuchinke, J. (1994). Stability of cell size and nucleolar size in Lewy body containing neurons of substantia nigra in Parkinson's disease. *Brain Research*, *637*(1–2), 339–341. https://doi.org/10.1016/0006-8993(94)91257-2

Giasson, B. I., Duda, J. E., Quinn, S. M., Zhang, B., Trojanowski, J. Q., & Lee, V. M.-Y. (2002). Neuronal alpha-synucleinopathy with severe movement disorder in mice expressing A53T human alpha-synuclein. *Neuron*, *34*(4), 521–533. https://doi.org/10.1016/s0896-6273(02)00682-7

Goers, J., Manning-Bog, A. B., McCormack, A. L., Millett, I. S., Doniach, S., Di Monte, D. A., Uversky, V. N., & Fink, A. L. (2003). Nuclear localization of alpha-synuclein and its interaction with histones. *Biochemistry*, *42*(28), 8465–8471. https://doi.org/10.1021/bi0341152

Goetz, C. G. (2011). The History of Parkinson's Disease: Early Clinical Descriptions and Neurological Therapies. *Cold Spring Harbor Perspectives in Medicine:*, *1*(1), a008862. https://doi.org/10.1101/cshperspect.a008862

Gomperts, S. N. (2016). Lewy Body Dementias: Dementia With Lewy Bodies and Parkinson Disease Dementia. *Continuum : Lifelong Learning in Neurology*, *22*(2 Dementia), 435–463. https://doi.org/10.1212/CON.0000000000000309

Gonçalves, S., & Outeiro, T. F. (2013a). Assessing the subcellular dynamics of alpha-synuclein using photoactivation microscopy. *Molecular Neurobiology*, *47*(3), 1081–1092. https://doi.org/10.1007/s12035-013-8406-x

Gonçalves, S., & Outeiro, T. F. (2013b). Assessing the subcellular dynamics of alpha-synuclein using photoactivation microscopy. *Molecular Neurobiology*, *47*(3), 1081–1092. https://doi.org/10.1007/s12035-013-8406-x

Gorbatyuk, O. S., Li, S., Sullivan, L. F., Chen, W., Kondrikova, G., Manfredsson, F. P., Mandel, R. J., & Muzyczka, N. (2008). The phosphorylation state of Ser-129 in human α-synuclein determines neurodegeneration in a rat model of Parkinson disease. *Proceedings of the National Academy of Sciences of the United States of America*, *105*(2), 763–768. https://doi.org/10.1073/pnas.0711053105

Gorell, J. M., Johnson, C. C., Rybicki, B. A., Peterson, E. L., & Richardson, R. J. (1998). The risk of Parkinson's disease with exposure to pesticides, farming, well water, and rural living. *Neurology*, *50*(5), 1346–1350. https://doi.org/10.1212/wnl.50.5.1346

Greffard, S., Verny, M., Bonnet, A.-M., Seilhean, D., Hauw, J.-J., & Duyckaerts, C. (2010). A stable proportion of Lewy body bearing neurons in the substantia nigra suggests a model in which the Lewy body causes neuronal death. *Neurobiology of Aging*, *31*(1), 99–103. https://doi.org/10.1016/j.neurobiolaging.2008.03.015

Greten-Harrison, B., Polydoro, M., Morimoto-Tomita, M., Diao, L., Williams, A. M., Nie, E. H., Makani, S., Tian, N., Castillo, P. E., Buchman, V. L., & Chandra, S. S. (2010). Aβγ-Synuclein triple knockout mice reveal age-dependent neuronal dysfunction. *Proceedings of the National Academy of Sciences*, *107*(45), 19573–19578. https://doi.org/10.1073/pnas.1005005107

Guerreiro, P. S., Huang, Y., Gysbers, A., Cheng, D., Gai, W. P., Outeiro, T. F., & Halliday, G. M. (2013). LRRK2 interactions with α-synuclein in Parkinson's disease brains and in cell models. *Journal of Molecular Medicine*, *91*(4), 513–522. https://doi.org/10.1007/s00109-012-0984-y

Hallacli, E., Kayatekin, C., Nazeen, S., Wang, X. H., Sheinkopf, Z., Sathyakumar, S., Sarkar, S., Jiang, X., Dong, X., Di Maio, R., Wang, W., Keeney, M. T., Felsky, D., Sandoe, J., Vahdatshoar, A., Udeshi, N. D., Mani, D. R., Carr, S. A., Lindquist, S., … Khurana, V. (2022). The Parkinson's disease protein alpha-synuclein is a modulator of processing bodies and mRNA stability. *Cell*, *185*(12), 2035-2056.e33. https://doi.org/10.1016/j.cell.2022.05.008

Heller, J., Dogan, I., Schulz, J. B., & Reetz, K. (2014). Evidence for gender differences in cognition, emotion and quality of life in Parkinson's disease? *Aging and Disease*, *5*(1), 63–75. https://doi.org/10.14366/AD.2014.050063

Hijaz, B. A., & Volpicelli-Daley, L. A. (2020). Initiation and propagation of α-synuclein aggregation in the nervous system. *Molecular Neurodegeneration*, *15*(1), 19. https://doi.org/10.1186/s13024-020-00368-6

Hu, S., Hu, M., Liu, J., Zhang, B., Zhang, Z., Zhou, F. H., Wang, L., & Dong, J. (2020). Phosphorylation of Tau and α-Synuclein Induced Neurodegeneration in MPTP Mouse

Model of Parkinson's Disease. *Neuropsychiatric Disease and Treatment*, *16*, 651–663. https://doi.org/10.2147/NDT.S235562

Huang, C.-H., Mirabelli, C. K., Jan, Y., & Crooke, S. T. (1981). Single-strand and double-strand deoxyribonucleic acid breaks produced by several bleomycin analogs. *Biochemistry*, *20*(2), 233–238. https://doi.org/10.1021/bi00505a001

Huang, Z., Xu, Z., Wu, Y., & Zhou, Y. (2011). Determining nuclear localization of alpha-synuclein in mouse brains. *Neuroscience*, *199*, 318–332. https://doi.org/10.1016/j.neuroscience.2011.10.016

Hyun, S.-Y., Hwan, H.-I., & Jang, Y.-J. (2014). Polo-like kinase-1 in DNA damage response. *BMB Reports*, *47*(5), 249–255. https://doi.org/10.5483/BMBRep.2014.47.5.061

Iliakis, G., Murmann, T., & Soni, A. (2015). Alternative end-joining repair pathways are the ultimate backup for abrogated classical non-homologous end-joining and homologous recombination repair: Implications for the formation of chromosome translocations. *Mutation Research. Genetic Toxicology and Environmental Mutagenesis*, *793*, 166–175. https://doi.org/10.1016/j.mrgentox.2015.07.001

Iliakis, G., Wang, H., Perrault, A. R., Boecker, W., Rosidi, B., Windhofer, F., Wu, W., Guan, J., Terzoudi, G., & Pantelias, G. (2004). Mechanisms of DNA double strand break repair and chromosome aberration formation. *Cytogenetic and Genome Research*, *104*(1–4), 14–20. https://doi.org/10.1159/000077461

Inglis, K. J., Chereau, D., Brigham, E. F., Chiou, S.-S., Schöbel, S., Frigon, N. L., Yu, M., Caccavello, R. J., Nelson, S., Motter, R., Wright, S., Chian, D., Santiago, P., Soriano, F., Ramos, C., Powell, K., Goldstein, J. M., Babcock, M., Yednock, T., … Anderson, J. P. (2009). Polo-like

kinase 2 (PLK2) phosphorylates alpha-synuclein at serine 129 in central nervous system. *The Journal of Biological Chemistry*, *284*(5), 2598–2602. https://doi.org/10.1074/jbc.C800206200

Ionov, I. D., & Severtsev, N. N. (2012). Somatostatin antagonist potentiates haloperidol-induced catalepsy in the aged rat. *Pharmacology, Biochemistry, and Behavior*, *103*(2), 295–298. https://doi.org/10.1016/j.pbb.2012.08.006

Ionov, I. D., & Severtsev, N. N. (2022). Editorial Expression of Concern: Histamine- and haloperidol-induced catalepsy in aged mice: differential responsiveness to L-DOPA. *Psychopharmacology*, *239*(8), 2709. https://doi.org/10.1007/s00213-022-06167-9

Ishii, A., Nonaka, T., Taniguchi, S., Saito, T., Arai, T., Mann, D., Iwatsubo, T., Hisanaga, S.-I., Goedert, M., & Hasegawa, M. (2007). Casein kinase 2 is the major enzyme in brain that phosphorylates Ser129 of human alpha-synuclein: Implication for alpha-synucleinopathies. *FEBS Letters*, *581*(24), 4711–4717. https://doi.org/10.1016/j.febslet.2007.08.067

Iwata, A., Miura, S., Kanazawa, I., Sawada, M., & Nukina, N. (2001). α-Synuclein forms a complex with transcription factor Elk-1. *Journal of Neurochemistry*, *77*(1), 239–252. https://doi.org/10.1046/j.1471-4159.2001.00232.x

Jasin, M., & Rothstein, R. (2013). Repair of Strand Breaks by Homologous Recombination. *Cold Spring Harbor Perspectives in Biology*, *5*(11), a012740. https://doi.org/10.1101/cshperspect.a012740

Kabotyanski, E. B., Gomelsky, L., Han, J. O., Stamato, T. D., & Roth, D. B. (1998). Double-strand break repair in Ku86- and XRCC4-deficient cells. *Nucleic Acids Research*, *26*(23), 5333–5342.

Kaech, S., & Banker, G. (2006). Culturing hippocampal neurons. *Nature Protocols*, *1*(5), Article 5. https://doi.org/10.1038/nprot.2006.356

Kalia, L. V., & Lang, A. E. (2015). Parkinson's disease. *Lancet (London, England)*, *386*(9996), 896–912. https://doi.org/10.1016/S0140-6736(14)61393-3

Kam, T.-I., Mao, X., Park, H., Chou, S.-C., Karuppagounder, S. S., Umanah, G. E., Yun, S. P., Brahmachari, S., Panicker, N., Chen, R., Andrabi, S. A., Qi, C., Poirier, G. G., Pletnikova, O., Troncoso, J. C., Bekris, L. M., Leverenz, J. B., Pantelyat, A., Ko, H. S., … Dawson, V. L. (2018). Poly(ADP-ribose) drives pathologic α-synuclein neurodegeneration in Parkinson's disease. *Science*, *362*(6414). https://doi.org/10.1126/science.aat8407

Kamel, F., Tanner, C., Umbach, D., Hoppin, J., Alavanja, M., Blair, A., Comyns, K., Goldman, S., Korell, M., Langston, J., Ross, G., & Sandler, D. (2007). Pesticide exposure and self-reported Parkinson's disease in the agricultural health study. *American Journal of Epidemiology*, *165*(4), 364–374. https://doi.org/10.1093/aje/kwk024

Kawahata, I., Finkelstein, D. I., & Fukunaga, K. (2022). Pathogenic Impact of α-Synuclein Phosphorylation and Its Kinases in α-Synucleinopathies. *International Journal of Molecular Sciences*, *23*(11), 6216. https://doi.org/10.3390/ijms23116216

Kim, J.-S., Krasieva, T. B., Kurumizaka, H., Chen, D. J., Taylor, A. M. R., & Yokomori, K. (2005). Independent and sequential recruitment of NHEJ and HR factors to DNA damage sites in

mammalian cells. *The Journal of Cell Biology*, *170*(3), 341–347. https://doi.org/10.1083/jcb.200411083

Kirik, D., Annett, L. E., Burger, C., Muzyczka, N., Mandel, R. J., & Björklund, A. (2003). Nigrostriatal α-synucleinopathy induced by viral vector-mediated overexpression of human α-synuclein: A new primate model of Parkinson's disease. *Proceedings of the National Academy of Sciences*, *100*(5), 2884–2889. https://doi.org/10.1073/pnas.0536383100

Kitada, T., Asakawa, S., Hattori, N., Matsumine, H., Yamamura, Y., Minoshima, S., Yokochi, M., Mizuno, Y., & Shimizu, N. (1998). Mutations in the parkin gene cause autosomal recessive juvenile parkinsonism. *Nature*, *392*(6676), 605–608. https://doi.org/10.1038/33416

Kontopoulos, E., Parvin, J. D., & Feany, M. B. (2006). α-synuclein acts in the nucleus to inhibit histone acetylation and promote neurotoxicity. *Human Molecular Genetics*, *15*(20), 3012–3023. https://doi.org/10.1093/hmg/ddl243

Kotzbauer, P. T., Trojanowski, J. Q., & Lee, V. M.-Y. (2001). Lewy body pathology in Alzheimer's disease. *Journal of Molecular Neuroscience*, *17*(2), 225–232. https://doi.org/10.1385/JMN:17:2:225

Krüger, R., Kuhn, W., Müller, T., Woitalla, D., Graeber, M., Kösel, S., Przuntek, H., Epplen, J. T., Schöls, L., & Riess, O. (1998). Ala30Pro mutation in the gene encoding alpha-synuclein in Parkinson's disease. *Nature Genetics*, *18*(2), 106–108. https://doi.org/10.1038/ng0298-106

Kumar, V., Singh, D., Singh, B. K., Singh, S., Mittra, N., Jha, R. R., Patel, D. K., & Singh, C. (2018). Alpha-synuclein aggregation, Ubiquitin proteasome system impairment, and l-Dopa response in zinc-induced Parkinsonism: Resemblance to sporadic Parkinson's disease. *Molecular and Cellular Biochemistry*, *444*(1), 149–160. https://doi.org/10.1007/s11010-017-3239-y

Langston, J. W., Ballard, P., Tetrud, J. W., & Irwin, I. (1983). Chronic Parkinsonism in humans due to a product of meperidine-analog synthesis. *Science (New York, N.Y.)*, *219*(4587), 979–980. https://doi.org/10.1126/science.6823561

Lashuel, H. A., Mahul-Mellier, A.-L., Novello, S., Hegde, R. N., Jasiqi, Y., Altay, M. F., Donzelli, S., DeGuire, S. M., Burai, R., Magalhães, P., Chiki, A., Ricci, J., Boussouf, M., Sadek, A., Stoops, E., Iseli, C., & Guex, N. (2022). Revisiting the specificity and ability of phospho-S129 antibodies to capture alpha-synuclein biochemical and pathological diversity. *Npj Parkinson's Disease*, *8*(1), 1–19. https://doi.org/10.1038/s41531-022-00388-7

Le, W., Rowe, D., Xie, W., Ortiz, I., He, Y., & Appel, S. H. (2001). Microglial Activation and Dopaminergic Cell Injury: An In Vitro Model Relevant to Parkinson's Disease. *The Journal of Neuroscience*, *21*(21), 8447–8455. https://doi.org/10.1523/JNEUROSCI.21-21-08447.2001

Lee Clough, R., & Stefanis, L. (2007). A novel pathway for transcriptional regulation of α-synuclein. *The FASEB Journal*, *21*(2), 596–607. https://doi.org/10.1096/fj.06-7111com

Lee, S.-Y., Jang, C., & Lee, K.-A. (2014). Polo-Like Kinases (Plks), a Key Regulator of Cell Cycle and New Potential Target for Cancer Therapy. *Development & Reproduction*, *18*(1), 65–71. https://doi.org/10.12717/DR.2014.18.1.065

Li, X., & Heyer, W.-D. (2008). Homologous recombination in DNA repair and DNA damage tolerance. *Cell Research*, *18*(1), 99–113. https://doi.org/10.1038/cr.2008.1

Li, Z., Li, J., Kong, Y., Yan, S., Ahmad, N., & Liu, X. (2017). Plk1 Phosphorylation of Mre11 Antagonizes the DNA Damage Response. *Cancer Research*, *77*(12), 3169–3180. https://doi.org/10.1158/0008-5472.CAN-16-2787

Liew, Z., Wang, A., Bronstein, J., & Ritz, B. (2014). Job exposure matrix (JEM)-derived estimates of lifetime occupational pesticide exposure and the risk of Parkinson's disease. *Archives of Environmental & Occupational Health*, *69*(4), 241–251. https://doi.org/10.1080/19338244.2013.778808

Lou, H., Montoya, S. E., Alerte, T. N. M., Wang, J., Wu, J., Peng, X., Hong, C.-S., Friedrich, E. E., Mader, S. A., Pedersen, C. J., Marcus, B. S., McCormack, A. L., Di Monte, D. A., Daubner, S. C., & Perez, R. G. (2010). Serine 129 phosphorylation reduces the ability of alpha-synuclein to regulate tyrosine hydroxylase and protein phosphatase 2A in vitro and in vivo. *The Journal of Biological Chemistry*, *285*(23), 17648–17661. https://doi.org/10.1074/jbc.M110.100867

Lu, L., Neff, F., Alvarez-Fischer, D., Henze, C., Xie, Y., Oertel, W. H., Schlegel, J., & Hartmann, A. (2005). Gene expression profiling of Lewy body-bearing neurons in Parkinson's disease. *Experimental Neurology*, *195*(1), 27–39. https://doi.org/10.1016/j.expneurol.2005.04.011

Luk, K. C., Kehm, V., Carroll, J., Zhang, B., O'Brien, P., Trojanowski, J. Q., & Lee, V. M.-Y. (2012). Pathological α-Synuclein Transmission Initiates Parkinson-like Neurodegeneration in

Non-transgenic Mice. *Science (New York, N.Y.)*, *338*(6109), 949–953. https://doi.org/10.1126/science.1227157

Luk, K. C., Kehm, V. M., Zhang, B., O'Brien, P., Trojanowski, J. Q., & Lee, V. M. Y. (2012). Intracerebral inoculation of pathological α-synuclein initiates a rapidly progressive neurodegenerative α-synucleinopathy in mice. *The Journal of Experimental Medicine*, *209*(5), 975–986. https://doi.org/10.1084/jem.20112457

Lv, Z., Hashemi, M., Banerjee, S., Zagorski, K., Rochet, J.-C., & Lyubchenko, Y. L. (2019). Assembly of α-synuclein aggregates on phospholipid bilayers. *Biochimica et Biophysica Acta (BBA) - Proteins and Proteomics*, *1867*(9), 802–812. https://doi.org/10.1016/j.bbapap.2019.06.006

Ma, M.-R., Hu, Z.-W., Zhao, Y.-F., Chen, Y.-X., & Li, Y.-M. (2016). Phosphorylation induces distinct alpha-synuclein strain formation. *Scientific Reports*, *6*(1), 37130. https://doi.org/10.1038/srep37130

Mah, L.-J., El-Osta, A., & Karagiannis, T. C. (2010). γH2AX as a molecular marker of aging and disease. *Epigenetics*, *5*(2), 129–136. https://doi.org/10.4161/epi.5.2.11080

Manning-Bog, A. B., McCormack, A. L., Li, J., Uversky, V. N., Fink, A. L., & Monte, D. A. D. (2002). The Herbicide Paraquat Causes Up-regulation and Aggregation of α-Synuclein in Mice: PARAQUAT AND α-SYNUCLEIN *. *Journal of Biological Chemistry*, *277*(3), 1641–1644. https://doi.org/10.1074/jbc.C100560200

Mao, Z., Bozzella, M., Seluanov, A., & Gorbunova, V. (2008). Comparison of nonhomologous end joining and homologous recombination in human cells. *DNA Repair*, *7*(10), 1765–1771. https://doi.org/10.1016/j.dnarep.2008.06.018

Maroteaux, L., Campanelli, J., & Scheller, R. (1988). Synuclein: A neuron-specific protein localized to the nucleus and presynaptic nerve terminal. *The Journal of Neuroscience*, *8*(8), 2804–2815. https://doi.org/10.1523/JNEUROSCI.08-08-02804.1988

Masliah, E., Rockenstein, E., Veinbergs, I., Mallory, M., Hashimoto, M., Takeda, A., Sagara, Y., Sisk, A., & Mucke, L. (2000). Dopaminergic loss and inclusion body formation in alpha-synuclein mice: Implications for neurodegenerative disorders. *Science (New York, N.Y.)*, *287*(5456), 1265–1269. https://doi.org/10.1126/science.287.5456.1265

Mbefo, M. K., Paleologou, K. E., Boucharaba, A., Oueslati, A., Schell, H., Fournier, M., Olschewski, D., Yin, G., Zweckstetter, M., Masliah, E., Kahle, P. J., Hirling, H., & Lashuel, H. A. (2010). Phosphorylation of Synucleins by Members of the Polo-like Kinase Family. *The Journal of Biological Chemistry*, *285*(4), 2807–2822. https://doi.org/10.1074/jbc.M109.081950

McFarland, M. A., Ellis, C. E., Markey, S. P., & Nussbaum, R. L. (2008). Proteomics Analysis Identifies Phosphorylation-dependent α-Synuclein Protein Interactions. *Molecular & Cellular Proteomics : MCP*, *7*(11), 2123–2137. https://doi.org/10.1074/mcp.M800116-MCP200

McFarland, N. R., Fan, Z., Xu, K., Schwarzschild, M. A., Feany, M. B., Hyman, B. T., & McLean, P. J. (2009). Alpha-Synuclein S129 Phosphorylation Mutants Do Not Alter Nigrostriatal Toxicity in a Rat Model of Parkinson Disease. *Journal of Neuropathology and Experimental Neurology*, *68*(5), 515–524. https://doi.org/10.1097/NEN.0b013e3181a24b53

McLean, P. J., Kawamata, H., Ribich, S., & Hyman, B. T. (2000). Membrane Association and Protein Conformation of α-Synuclein in Intact Neurons: EFFECT OF PARKINSON'S DISEASE-LINKED MUTATIONS *. *Journal of Biological Chemistry*, *275*(12), 8812–8816. https://doi.org/10.1074/jbc.275.12.8812

McNaught, K. S. P., Belizaire, R., Isacson, O., Jenner, P., & Olanow, C. W. (2003). Altered proteasomal function in sporadic Parkinson's disease. *Experimental Neurology*, *179*(1), 38–46. https://doi.org/10.1006/exnr.2002.8050

Mencke, P., Boussaad, I., Romano, C. D., Kitami, T., Linster, C. L., & Krüger, R. (2021). The Role of DJ-1 in Cellular Metabolism and Pathophysiological Implications for Parkinson's Disease. *Cells*, *10*(2), 347. https://doi.org/10.3390/cells10020347

Milanese, C., Cerri, S., Ulusoy, A., Gornati, S. V., Plat, A., Gabriels, S., Blandini, F., Di Monte, D. A., Hoeijmakers, J. H., & Mastroberardino, P. G. (2018). Activation of the DNA damage response in vivo in synucleinopathy models of Parkinson's disease. *Cell Death & Disease*, *9*(8), 818. https://doi.org/10.1038/s41419-018-0848-7

Milán-Tomás, Á., Fernández-Matarrubia, M., & Rodríguez-Oroz, M. C. (2021). Lewy Body Dementias: A Coin with Two Sides? *Behavioral Sciences*, *11*(7), 94. https://doi.org/10.3390/bs11070094

Mizuno, H., Fujikake, N., Wada, K., & Nagai, Y. (2010). *α*-Synuclein Transgenic *Drosophila* As a Model of Parkinson's Disease and Related Synucleinopathies. *Parkinson's Disease*, *2011*, e212706. https://doi.org/10.4061/2011/212706

Neal, J. A., Dang, V., Douglas, P., Wold, M. S., Lees-Miller, S. P., & Meek, K. (2011). Inhibition of homologous recombination by DNA-dependent protein kinase requires kinase activity, is

titratable, and is modulated by autophosphorylation. *Molecular and Cellular Biology*, *31*(8), 1719–1733. https://doi.org/10.1128/MCB.01298-10

Neal, J. A., & Meek, K. (2011). Choosing the right path: Does DNA-PK help make the decision? *Mutation Research*, *711*(1–2), 73–86. https://doi.org/10.1016/j.mrfmmm.2011.02.010

Neumann, M., Kahle, P. J., Giasson, B. I., Ozmen, L., Borroni, E., Spooren, W., Müller, V., Odoy, S., Fujiwara, H., Hasegawa, M., Iwatsubo, T., Trojanowski, J. Q., Kretzschmar, H. A., & Haass, C. (2002). Misfolded proteinase K–resistant hyperphosphorylated α-synuclein in aged transgenic mice with locomotor deterioration and in human α-synucleinopathies. *The Journal of Clinical Investigation*, *110*(10), 1429–1439. https://doi.org/10.1172/JCI15777

Nick McElhinny, S. A., Havener, J. M., Garcia-Diaz, M., Juárez, R., Bebenek, K., Kee, B. L., Blanco, L., Kunkel, T. A., & Ramsden, D. A. (2005). A Gradient of Template Dependence Defines Distinct Biological Roles for Family X Polymerases in Nonhomologous End Joining. *Molecular Cell*, *19*(3), 357–366. https://doi.org/10.1016/j.molcel.2005.06.012

Nübling, G. S., Levin, J., Bader, B., Lorenzl, S., Hillmer, A., Högen, T., Kamp, F., & Giese, A. (2014). Modelling Ser129 Phosphorylation Inhibits Membrane Binding of Pore-Forming Alpha-Synuclein Oligomers. *PLOS ONE*, *9*(6), e98906. https://doi.org/10.1371/journal.pone.0098906

Osterberg, V. R., Spinelli, K. J., Weston, L. J., Luk, K. C., Woltjer, R. L., & Unni, V. K. (2015). Progressive aggregation of alpha-synuclein and selective degeneration of lewy inclusion-bearing neurons in a mouse model of parkinsonism. *Cell Reports*, *10*(8), 1252–1260. https://doi.org/10.1016/j.celrep.2015.01.060

Ou, Z., Pan, J., Tang, S., Duan, D., Yu, D., Nong, H., & Wang, Z. (2021). Global Trends in the Incidence, Prevalence, and Years Lived With Disability of Parkinson's Disease in 204 Countries/Territories From 1990 to 2019. *Frontiers in Public Health*, *9*, 776847. https://doi.org/10.3389/fpubh.2021.776847

Oueslati, A. (2016). Implication of Alpha-Synuclein Phosphorylation at S129 in Synucleinopathies: What Have We Learned in the Last Decade? *Journal of Parkinson's Disease*, *6*(1), 39–51. https://doi.org/10.3233/JPD-160779

Oueslati, A., Schneider, B. L., Aebischer, P., & Lashuel, H. A. (2013). Polo-like kinase 2 regulates selective autophagic α-synuclein clearance and suppresses its toxicity in vivo. *Proceedings of the National Academy of Sciences of the United States of America*, *110*(41), E3945-3954. https://doi.org/10.1073/pnas.1309991110

Paiva, I., Pinho, R., Pavlou, M. A., Hennion, M., Wales, P., Schütz, A.-L., Rajput, A., Szego, É. M., Kerimoglu, C., Gerhardt, E., Rego, A. C., Fischer, A., Bonn, S., & Outeiro, T. F. (2017). Sodium butyrate rescues dopaminergic cells from alpha-synuclein-induced transcriptional deregulation and DNA damage. *Human Molecular Genetics*, *26*(12), 2231–2246. https://doi.org/10.1093/hmg/ddx114

Paleologou, K. E., Schmid, A. W., Rospigliosi, C. C., Kim, H.-Y., Lamberto, G. R., Fredenburg, R. A., Lansbury, P. T., Fernandez, C. O., Eliezer, D., Zweckstetter, M., & Lashuel, H. A. (2008). Phosphorylation at Ser-129 but not the phosphomimics S129E/D inhibits the fibrillation of alpha-synuclein. *The Journal of Biological Chemistry*, *283*(24), 16895–16905. https://doi.org/10.1074/jbc.M800747200

Parihar, M. S., Parihar, A., Fujita, M., Hashimoto, M., & Ghafourifar, P. (2009). Alpha-synuclein overexpression and aggregation exacerbates impairment of mitochondrial functions by augmenting oxidative stress in human neuroblastoma cells. *The International Journal of Biochemistry & Cell Biology*, *41*(10), 2015–2024. https://doi.org/10.1016/j.biocel.2009.05.008

Parkinson, J. (1817). *An Essay on the Shaking Palsy*. Dawson.

Perni, M., van der Goot, A., Limbocker, R., van Ham, T. J., Aprile, F. A., Xu, C. K., Flagmeier, P., Thijssen, K., Sormanni, P., Fusco, G., Chen, S. W., Challa, P. K., Kirkegaard, J. B., Laine, R. F., Ma, K. Y., Müller, M. B. D., Sinnige, T., Kumita, J. R., Cohen, S. I. A., … Dobson, C. M. (2021). Comparative Studies in the A30P and A53T α-Synuclein C. elegans Strains to Investigate the Molecular Origins of Parkinson's Disease. *Frontiers in Cell and Developmental Biology*, *9*, 552549. https://doi.org/10.3389/fcell.2021.552549

Perrault, R., Wang, H., Wang, M., Rosidi, B., & Iliakis, G. (2004). Backup pathways of NHEJ are suppressed by DNA-PK. *Journal of Cellular Biochemistry*, *92*(4), 781–794. https://doi.org/10.1002/jcb.20104

Pezzoli, G., & Cereda, E. (2013). Exposure to pesticides or solvents and risk of Parkinson disease. *Neurology*, *80*(22), 2035–2041. https://doi.org/10.1212/WNL.0b013e318294b3c8

Piltonen, M., Savolainen, M., Patrikainen, S., Baekelandt, V., Myöhänen, T. T., & Männistö, P. T. (2013). Comparison of motor performance, brain biochemistry and histology of two A30P α-synuclein transgenic mouse strains. *Neuroscience*, *231*, 157–168. https://doi.org/10.1016/j.neuroscience.2012.11.045

Pinho, R., Paiva, I., Jerčić, K. G., Fonseca-Ornelas, L., Gerhardt, E., Fahlbusch, C., Garcia-Esparcia, P., Kerimoglu, C., Pavlou, M. A. S., Villar-Piqué, A., Szegő, É., Lopes da Fonseca, T., Odoardi, F., Soeroes, S., Rego, A. C., Fischle, W., Schwamborn, J. C., Meyer, T., Kügler, S., … Outeiro, T. F. (2019). Nuclear localization and phosphorylation modulate pathological effects of alpha-synuclein. *Human Molecular Genetics*, *28*(1), 31–50. https://doi.org/10.1093/hmg/ddy326

Pismataro, M. C., Astolfi, A., Barreca, M. L., Pacetti, M., Schenone, S., Bandiera, T., Carbone, A., & Massari, S. (2023). Small Molecules Targeting DNA Polymerase Theta (POLθ) as Promising Synthetic Lethal Agents for Precision Cancer Therapy. *Journal of Medicinal Chemistry*, *66*(10), 6498–6522. https://doi.org/10.1021/acs.jmedchem.2c02101

Polymeropoulos, M. H., Lavedan, C., Leroy, E., Ide, S. E., Dehejia, A., Dutra, A., Pike, B., Root, H., Rubenstein, J., Boyer, R., Stenroos, E. S., Chandrasekharappa, S., Athanassiadou, A., Papapetropoulos, T., Johnson, W. G., Lazzarini, A. M., Duvoisin, R. C., Di Iorio, G., Golbe, L. I., & Nussbaum, R. L. (1997). Mutation in the alpha-synuclein gene identified in families with Parkinson's disease. *Science (New York, N.Y.)*, *276*(5321), 2045–2047. https://doi.org/10.1126/science.276.5321.2045

Pouchieu, C., Piel, C., Carles, C., Gruber, A., Helmer, C., Tual, S., Marcotullio, E., Lebailly, P., & Baldi, I. (2018). Pesticide use in agriculture and Parkinson's disease in the AGRICAN cohort study. *International Journal of Epidemiology*, *47*(1), 299–310. https://doi.org/10.1093/ije/dyx225

Priyadarshi, A., Khuder, S. A., Schaub, E. A., & Priyadarshi, S. S. (2001). Environmental risk factors and Parkinson's disease: A metaanalysis. *Environmental Research*, *86*(2), 122–127. https://doi.org/10.1006/enrs.2001.4264

Pronin, A. N., Morris, A. J., Surguchov, A., & Benovic, J. L. (2000). Synucleins are a novel class of substrates for G protein-coupled receptor kinases. *The Journal of Biological Chemistry*, *275*(34), 26515–26522. https://doi.org/10.1074/jbc.M003542200

Przedborski, S., Jackson-Lewis, V., Naini, A. B., Jakowec, M., Petzinger, G., Miller, R., & Akram, M. (2001). The parkinsonian toxin 1-methyl-4-phenyl-1,2,3,6-tetrahydropyridine (MPTP): A technical review of its utility and safety. *Journal of Neurochemistry*, *76*(5), 1265–1274. https://doi.org/10.1046/j.1471-4159.2001.00183.x

Qing, H., Wong, W., McGeer, E. G., & McGeer, P. L. (2009). Lrrk2 phosphorylates alpha synuclein at serine 129: Parkinson disease implications. *Biochemical and Biophysical Research Communications*, *387*(1), 149–152. https://doi.org/10.1016/j.bbrc.2009.06.142

Ray, S., Singh, N., Kumar, R., Patel, K., Pandey, S., Datta, D., Mahato, J., Panigrahi, R., Navalkar, A., Mehra, S., Gadhe, L., Chatterjee, D., Sawner, A. S., Maiti, S., Bhatia, S., Gerez, J. A., Chowdhury, A., Kumar, A., Padinhateeri, R., … Maji, S. K. (2020). α-Synuclein aggregation nucleates through liquid–liquid phase separation. *Nature Chemistry*, *12*(8), Article 8. https://doi.org/10.1038/s41557-020-0465-9

Rietdijk, C. D., Perez-Pardo, P., Garssen, J., van Wezel, R. J. A., & Kraneveld, A. D. (2017). Exploring Braak's Hypothesis of Parkinson's Disease. *Frontiers in Neurology*, *8*, 37. https://doi.org/10.3389/fneur.2017.00037

Rocha, E. M., Keeney, M. T., Maio, R. D., Miranda, B. R. D., & Greenamyre, J. T. (2022). LRRK2 and idiopathic Parkinson's disease. *Trends in Neurosciences*, *45*(3), 224–236. https://doi.org/10.1016/j.tins.2021.12.002

Rockenstein, E., Mallory, M., Hashimoto, M., Song, D., Shults, C. W., Lang, I., & Masliah, E. (2002). Differential neuropathological alterations in transgenic mice expressing alpha-synuclein from the platelet-derived growth factor and Thy-1 promoters. *Journal of Neuroscience Research*, *68*(5), 568–578. https://doi.org/10.1002/jnr.10231

Rose, E. P., Osterberg, V. R., Banga, J. S., Gorbunova, V., & Unni, V. K. (2024). *Alpha-synuclein regulates the repair of genomic DNA double-strand breaks in a DNA-PKcs-dependent manner* (p. 2024.02.29.582819). bioRxiv. https://doi.org/10.1101/2024.02.29.582819

Ryu, M. Y., Kim, D. W., Arima, K., Mouradian, M. M., Kim, S. U., & Lee, G. (2008). Localization of CKII beta subunits in Lewy bodies of Parkinson's disease. *Journal of the Neurological Sciences*, *266*(1–2), 9–12. https://doi.org/10.1016/j.jns.2007.08.027

Saint-Pierre, M., Tremblay, M.-E., Sik, A., Gross, R. E., & Cicchetti, F. (2006). Temporal effects of paraquat/maneb on microglial activation and dopamine neuronal loss in older rats. *Journal of Neurochemistry*, *98*(3), 760–772. https://doi.org/10.1111/j.1471-4159.2006.03923.x

Samuel, F., Flavin, W. P., Iqbal, S., Pacelli, C., Renganathan, S. D. S., Trudeau, L.-E., Campbell, E. M., Fraser, P. E., & Tandon, A. (2016). Effects of Serine 129 Phosphorylation on α-Synuclein Aggregation, Membrane Association, and Internalization. *Journal of Biological Chemistry*, *291*(9), 4374–4385. https://doi.org/10.1074/jbc.M115.705095

Sano, K., Iwasaki, Y., Yamashita, Y., Irie, K., Hosokawa, M., Satoh, K., & Mishima, K. (2021). Tyrosine 136 phosphorylation of α-synuclein aggregates in the Lewy body dementia brain: Involvement of serine 129 phosphorylation by casein kinase 2. *Acta Neuropathologica Communications*, *9*(1), 182. https://doi.org/10.1186/s40478-021-01281-9

Santiago, J. A., Bottero, V., & Potashkin, J. A. (2017). Biological and Clinical Implications of Comorbidities in Parkinson's Disease. *Frontiers in Aging Neuroscience*, *9*. https://doi.org/10.3389/fnagi.2017.00394

Sato, H., Arawaka, S., Hara, S., Fukushima, S., Koga, K., Koyama, S., & Kato, T. (2011). Authentically phosphorylated α-synuclein at Ser129 accelerates neurodegeneration in a rat model of familial Parkinson's disease. *The Journal of Neuroscience: The Official Journal of the Society for Neuroscience*, *31*(46), 16884–16894. https://doi.org/10.1523/JNEUROSCI.3967-11.2011

Schaser, A. J., Osterberg, V. R., Dent, S. E., Stackhouse, T. L., Wakeham, C. M., Boutros, S. W., Weston, L. J., Owen, N., Weissman, T. A., Luna, E., Raber, J., Luk, K. C., McCullough, A. K., Woltjer, R. L., & Unni, V. K. (2019). Alpha-synuclein is a DNA binding protein that modulates DNA repair with implications for Lewy body disorders. *Scientific Reports*, *9*(1), Article 1. https://doi.org/10.1038/s41598-019-47227-z

Schaser, A. J., Stackhouse, T. L., Weston, L. J., Kerstein, P. C., Osterberg, V. R., López, C. S., Dickson, D. W., Luk, K. C., Meshul, C. K., Woltjer, R. L., & Unni, V. K. (2020). Trans-synaptic and retrograde axonal spread of Lewy pathology following pre-formed fibril injection in an in vivo A53T alpha-synuclein mouse model of synucleinopathy. *Acta*

Neuropathologica Communications, *8*(1), 150. https://doi.org/10.1186/s40478-020-01026-0

Schulz-Schaeffer, W. J. (2010). The synaptic pathology of alpha-synuclein aggregation in dementia with Lewy bodies, Parkinson's disease and Parkinson's disease dementia. *Acta Neuropathologica*, *120*(2), 131–143. https://doi.org/10.1007/s00401-010-0711-0

Seirafi, M., Kozlov, G., & Gehring, K. (2015). Parkin structure and function. *The Febs Journal*, *282*(11), 2076–2088. https://doi.org/10.1111/febs.13249

Sekiguchi, M., & Sakumi, K. (1997). Roles of DNA repair methyltransferase in mutagenesis and carcinogenesis. *Japanese Journal of Human Genetics*, *42*(3), 389–399. https://doi.org/10.1007/BF02766939

Seluanov, A., Mao, Z., & Gorbunova, V. (2010). Analysis of DNA Double-strand Break (DSB) Repair in Mammalian Cells. *Journal of Visualized Experiments : JoVE*, *43*. https://doi.org/10.3791/2002

Sfeir, A., & Symington, L. S. (2015). Microhomology-Mediated End Joining: A Back-up Survival Mechanism or Dedicated Pathway? *Trends in Biochemical Sciences*, *40*(11), 701–714. https://doi.org/10.1016/j.tibs.2015.08.006

Singleton, A. B., Farrer, M., Johnson, J., Singleton, A., Hague, S., Kachergus, J., Hulihan, M., Peuralinna, T., Dutra, A., Nussbaum, R., Lincoln, S., Crawley, A., Hanson, M., Maraganore, D., Adler, C., Cookson, M. R., Muenter, M., Baptista, M., Miller, D., … Gwinn-Hardy, K. (2003). α-Synuclein Locus Triplication Causes Parkinson's Disease. *Science*, *302*(5646), 841–841. https://doi.org/10.1126/science.1090278

Smith, L., & Schapira, A. H. V. (2022). GBA Variants and Parkinson Disease: Mechanisms and Treatments. *Cells*, *11*(8), 1261. https://doi.org/10.3390/cells11081261

Solla, P., Cannas, A., Ibba, F. C., Loi, F., Corona, M., Orofino, G., Marrosu, M. G., & Marrosu, F. (2012). Gender differences in motor and non-motor symptoms among Sardinian patients with Parkinson's disease. *Journal of the Neurological Sciences*, *323*(1–2), 33–39. https://doi.org/10.1016/j.jns.2012.07.026

Somayaji, M., Lanseur, Z., Choi, S. J., Sulzer, D., & Mosharov, E. V. (2021). Roles for α-Synuclein in Gene Expression. *Genes*, *12*(8), Article 8. https://doi.org/10.3390/genes12081166

Spinelli, K. J., Taylor, J. K., Osterberg, V. R., Churchill, M. J., Pollock, E., Moore, C., Meshul, C. K., & Unni, V. K. (2014). Presynaptic Alpha-Synuclein Aggregation in a Mouse Model of Parkinson's Disease. *The Journal of Neuroscience*, *34*(6), 2037–2050. https://doi.org/10.1523/JNEUROSCI.2581-13.2014

Steidl, J. V., Gomez-Isla, T., Mariash, A., Ashe, K. H., & Boland, L. M. (2003). Altered short-term hippocampal synaptic plasticity in mutant alpha-synuclein transgenic mice. *Neuroreport*, *14*(2), 219–223. https://doi.org/10.1097/00001756-200302100-00012

Steinberg, R. C., Liu, J., Vaghasia, A. M., Giovinazzo, H., Pham, M.-T., Tselenchuk, D., Chikarmane, R., Haffner, M. C., Nelson, W. G., & Yegnasubramanian, S. (2023). *RepairSwitch: Simultaneous functional assessment of homologous recombination vs end joining DNA repair pathways in living cells* (p. 2023.01.17.524235). bioRxiv. https://doi.org/10.1101/2023.01.17.524235

Stewart, T., Sossi, V., Aasly, J. O., Wszolek, Z. K., Uitti, R. J., Hasegawa, K., Yokoyama, T., Zabetian, C. P., Leverenz, J. B., Stoessl, A. J., Wang, Y., Ginghina, C., Liu, C., Cain, K. C., Auinger, P.,

Kang, U. J., Jensen, P. H., Shi, M., & Zhang, J. (2015). Phosphorylated α-synuclein in Parkinson's disease: Correlation depends on disease severity. *Acta Neuropathologica Communications*, *3*(1), 7. https://doi.org/10.1186/s40478-015-0185-3

Stoker, T. B., Camacho, M., Winder-Rhodes, S., Liu, G., Scherzer, C. R., Foltynie, T., Barker, R. A., & Williams-Gray, C. H. (2020). A common polymorphism in SNCA is associated with accelerated motor decline in GBA-Parkinson's disease. *Journal of Neurology, Neurosurgery & Psychiatry*, *91*(6), 673–674. https://doi.org/10.1136/jnnp-2019-322210

Subramaniam, S. R., Vergnes, L., Franich, N. R., Reue, K., & Chesselet, M.-F. (2014). Region specific mitochondrial impairment in mice with widespread overexpression of alpha-synuclein. *Neurobiology of Disease*, *70*, 204–213. https://doi.org/10.1016/j.nbd.2014.06.017

Surguchov, A. (2015). Intracellular Dynamics of Synucleins: "Here, There and Everywhere." *International Review of Cell and Molecular Biology*, *320*, 103–169. https://doi.org/10.1016/bs.ircmb.2015.07.007

Takahashi, M., Kanuka, H., Fujiwara, H., Koyama, A., Hasegawa, M., Miura, M., & Iwatsubo, T. (2003). Phosphorylation of α-synuclein characteristic of synucleinopathy lesions is recapitulated in α-synuclein transgenic *Drosophila*. *Neuroscience Letters*, *336*(3), 155–158. https://doi.org/10.1016/S0304-3940(02)01258-2

Tanner, C. M., Kamel, F., Ross, G. W., Hoppin, J. A., Goldman, S. M., Korell, M., Marras, C., Bhudhikanok, G. S., Kasten, M., Chade, A. R., Comyns, K., Richards, M. B., Meng, C., Priestley, B., Fernandez, H. H., Cambi, F., Umbach, D. M., Blair, A., Sandler, D. P., &

Langston, J. W. (2011). Rotenone, paraquat, and Parkinson's disease. *Environmental Health Perspectives*, *119*(6), 866–872. https://doi.org/10.1289/ehp.1002839

Tenreiro, S., Eckermann, K., & Outeiro, T. F. (2014). Protein phosphorylation in neurodegeneration: Friend or foe? *Frontiers in Molecular Neuroscience*, *7*, 42. https://doi.org/10.3389/fnmol.2014.00042

Thiruchelvam, M., Brockel, B. J., Richfield, E. K., Baggs, R. B., & Cory-Slechta, D. A. (2000). Potentiated and preferential effects of combined paraquat and maneb on nigrostriatal dopamine systems: Environmental risk factors for Parkinson's disease? *Brain Research*, *873*(2), 225–234. https://doi.org/10.1016/S0006-8993(00)02496-3

Tolosa, E., Vila, M., Klein, C., & Rascol, O. (2020). LRRK2 in Parkinson disease: Challenges of clinical trials. *Nature Reviews Neurology*, *16*(2), Article 2. https://doi.org/10.1038/s41582-019-0301-2

Tripathy, B. K., Pal, K., Shabrish, S., & Mittra, I. (2021). A New Perspective on the Origin of DNA Double-Strand Breaks and Its Implications for Ageing. *Genes*, *12*(2), 163. https://doi.org/10.3390/genes12020163

Udayakumar, D., Bladen, C. L., Hudson, F. Z., & Dynan, W. S. (2003). Distinct pathways of nonhomologous end joining that are differentially regulated by DNA-dependent protein kinase-mediated phosphorylation. *The Journal of Biological Chemistry*, *278*(43), 41631–41635. https://doi.org/10.1074/jbc.M306470200

Vaikath, N. N., Hmila, I., Gupta, V., Erskine, D., Ingelsson, M., & El-Agnaf, O. M. A. (2019). Antibodies against alpha-synuclein: Tools and therapies. *Journal of Neurochemistry*, *150*(5), 612–625. https://doi.org/10.1111/jnc.14713

Valente, E. M., Bentivoglio, A. R., Dixon, P. H., Ferraris, A., Ialongo, T., Frontali, M., Albanese, A., & Wood, N. W. (2001). Localization of a novel locus for autosomal recessive early-onset parkinsonism, PARK6, on human chromosome 1p35-p36. *American Journal of Human Genetics*, *68*(4), 895–900. https://doi.org/10.1086/319522

Vasquez, V., Mitra, J., Hegde, P. M., Pandey, A., Sengupta, S., Mitra, S., Rao, K. S., & Hegde, M. L. (2017). Chromatin-Bound Oxidized α-Synuclein Causes Strand Breaks in Neuronal Genomes in in vitro Models of Parkinson's Disease. *Journal of Alzheimer's Disease: JAD*, *60*(s1), S133–S150. https://doi.org/10.3233/JAD-170342

Waku, I., Magalhães, M. S., Alves, C. O., & de Oliveira, A. R. (2021). Haloperidol-induced catalepsy as an animal model for parkinsonism: A systematic review of experimental studies. *The European Journal of Neuroscience*, *53*(11), 3743–3767. https://doi.org/10.1111/ejn.15222

Wang, H., Qiu, Z., Liu, B., Wu, Y., Ren, J., Liu, Y., Zhao, Y., Wang, Y., Hao, S., Li, Z., Peng, B., & Xu, X. (2018). PLK1 targets CtIP to promote microhomology-mediated end joining. *Nucleic Acids Research*, *46*(20), 10724–10739. https://doi.org/10.1093/nar/gky810

Wang, L., Das, U., Scott, D. A., Tang, Y., McLean, P. J., & Roy, S. (2014). α-synuclein multimers cluster synaptic vesicles and attenuate recycling. *Current Biology: CB*, *24*(19), 2319–2326. https://doi.org/10.1016/j.cub.2014.08.027

Wang, Y., Shi, M., Chung, K. A., Zabetian, C. P., Leverenz, J. B., Berg, D., Srulijes, K., Trojanowski, J. Q., Lee, V. M.-Y., Siderowf, A. D., Hurtig, H., Litvan, I., Schiess, M. C., Peskind, E. R., Masuda, M., Hasegawa, M., Lin, X., Pan, C., Galasko, D., … Zhang, J. (2012).

Phosphorylated α-Synuclein in Parkinson's Disease. *Science Translational Medicine*, *4*(121), 121ra20. https://doi.org/10.1126/scitranslmed.3002566

Ward, C. D., Duvoisin, R. C., Ince, S. E., Nutt, J. D., Eldridge, R., & Calne, D. B. (1983). Parkinson's disease in 65 pairs of twins and in a set of quadruplets. *Neurology*, *33*(7), 815–824. https://doi.org/10.1212/wnl.33.7.815

Waxman, E. A., & Giasson, B. I. (2011). Characterization of kinases involved in the phosphorylation of aggregated α-synuclein. *Journal of Neuroscience Research*, *89*(2), 231–247. https://doi.org/10.1002/jnr.22537

Webber, C. J., Lei, S. (Eric), & Wolozin, B. (2020). The pathophysiology of neurodegenerative disease: Disturbing the balance between phase separation and irreversible aggregation. *Progress in Molecular Biology and Translational Science*, *174*, 187–223. https://doi.org/10.1016/bs.pmbts.2020.04.021

Weber Boutros, S., Unni, V. K., & Raber, J. (2022). An Adaptive Role for DNA Double-Strand Breaks in Hippocampus-Dependent Learning and Memory. *International Journal of Molecular Sciences*, *23*(15), 8352. https://doi.org/10.3390/ijms23158352

Weston, L. J., Stackhouse, T. L., Spinelli, K. J., Boutros, S. W., Rose, E. P., Osterberg, V. R., Luk, K. C., Raber, J., Weissman, T. A., & Unni, V. K. (2021). Genetic deletion of Polo-like kinase 2 reduces alpha-synuclein serine-129 phosphorylation in presynaptic terminals but not Lewy bodies. *Journal of Biological Chemistry*, *296*, 100273. https://doi.org/10.1016/j.jbc.2021.100273

Winslow, A. R., Chen, C.-W., Corrochano, S., Acevedo-Arozena, A., Gordon, D. E., Peden, A. A., Lichtenberg, M., Menzies, F. M., Ravikumar, B., Imarisio, S., Brown, S., O'Kane, C. J., &

Rubinsztein, D. C. (2010). α-Synuclein impairs macroautophagy: Implications for Parkinson's disease. *The Journal of Cell Biology*, *190*(6), 1023–1037. https://doi.org/10.1083/jcb.201003122

Wright, W. D., Shah, S. S., & Heyer, W.-D. (2018). Homologous recombination and the repair of DNA double-strand breaks. *The Journal of Biological Chemistry*, *293*(27), 10524–10535. https://doi.org/10.1074/jbc.TM118.000372

Wu, W., Sung, C. C., Yu, P., Li, J., & Chung, K. K. K. (2020). S-Nitrosylation of G protein-coupled receptor kinase 6 and Casein kinase 2 alpha modulates their kinase activity toward alpha-synuclein phosphorylation in an animal model of Parkinson's disease. *PloS One*, *15*(4), e0232019. https://doi.org/10.1371/journal.pone.0232019

Wyatt, D. W., Feng, W., Conlin, M. P., Yousefzadeh, M. J., Roberts, S. A., Mieczkowski, P., Wood, R. D., Gupta, G. P., & Ramsden, D. A. (2016). Essential Roles for Polymerase θ-Mediated End Joining in the Repair of Chromosome Breaks. *Molecular Cell*, *63*(4), 662–673. https://doi.org/10.1016/j.molcel.2016.06.020

Xilouri, M., Brekk, O. R., & Stefanis, L. (2016). Autophagy and Alpha-Synuclein: Relevance to Parkinson's Disease and Related Synucleopathies. *Movement Disorders: Official Journal of the Movement Disorder Society*, *31*(2), 178–192. https://doi.org/10.1002/mds.26477

Xiong, Y., Dawson, T. M., & Dawson, V. L. (2017). Models of LRRK2 associated Parkinson's disease. *Advances in Neurobiology*, *14*, 163–191. https://doi.org/10.1007/978-3-319-49969-7_9

Xu, J., Kawahata, I., Izumi, H., & Fukunaga, K. (2021). T-Type Ca2+ Enhancer SAK3 Activates CaMKII and Proteasome Activities in Lewy Body Dementia Mice Model. *International Journal of Molecular Sciences*, *22*(12), Article 12. https://doi.org/10.3390/ijms22126185

Yamada, M., Iwatsubo, T., Mizuno, Y., & Mochizuki, H. (2004). Overexpression of α-synuclein in rat substantia nigra results in loss of dopaminergic neurons, phosphorylation of α-synuclein and activation of caspase-9: Resemblance to pathogenetic changes in Parkinson's disease. *Journal of Neurochemistry*, *91*(2), 451–461. https://doi.org/10.1111/j.1471-4159.2004.02728.x

Ysselstein, D., Joshi, M., Mishra, V., Griggs, A. M., Asiago, J. M., McCabe, G. P., Stanciu, L. A., Post, C. B., & Rochet, J.-C. (2015). Effects of impaired membrane interactions on α-synuclein aggregation and neurotoxicity. *Neurobiology of Disease*, *79*, 150–163. https://doi.org/10.1016/j.nbd.2015.04.007

Yuan, Y.-H., Yan, W.-F., Sun, J.-D., Huang, J.-Y., Mu, Z., & Chen, N.-H. (2015). The molecular mechanism of rotenone-induced α-synuclein aggregation: Emphasizing the role of the calcium/GSK3β pathway. *Toxicology Letters*, *233*(2), 163–171. https://doi.org/10.1016/j.toxlet.2014.11.029

Zarranz, J. J., Alegre, J., Gómez-Esteban, J. C., Lezcano, E., Ros, R., Ampuero, I., Vidal, L., Hoenicka, J., Rodriguez, O., Atarés, B., Llorens, V., Gomez Tortosa, E., del Ser, T., Muñoz, D. G., & de Yebenes, J. G. (2004). The new mutation, E46K, of alpha-synuclein causes Parkinson and Lewy body dementia. *Annals of Neurology*, *55*(2), 164–173. https://doi.org/10.1002/ana.10795

Zhao, X., Wei, C., Li, J., Xing, P., Li, J., Zheng, S., & Chen, X. (2017). Cell cycle-dependent control of homologous recombination. *Acta Biochimica Et Biophysica Sinica*, *49*(8), 655–668. https://doi.org/10.1093/abbs/gmx055

Zharikov, A. D., Cannon, J. R., Tapias, V., Bai, Q., Horowitz, M. P., Shah, V., Ayadi, A. E., Hastings, T. G., Greenamyre, J. T., & Burton, E. A. (2015). shRNA targeting α-synuclein prevents neurodegeneration in a Parkinson's disease model. *The Journal of Clinical Investigation*, *125*(7), 2721–2735. https://doi.org/10.1172/JCI64502

Zhou, Y., Lee, J.-H., Jiang, W., Crowe, J. L., Zha, S., & Paull, T. T. (2017). Regulation of the DNA Damage Response by DNA-PKcs Inhibitory Phosphorylation of ATM. *Molecular Cell*, *65*(1), 91–104. https://doi.org/10.1016/j.molcel.2016.11.004

Zimprich, A., Biskup, S., Leitner, P., Lichtner, P., Farrer, M., Lincoln, S., Kachergus, J., Hulihan, M., Uitti, R. J., Calne, D. B., Stoessl, A. J., Pfeiffer, R. F., Patenge, N., Carbajal, I. C., Vieregge, P., Asmus, F., Müller-Myhsok, B., Dickson, D. W., Meitinger, T., … Gasser, T. (2004). Mutations in LRRK2 cause autosomal-dominant parkinsonism with pleomorphic pathology. *Neuron*, *44*(4), 601–607. https://doi.org/10.1016/j.neuron.2004.11.005